

Development of a Selective Dual Discoidin Domain Receptor (DDR)/p38

Kinase Chemical Probe

Sandra Röhm^{†,‡}, Benedict-Tilman Berger^{†,‡}, Martin Schröder^{†,‡}, Deep Chatterjee^{†,‡}, Sebastian Mathea^{†,‡}, Andreas C. Joerger^{†,‡}, Daniel M. Pinkas[§], Joshua C. Bufton[§], Amelie Tjaden^{†,‡}, Lohitesh Kovooru^{‡,¶}, Mark Kudolo[♢], Christian Pohl^{‡,¶,♢}, Alex N. Bullock[§], Susanne Müller^{†,‡}, Stefan Laufer[♢], Stefan Knapp^{*,†,‡}

[†]Johann Wolfgang Goethe University, Institute of Pharmaceutical Chemistry, Max-von-Laue-Str. 9, 60438 Frankfurt am Main, Germany

[‡]Structural Genomics Consortium (SGC), Buchmann Institute for Molecular Life Sciences, Max-von-Laue-Str. 15, 60438, Frankfurt am Main, Germany.

[♢]Department of Pharmaceutical/Medicinal Chemistry, Eberhard Karls University Tübingen, Auf der Morgenstelle 8, 72076 Tübingen, Germany

[§]Centre for Medicines Discovery, University of Oxford, Old Road Campus, Roosevelt Drive, Oxford, OX3 7DQ, UK

[¶]Institute of Biochemistry II, Faculty of Medicine, Johann Wolfgang Goethe University, Max-von-Laue-Str. 15, 60438, Frankfurt am Main, Germany.

[#]Current affiliation: Neuroscience Discovery, AbbVie Deutschland GmbH & Co KG, Knollstraße 50, 67061 Ludwigshafen, Germany

Correspondence: Stefan Knapp, e-mail: knapp@pharmchem.uni-frankfurt.de

ABSTRACT

Discoidin domain receptors 1/2 (DDR1/2) play a central role in fibrotic disorders, such as renal and pulmonary fibrosis, atherosclerosis and various forms of cancer. Potent and selective inhibitors, so-called chemical probe compounds, have been developed to study DDR1/2 kinase signaling. However, these inhibitors showed undesired activity on other kinases such as the tyrosine-protein kinase receptor TIE (tropomyosin receptor kinases), which are related to angiogenesis and neuronal toxicity. In this study, we optimized our recently published p38 mitogene activated protein kinase inhibitor **7** towards a potent and cell-active active dual DDR/p38 chemical probe and developed a structurally related negative control. The structure-guided design approach used provided insights into the P-loop folding process of p38 and how targeting of non-conserved amino acids modulates inhibitor selectivity. The developed and comprehensively characterized DDR/p38-probe, **30** (SR-302), is a valuable tool for studying the role of DDR-kinase in normal physiology and in disease development.

Key words: Discoidin domain receptor, DDR1, DDR2, protein kinase, structure based design, chemical probe

INTRODUCTION

The discoidin domain receptor (DDR) kinases DDR1 and DDR2 were first identified in the early 1990s as members of the receptor tyrosine kinase (RTK) family. DDR2 is expressed as a single type-I transmembrane protein, whereas five isoforms of DDR1 produced by alternative splicing have been discovered, namely, DDR1a, DDR1b, DDR1c, DDR1d, and DDR1e.^{1, 2} DDR kinases share a high similarity in their extracellular discoidin domain structure, but differ in their intracellular region. Whereas DDR1a-c and DDR2 share an intracellular kinase domain, the isoforms DDR1d and DDR1e are truncated, kinase-deficient receptors.³ Typically, RTKs

are activated by peptide-like growth factors extracellularly, followed by receptor dimerization, cross-phosphorylation, and fast activation of the signaling cascade. Interestingly, DDR kinases are characterized by a unique mechanism of activation by various forms of triple-helical collagens present in the extracellular matrix.^{1,2,4} Furthermore, in contrast to other RTKs, DDRs exist in preformed autoinhibited receptor homo- or heterodimers in the transmembrane, an assembly which enhances collagen binding.⁵ Linked to the extracellular matrix, DDR kinases regulate fundamental physiological processes such as cellular adhesion, migration, proliferation, differentiation, matrix remodeling, and survival.⁶ Aberrant kinase activation of DDR kinases plays an important role in fibrotic disorders of lung, kidney, and liver.

DDR1/2 kinases exist mostly in their inactive states if not stimulated by extracellular collagen ligands. The low cellular activity of DDR1 kinase is also caused by an intrinsic autoinhibitory YxxxYY motif, in which the N-terminal tyrosine (Tyr755) controls the autoinhibitory state by phosphorylation.⁶ A similar structural motif has previously been described for the insulin-receptor tyrosine kinase (IRK), where phosphorylation of a tyrosine reverses autoinhibition and thus enables catalytic activity.^{7, 8} Another molecular mechanism discussed mediating the unexpected low DDR1 kinase activity inside the cell is a rarely seen salt bridge between Asp671 (α D helix) and Arg752 (A-loop), which stabilizes the inactivating DFG-out conformation.⁹ This polar interaction strongly impairs the formation of a catalytically active DFG-in conformation and may explain why crystal structures of DDR1 kinase in complex with type-I inhibitors always show the inactive DFG-out conformation. Interestingly, this stabilizing salt bridge has also been observed in six other kinases, KIT, CSF1R, MEK5, YSK4, and PDGFR α/β , and it has been suggested to play a role in inhibitor promiscuity.¹⁰ Although DDR kinases have been described as enzymes that bind many diverse inhibitors, and selectivity profiles of kinase inhibitors, such as imatinib, frequently show DDR kinases as off-targets, few publications have focused on the design of selective DDR inhibitors.¹⁰ So far, the published inhibitor landscape

is of limited scaffold diversity, covering urea compounds designed by derivatization of inhibitors with known DDR1/2 kinase activity, such as imatinib, dasatinib, and BIRB-796.¹¹⁻¹³ For instance, a recent study has focused on ponatinib derivatives, and a diverse set of pyrazolopyrimidine (eg. **1**) and imidazopyrazine derivatives have been evaluated as DDR inhibitor.^{14, 15} In 2016, Wang et al. reported of tetrahydroisoquinoline-7-carboxamides as very potent and selective DDR1 inhibitors.^{16, 17} However, these inhibitors, including also the DDR-TRK-1 chemical probe (**5**),¹⁸ show undesired off-target activities on tropomyosin receptor kinases (TRKA-C), which are important for the normal function of the central and peripheral nervous systems.^{16, 17, 19, 20} BAY-826 (**6**) has been used to probe DDR1/2 kinases, but originally this inhibitor was developed to study the role of TIE1/2 in angiogenesis, two related receptor tyrosine kinases TIE1/2 that are potently inhibited by BAY-826.²¹ Roche Pharma discovered a set of very promising potent and selective spiroindolinone derivatives using a DNA-encoded library screening approach. In this study, **2** prohibited collagen-induced activation of renal epithelial cells expressing DDR1.²²

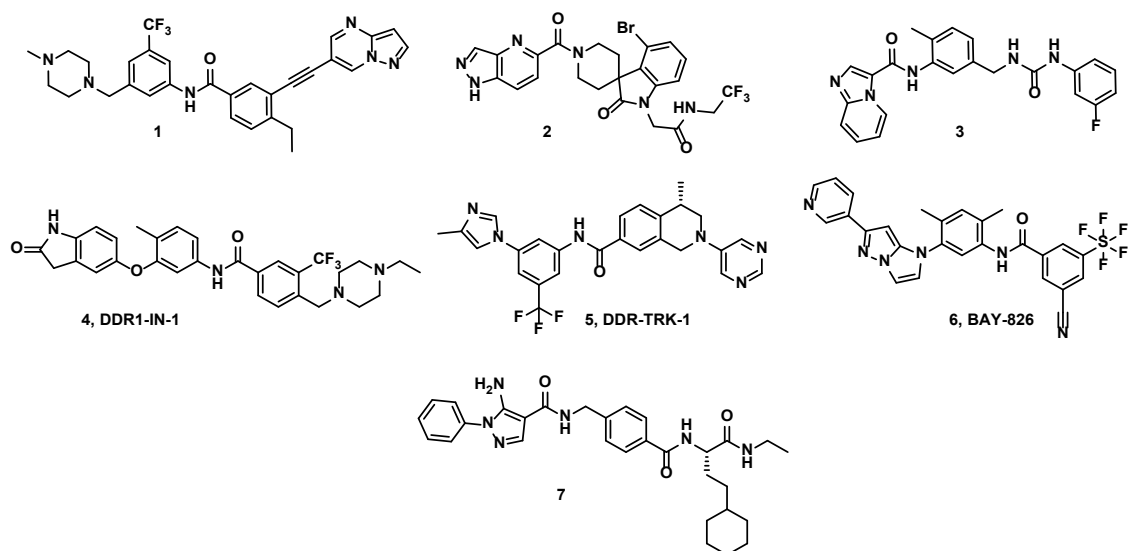


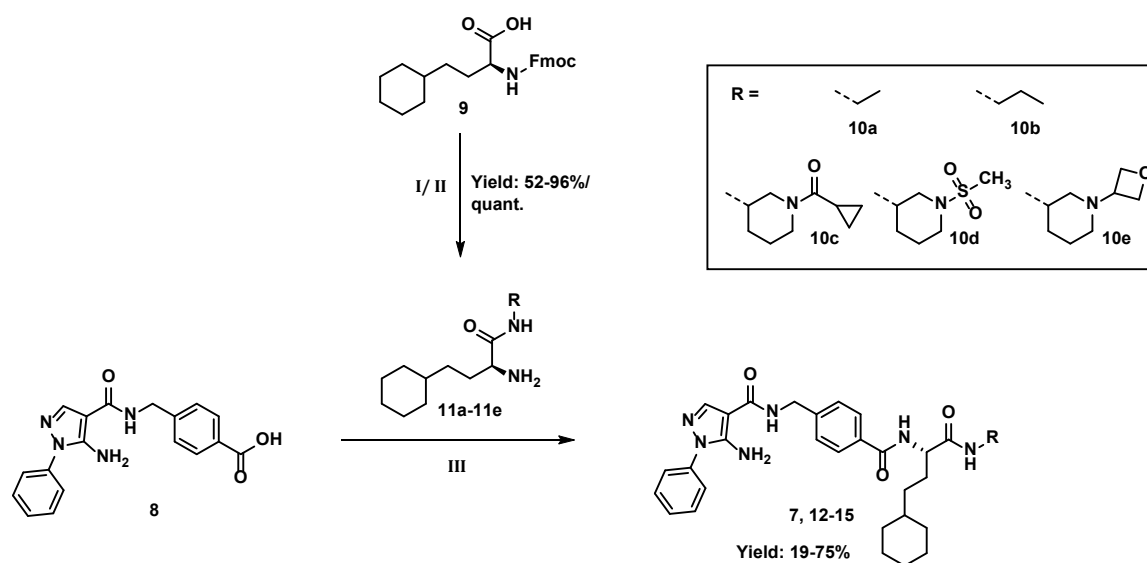
Figure 1. Inhibitor landscape of published DDR1/2 kinase inhibitors (**1-6**) and the p38 lead compound used for the development of a DDR/p38 chemical probe (**7**).

To enrich the scaffold diversity of DDR1/2 inhibitors and to enable mechanistic studies on DDR-kinase signaling, we optimized the p38 inhibitor VPC-00628²³ **7** for targeting DDR1/2 kinases.²⁴ In our comprehensive characterization of **7**, potent activity on DDR1/2 kinases (K_d = 31 nM/40 nM for DDR1/2) was disclosed.²⁴ Therefore, we chose **7** as a starting point for the synthesis of a comprehensive set of DDR1/2 kinase inhibitors using this chemical scaffold. Structure variations targeting the back pocket and the hinge-binding motif in DDR1/2 kinase provided important structural and mechanistic insights into inhibitor binding. Furthermore, we optimized this series to yield a potent, cell active dual DDR/p38 chemical probe **30** with excellent selectivity against the kinome as well as a structurally related negative control.

CHEMISTRY

For the synthesis of **7** and its derivatives **12-15**, Fmoc-homocyclohexyl-L-alanine (**9**) was activated with HATU, DIPEA in DMF, and reacted with the corresponding amine **10a-10e** in an amide coupling reaction. The Fmoc-protecting group was then cleaved under basic conditions, and the unnatural amino acids **11a-11e** were each reacted with 4-((5-amino-1-phenyl-1*H*-pyrazole-4-carboxamido)methyl)benzoic acid (**8**), HATU, DIPEA and DMF to obtain the final compounds **7**, **12-15** in yields between 19-75%.

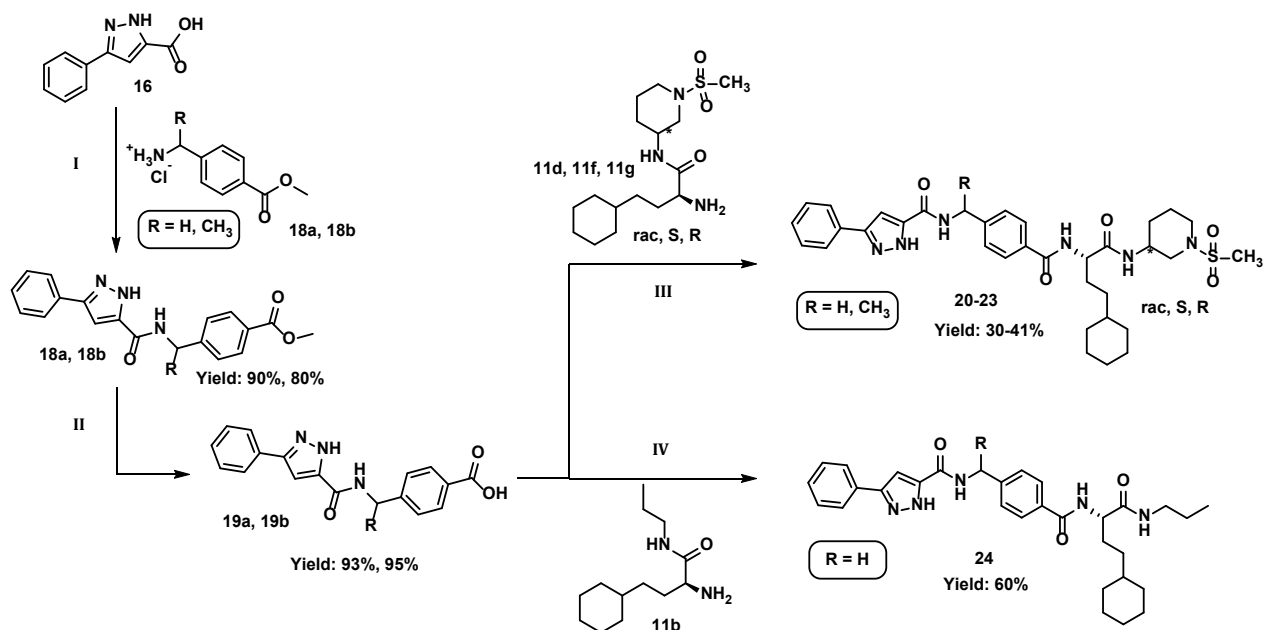
Scheme 1. Synthetic route for the preparation of compounds **7** and **12-15**.^a



^aReagents and conditions: (I) **9**, RNH_2 , HATU, DIPEA, DMF, RT; (II) piperidine, DMF, RT; (III) **11a-11e**, HATU, DIPEA, DMF, RT.

For optimizing the hinge-binding head decoration, various heteroaromatic moieties were selected for synthesis (Scheme 2 and Scheme 3). For compounds **20-24**, 3-phenyl-1*H*-pyrazole-5-carboxylic acid (**16**) was used as starting material, which was activated with EDC-HCl, HOBt, and DIPEA, and then reacted with either benzylamine derivative **17a** or **17b** (Scheme 2). The ester functionality was cleaved with lithium hydroxide in a tetrahydrofuran-water mixture to obtain **19a** and **19b** by precipitation with hydrochloric acid. In the final step, the carboxylic acid was activated by HATU and DIPEA in DMF, and the corresponding amine (**11b**, **11d**, **11f**, **11g**) was added, leading to the compounds of interest at yields between 30% and 60%.

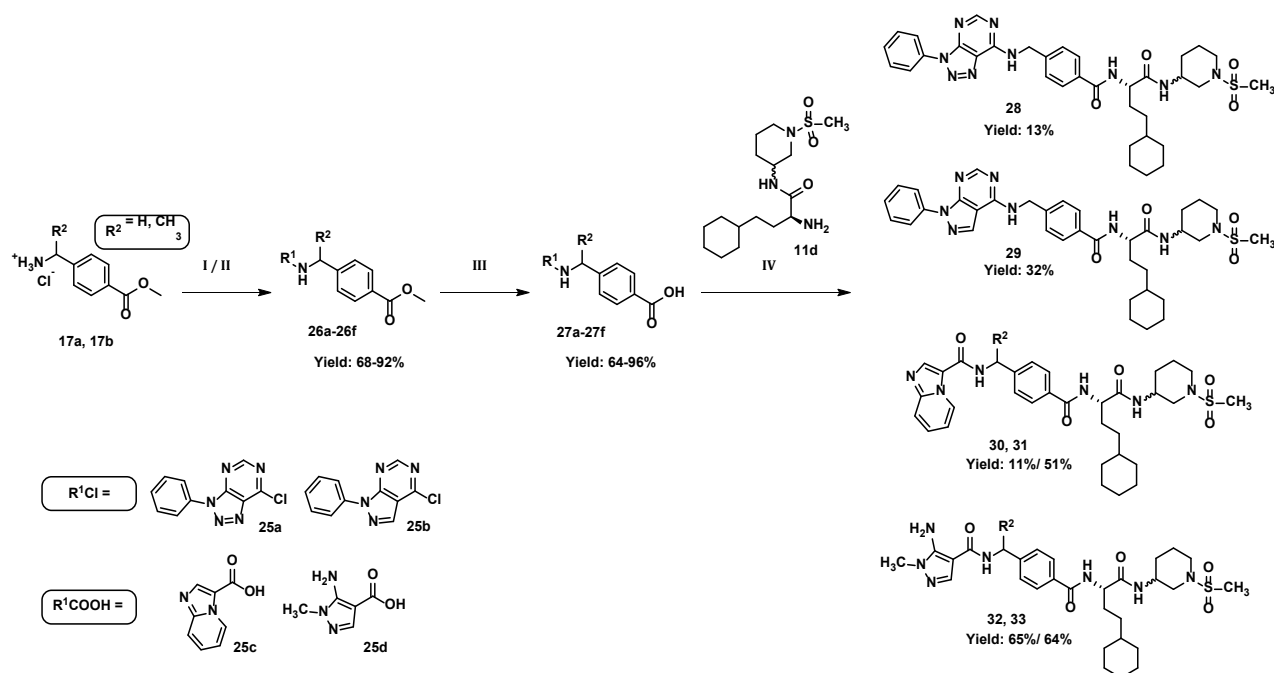
Scheme 2. Synthetic route for the preparation of compounds **20-24**.^a



^aReagents and conditions: (I) EDC-HCl, HOBt, DIPEA, DMF, RT; (II) LiOH, THF/H₂O, RT; (III) **11d**, **11f**, **11g**, HATU, DIPEA, DMF, RT; (IV) **11b**, HATU, DIPEA, DMF, RT.

A nucleophilic aromatic substitution reaction was applied for the synthesis of compounds **26a** and **26b**, using the benzylamine derivative **17a** or **17b** and either triazolopyrimidine **25a** or pyrazolopyrimidine **25b** as starting material (Scheme 3). For compounds **26c-26f**, an amide coupling reaction was performed with imidazo[1,2-*a*]pyridine-3-carboxylic acid (**25c**) or 5-amino-1-methyl-1*H*-pyrazole-4-carboxylic acid (**25d**), which were activated by HATU and DIPEA in DMF before the corresponding benzylamine derivative **17a** or **17b** was added. In the next step, the ester functionality of all compounds synthesized was hydrolyzed with lithium hydroxide to yield the desired acid. Compounds **27a-27f**, which were prepared according to this protocol, were then reacted with (S)-2-amino-4-cyclohexyl-N-((SR)-1-(methylsulfonyl)piperidin-3-yl)butanamide (**11d**) in a second amine coupling reaction to give the final compounds **28-33** at yields between 11-65%.

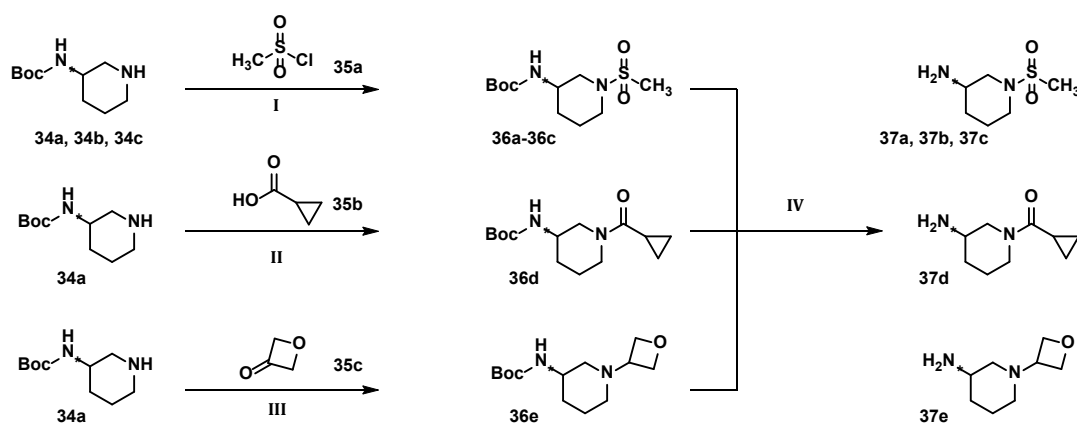
Scheme 3. Synthetic route for the preparation of compounds **28-33**.^a



^aReagents and conditions: (I) for nucleophilic substitution: DIPEA, THF, 60 °C; (II) for amide coupling: EDC-HCl, HOBT, DIPEA, DMF, RT; (III) LiOH, THF/H₂O, RT; (IV) HATU, DIPEA, DMF, RT.

The substituted 3-amino piperidine derivatives used in those amide coupling reactions were synthesized from racemic and/or enantiomeric pure (*R*), (*S*) *tert*-butyl piperidine-3-ylcarbamate (**34a-34c**, Scheme 4). For the sulfonamide decoration, the different 3-amino piperidines **34a-34c** were each reacted with methanesulfonyl chloride (**35a**) in a nucleophilic substitution reaction to obtain compounds **36a-36c**. The cyclopropyl decoration was introduced with cyclopropane carboxylic acid (**35b**), which was reacted with *rac* 3-amino piperidine (**34a**) in an HATU-assisted amide coupling reaction. For the oxetane derivative **36e**, a reductive amination reaction with oxetane-3-one (**34c**) and sodium triacetoxyborohydride under acidic conditions was performed. The Boc protecting group of all compounds synthesized was removed with trifluoroacetic acid to quantitatively obtain the free amines **37a-37e**.

Scheme 4. Synthetic route for the preparation of amine intermediates (**37a-37e**).^a



^aReagents and conditions: (I) TEA, DCM, -20 °C → RT; (II) HATU, DIPEA, DMF, RT; (III) NaBH(OAc)₃, HOAc, DCM, RT; (IV) TFA, DCM, 0 °C → RT.

RESULTS AND DISCUSSION

In order to obtain initial data on the most suitable building blocks for the development of a DDR inhibitor, our previously published p38 compound library covering 127 inhibitors was screened by differential scanning fluorimetry (DSF) against the most potent targets found in the selectivity profiling of **7**.²⁴ The p38 compound library contained VPC-00628 derivatives,²⁵ a set of back-pocket modified type-II inhibitors, and allosteric fragments derived from BIRB-796.²⁴ Thermal shift values (ΔT_m) were determined for DDR1/2, abelson tyrosine-protein kinase 1 (ABL1) as well as mitogen-activated protein kinase kinase kinase 20 (ZAK) and compared with p38 α/β (Supplement Table S1, Table S2). Because the ΔT_m values typically correlate well with K_d values, potencies of new derivatives were estimated by comparing the corresponding thermal shift values. Compound **7** with known K_d values was used as a control in these experiments (p38 α/β [K_d = 6.3/20 nM], DDR1/2 [K_d = 31/40 nM], ZAK [K_d = 120 nM], ABL1 [K_d = 130 nM]). Comparing the screening data for this compound collection²⁴ revealed that thermal stabilization of DDR1/2 followed ΔT_m values measured for p38 α , despite the low

sequence homology of these two kinases. A similar behavior was found for the off-targets ZAK and ABL1. The highest temperature shifts for DDR1 ($\Delta T_m > 4\text{ }^\circ\text{C}$) were measured for compounds **7** and **13-15**. The amino-piperidine back-pocket decorations of compounds **13-15** were therefore considered the most useful starting point for the synthesis of new DDR1/2 inhibitors. For our VPC-00628^{23, 25} based library compounds, the highest thermal shifts for DDR1 ($\Delta T_m > 4\text{ }^\circ\text{C}$) were found for VPC-00628, MCP-040, MCP-042, MCP-047, MCP-074 as well as MCP-081 (structures depicted in Supplement Table S1 and Table S2). In this screen, VPC-00628 and MCP-074 showed off-target activities similar to **7** on all five targets investigated. Besides DDR1, MCP-040 also displayed thermal stabilization of ZAK and ABL1. Compound MCP-042 led to a robust stabilization of DDR1 kinase ($\Delta T_m = 4.3\text{ }^\circ\text{C}$), but it also showed the highest thermal shift for the off-target ZAK ($\Delta T_m = 6.5\text{ }^\circ\text{C}$). The affinity for p38 α/β was slightly reduced in comparison with **7**, which may be due to the CF₃-decorated pyrazole hinge-binding motif. The latter plays an important role in stabilizing the P-loop in a specific conformation, as confirmed by crystal structure determination of MCP-042 in complex with p38 α .²⁵ Interestingly, MCP-047 was the only compound that showed preferential stabilization of DDR1 ($\Delta T_m = 4.4\text{ }^\circ\text{C}$), with negligible temperature shifts for all other kinase targets investigated. MCP-047 and VPC-00628 have a similar back-pocket decoration, but they differ in their hinge-binding moiety, which is a 3-phenyl-1*H*-pyrazole-5-carboxamide moiety in the case of MCP-047. This building block might therefore be useful as a hinge-binding moiety to optimize **7** for the inhibition of DDR1/2 kinase. The chimera of VPC-00628²³ and BIRB-796, MCP-081, previously published and discussed because of its increased α -isoform selectivity,^{24, 25} showed a slight preference for DDR1 kinase in the thermal shift assays ($\Delta T_m = 5.3\text{ }^\circ\text{C}$). However, BIRB-like fragments were evaluated in DSF assays (Supplement Table S1) and appeared not to be optimal for improving activity towards DDR1/2. We speculated that the sulfonamide, cyclopropyl amide or oxetane decorated 3-amino piperidines **13-15** might be better suited for targeting the back pocket of DDR1/2 kinase.

Next, we crystallized **13** in complexes with DDR1 and p38 α kinase, respectively, to compare binding modes and to reveal potential sites for DDR1 kinase selectivity (Figure 2A).

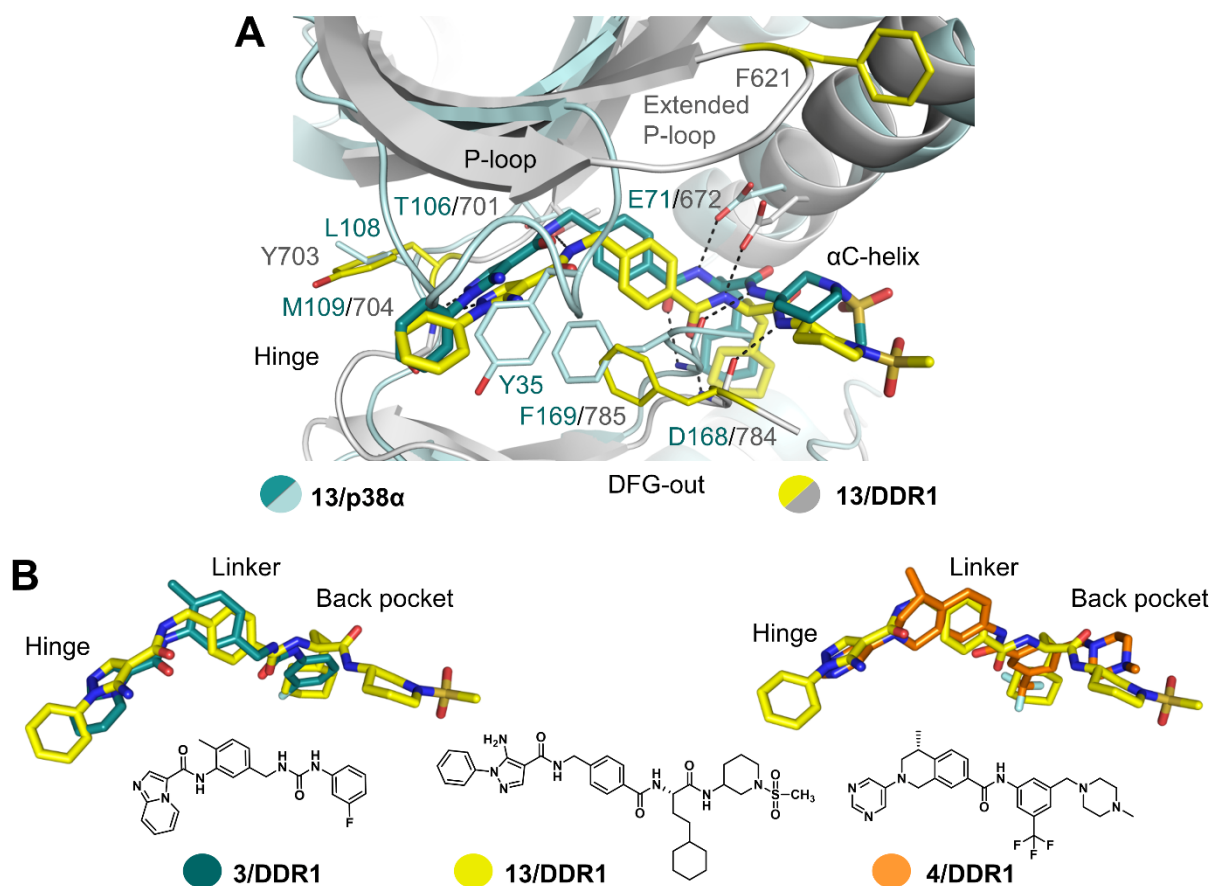


Figure 2. Differences in the binding mode of 13 in p38 α and DDR1 and shape similarities with published DDR1 kinase inhibitors. A) Structure alignment of 13/p38 α (light blue, inhibitor in teal, PDB: 7BE4) and 13/DDR1 kinase complex (gray, inhibitor in yellow, PDB: 7BE6). Hydrogen bonds are highlighted as black dashed lines; important structural motifs are labeled (teal for DDR1 and gray for p38 α). B) Superimposed binding modes of 13 (yellow, PDB: 7BE6), compound 3 (teal, PDB: 5BVN) published by Astex and the DDR-TRK-1 precursor 4 (orange, PDB: 5FDX).

Although both kinases belong to different kinase groups (DDR1 is a receptor tyrosine kinase and p38 α a CMGC family member) and thus share low sequence identity, key interactions with the inhibitor were however conserved, including the canonical hinge backbone interactions and polar interactions with the conserved α C glutamate. While **13** engaged the P-loop inside the

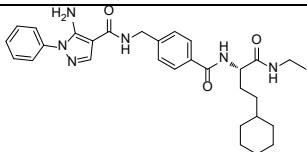
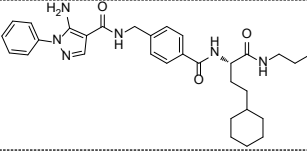
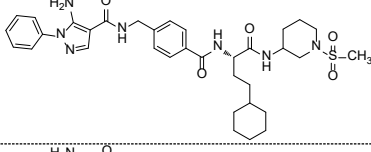
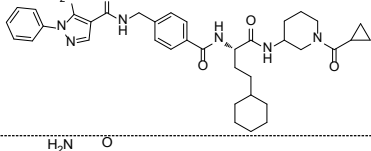
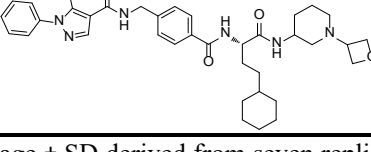
ATP-binding pocket in p38 α via interaction with Tyr35, an extended, active P-loop conformation was observed in the DDR1 complex. In both structures, inhibitor binding stabilized a (DFG-out) type-II binding mode, with the cyclohexyl moiety protruding into the allosteric DFG-out pocket. Only weak electron density was observed for the sulfonamide moiety, suggesting that it is flexible and does not form specific interactions with the protein, or that it adopts alternative binding modes. The hinge region seemed an attractive target for improving inhibitor activity for DDR1/2 because of its high degree of sequence diversity. To identify the most promising hinge-binding moieties, all inhibitors crystallized in complex with DDR1 kinase and published in the KLIFs database (<https://klifs.vu-compmedchem.nl/>) were compared with the structure in complex with **13** to potentially reveal differences in inhibitor binding modes. The most similar compound to our series was **3** from Astex Pharmaceuticals¹² and the DDR-TRK-1 precursor **4** (Figure 2B). Although derived from a completely different scaffold, **3** showed conformational similarity with **13** and its interactions with the hinge and the DFG-out pocket regions. Furthermore, **3** had a lower molecular weight and did not contain an allosteric, solvent-exposed sulfonamide decoration. An imidazo[1,2-*a*]pyridine hinge-binding motif was used in **3**, forming polar contacts with Met704. The flat geometry of the heterocycle enabled weak face-to-face π -interactions with Tyr703. For **13**, an orthogonal geometry between the pyrazole-phenyl decoration was observed, which partially extended into the front pocket. Thus, changing the hinge-binding head group of **13** to an imidazo[1,2-*a*]pyridine moiety might improve potency toward the DDR1 kinase. The alignment of DDR1-TRK-1 precursor **4** and **13** highlighted shape similarities in the allosteric DFG-out pocket region and the solvent-exposed region. Although the 1,2,3,4-tetrahydroisoquinoline moiety in **4** is more rigid, both chemical scaffolds adopted a similar geometry in the linker and hinge region. The DDR1-TRK-1 precursor **4** formed hydrogen bonds with Met704 via its pyrimidine heterocycle nitrogen atom. Furthermore, both database-derived compounds harbored a methyl decoration in the linker part that targeted the hydrophobic pocket behind the gatekeeper residue Thr701. We, therefore,

speculated that the introduction of a methyl group to the benzyl linker of **13** may also improve DDR1/2 kinase activity.

To validate the ΔT_m values determined for the inhibitors targeting the allosteric back pocket, *in cellulo* IC_{50} values of compounds **7** and **12-15** for p38 α as well as DDR1 and DDR2 kinase were determined (Table 1). Although nanomolar potencies were measured for p38 α , IC_{50} values for DDR1 and DDR2 were collectively higher in the cellular environment. For **7**, an approximately >100 times reduced cellular potency on DDR1/2 was determined compared with the K_d values on the isolated enzyme. Differences in potency observed intracellularly compared with K_d values determined on isolated enzyme were not surprising, given that NanoBRET assays usually measure kinase binding in the full-length proteins at cellular ATP concentrations.

Although the potency for p38 α kinase was largely retained for compound **12**, potencies for DDR1/2 kinases increased 3.2-fold and 1.3-fold. As expected from the very similar ΔT_m values obtained for the sulfonamide, cyclopropanamide, and oxetane decorated amino piperidines, low nanomolar affinity binding of p38 α was determined. While **13** and **15** inhibited both DDR1/2 kinases with micromolar potencies, **14** showed the best potency in this series, with IC_{50} values of 1.31 μ M and 1.75 μ M for DDR1/2 kinase, respectively.

Table 1. Back-pocket optimization. Potency of compounds **7** and **12-15** as determined by DSF and *in cellulo* NanoBRET assays for p38 α and DDR1/2.

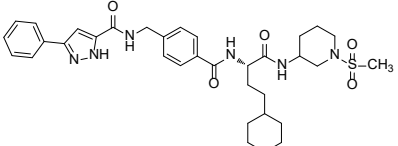
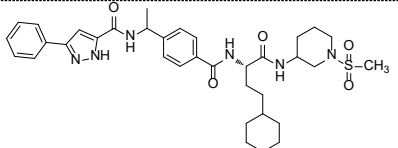
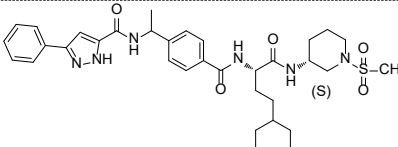
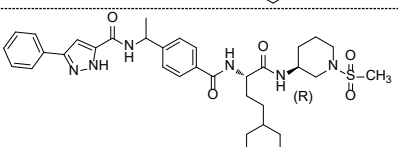
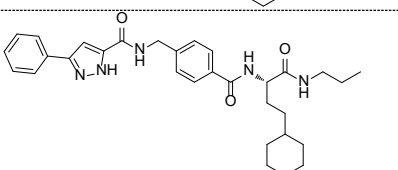
No.	Structure	ΔT_m^a [°C] p38 α	ΔT_m^a [°C] DDR1	ΔT_m^a [°C] DDR2	IC_{50}^b [μ M] p38 α	IC_{50}^b [μ M] DDR1	IC_{50}^b [μ M] DDR2
7		16.4 \pm 0.2	4.4 \pm 0.1	5.1 \pm 0.4	0.014 \pm 0.006 ^f	4.19 \pm 0.84	4.00 \pm 0.72
12		13.7 \pm 0.5	2.8 \pm 0.2	3.8 \pm 0.3	0.017 \pm 0.003 ^d	13.6 ^c	5.25 \pm 2.84 ^d
13		14.1 \pm 0.4	4.6 \pm 0.2	4.8 \pm 0.4	0.033 \pm 0.002 ^e	2.37 \pm 0.28 ^e	3.46 \pm 0.32 ^e
14		14.7 \pm 0.5	4.6 \pm 0.2	5.4 \pm 0.2	0.092 \pm 0.004	1.31 \pm 0.12 ^e	1.75 \pm 0.10 ^e
15		14.4 \pm 0.2	4.9 \pm 0.1	5.8 \pm 0.0	0.057 \pm 0.002	2.43 \pm 0.66 ^d	3.72 \pm 0.30 ^d

^a ΔT_m average \pm SD derived from seven replicates for p38 α and three replicates for DDR1/DDR2 at a compound concentration of 10 μ M; ^b Cellular IC_{50} values determined by NanoBRET assay in HEK293T cells, IC_{50} values \pm SEM were derived from technical replicates (n = 3); ^c n = 1; ^d n = 2; ^e n = 4; ^f n = 6.

Because the previously used hinge-binding motif seemed to be less optimal for DDR1/2 inhibition, further heterocyclic compounds were evaluated (Table 2). The sulfonamide decoration was left unchanged, and the hinge binding moiety of **13** was replaced by a 3-phenyl-1H-pyrazole isomer (compounds **20-24**). This structural element has already been used for the synthesis of VPC-00628 derivatives,²⁵ and DSF assays with **7** (Supplemental Table S2) showed that this heterocycle in compound MCP-047 resulted in better thermal stabilization of DDR1. In order to find out whether the exact stereochemistry of the racemic aminopiperidine derivative in **13** played a role in the binding to DDR kinases, enantiomerically pure (*S*)- and (*R*)-configured

derivatives were synthesized and investigated. Known DDR kinase inhibitors, such as compounds **3**, DDR-1-IN-1, DDR-1-IN-2 and the DDR-TRK-1 probe, all contain a methyl group targeting the hydrophobic pocket located adjacent to the gatekeeper. To investigate the role of the methyl group, a methyl group was incorporated into the benzyl linker of compounds **21-23**. In compound **24**, the sulfonamide decoration was finally replaced by a propyl residue to investigate the contribution of 3-phenyl-1*H*-pyrazole as a hinge binder and to exclude combinatorial mismatch effects.

Table 2. Hinge-binder optimization A. Potency of compounds **20-24** determined by ΔT_m and *in cellulo* IC_{50} values for p38 α and DDR1/2.

No.	Structure	ΔT_m^a [°C] p38 α	ΔT_m^a [°C] DDR1	ΔT_m^a [°C] DDR2	IC_{50}^b [μ M] p38 α	IC_{50}^b [μ M] DDR1	IC_{50}^b [μ M] DDR2
20		1.9 \pm 0.4	1.3 \pm 0.4	2.0 \pm 0.1	12.5 \pm 5.8	39.4 \pm 19.2	21.5 \pm 2.52
21		-0.3 \pm 0.2	1.7 \pm 0.2	1.7 \pm 0.0	18.9 \pm 0.9	16.5 ^c	27.7 \pm 11.3
22		0.4 \pm 0.3	1.1 \pm 0.2	1.5 \pm 0.0	6.0 \pm 2.5	45.2 \pm 17.9	22.0 \pm 7.10
23		0.0 \pm 0.3	1.7 \pm 0.2	1.9 \pm 0.1	6.9 \pm 0.5	13.2 ^c	35.2 \pm 9.4
24		1.0 \pm 0.3	0.1 \pm 0.3	1.1 \pm 0.1	7.2 \pm 0.4	10.4 ^c	59.2 \pm 35.8

^a ΔT_m average \pm SD derived from seven replicates for p38 α and three replicates for DDR1/DDR2 at a compound concentration of 10 μ M; ^b Cellular IC_{50} values \pm SEM determined by NanoBRETTM assay in HEK293T cells, IC_{50} values were derived from technical duplicates (n = 2); ^c n = 1; ^d n = 3.

Consistent with the data presented in Supplemental Table S1 and in our previous publication,²⁵ the introduction of a 3-phenyl-1*H*-pyrazole decoration prevented binding to p38 α . However, micromolar potencies and negligible thermal shift values were determined also for DDR1/2 kinases. Regarding the role of the configuration of the amino piperidines, very similar binding potencies were obtained for both stereoisomers, highlighting that the stereochemistry at this particular position does not affect inhibitor potency. These observations are in agreement with the crystal structure of **13** in complex with DDR1 kinase, showing that the (*S*)- and (*R*)-configured amino piperidine moiety pointed towards the solvent. Comparing the ΔT_m and IC_{50} values determined for all kinase targets of **21** (with methyl group) and **20** (without methyl-decorated benzyl linker), no significant difference in binding potency was apparent. Due to the unfavorable 3-phenyl-1*H*-pyrazole hinge-binding building block, only negligible inhibitory effects were determined for compound **24** with a propyl back-pocket decoration.

Next, we focused on the decoration of the amino-pyrazole moiety in **13** (Table 3). In **32** and **33**, the phenyl moiety thought to be crucial for P-loop stabilization in p38 MAPK and, hence, inhibitor selectivity was truncated. Thermal stabilization of p38 α by **32** ($\Delta T_m = 9.8$ °C) and **33** ($\Delta T_m = 8.7$ °C) was significantly lower than that by **13** ($\Delta T_m = 14.1$ °C), supporting our hypothesis. Interestingly, thermal stabilization of DDR1/2 kinases was even higher for the phenyl-truncated compounds, which was confirmed by BRET assays. While **32** and **33** showed an about 58-fold and 90-fold reduction in potency for p38 α compared with **13**, IC_{50} values of 1.33 μ M and 1.16 μ M were determined for **32** for DDR1/DDR2 kinases. Compound **33** had slightly higher IC_{50} values for all kinase targets, presumably due to unfavorable contacts of the methyl-stabilized benzyl linker. To study if the reduced affinity for p38 MAPK is caused by altered P-loop folding/interactions, a crystal structure of **32** in complex with p38 α kinase was determined (Figure 3).

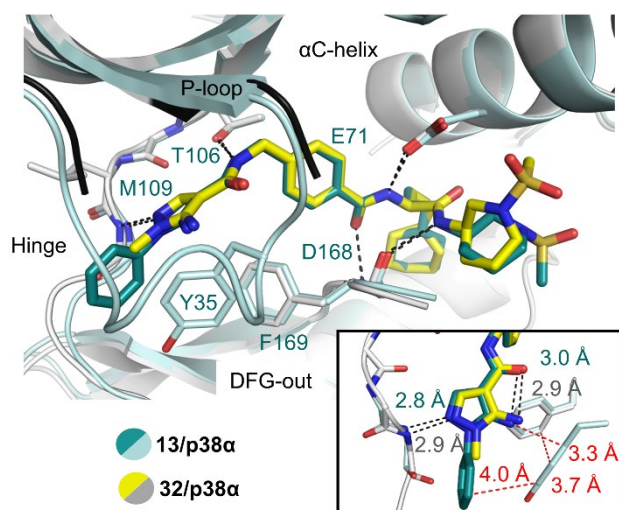


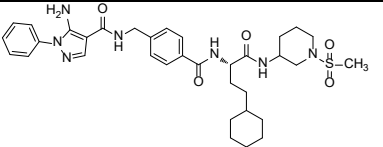
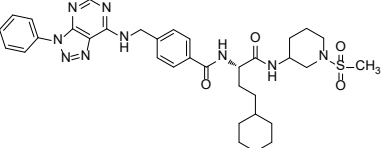
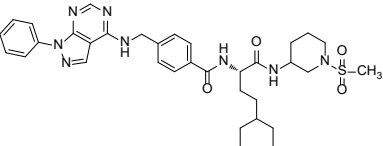
Figure 3. Mechanism of P-loop folding in p38 MAPK. Alignment of **13** (teal, PDB: 7BE4) with **32** (yellow, PDB: 7BE5) in complex with p38 α . **13** engages the P-loop in a folded conformation (teal). With the phenyl-deficient compound **32**, the P-loop was disordered and could not be modeled. Hydrogen bonds are highlighted by black dashed lines. Insert: stabilization of the P-loop by **13** with shown hydrogen bonds (black dashed lines), distance measurements (red dashed lines). Important structural motifs are labeled.

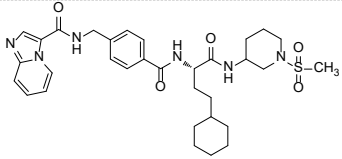
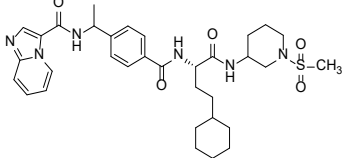
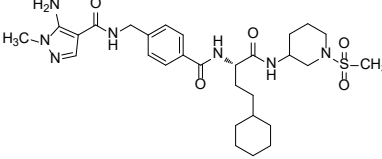
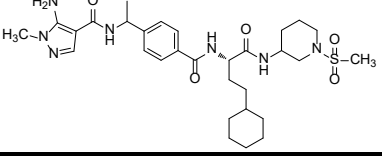
When comparing the crystal structures of p38 α with compounds **13** and **32**, remarkable differences in the P-loop conformation became apparent. While **13** engaged the P-loop via its phenyl residue by a face-to-face stacking interaction with Tyr35 and side-on stacking interaction with Phe169 from the DFG-motif, the P-loop was disordered in the complex with **32**. This observation confirmed the hypothesis that the p38 α hinge-targeting phenyl moiety of **32** was crucial for inhibitor potency and for trapping the P-loop inside the ATP-binding pocket. During the development of the p38 α / β type-II probe SR-318 and its negative control compound SR-321, the free amine at the pyrazole ring system was also found to be important for the P-loop interaction,²⁵ but the structural analysis above suggests that the phenyl-mediated interactions are the driving force for stabilizing the P-loop conformation.

Analysis of the crystal structures revealed that an intramolecular hydrogen bond was formed between the pyrazole-free amine group and the neighboring carbonyl oxygen atom. This

hydrogen bond stabilized the heterocycle and the amide group in a planar conformation, facilitating hinge-binding interaction with Met109 and the gatekeeper Thr106. Bridging of both groups was therefore considered. Compounds **29** and **28** were successfully prepared by the use of a 1-phenyl-1*H*-pyrazolo[3,4-*d*]pyrimidine or 3-phenyl-3*H*-[1,2,3]triazolo[4,5-*d*]pyrimidine building block. ΔT_m and IC_{50} values were determined for both compounds, giving somewhat unexpected results. For compound **29** (IC_{50} (DDR1/2) = 1.04/2.06 μ M), the potency towards DDR1/2 was improved compared with **13**. However, affinity for p38 α remained unaffected, which was probably caused by the phenyl decoration in the hinge region. Interestingly, for **28** binding to p38 α , DDR1 and DDR2 was impaired, and only negligible thermal shift values and potencies in NanoBRET assays were determined. The latter finding was unexpected in so far as only a single carbon atom of the pyrazole was replaced by a nitrogen in the triazolo-decoration. These data suggested that the triazolo[4,5-*d*]pyrimidine in **28** impaired binding due to altered electrostatic complementarity. Compound **28** might therefore be used as a potential negative control compound.

Table 3. Hinge-binder optimization B. Potency of compounds **13** and **27-32** for p38 α and DDR1/2 determined by DSF and NanoBRET assays.

No.	Structure	ΔT_m^a [°C] p38 α	ΔT_m^a [°C] DDR1	ΔT_m^a [°C] DDR2	IC_{50}^b [μ M] p38 α	IC_{50}^b [μ M] DDR1	IC_{50}^b [μ M] DDR2
13		14.1 \pm 0.4	4.6 \pm 0.2	4.8 \pm 0.4	0.033 \pm 0.002 ^d	2.37 \pm 0.28 ^d	3.46 \pm 0.32 ^d
28		0.5 \pm 0.5	0.3 \pm 0.1	0.6 \pm 0.0	5.39 \pm 3.10	21.9 \pm 5.44	15.5 \pm 5.08
29		6.6 \pm 0.3	5.7 \pm 0.7	6.1 \pm 0.7	0.24 \pm 0.02	1.04 \pm 0.17 ^d	2.06 \pm 0.27 ^d

30		11.1 ± 0.5	7.1 ± 0.1	9.1 ± 0.6	0.125 ± 0.011^c	0.023 ± 0.002	0.018 ± 0.002
31		n.d.	7.3 ± 0.3	7.9 ± 0.3	0.284 ± 0.007^c	0.044 ± 0.001^c	0.032 ± 0.005^c
32		9.8 ± 0.3	6.9 ± 0.2	8.7 ± 0.1	1.93 ± 0.05	1.33 ± 0.27	1.16 ± 0.07
33		8.7 ± 0.2	6.1 ± 0.5	6.7 ± 0.5	2.97 ± 0.06	2.27 ± 0.16	7.46 ± 2.38

^a ΔT_m average \pm SD derived from seven replicates for p38 α and three replicates for DDR1/DDR2 at a compound concentration of 10 μ M; ^b Cellular IC_{50} values \pm SEM determined by NanoBRET assay in HEK293T cells, IC_{50} values were derived from triplicates (n = 3); ^c n = 2; ^d n = 4.

In compounds **30** and **31**, the hinge-binding heterocycle was replaced by a bicyclic imidazo[1,2-*a*]pyridine decoration, reminiscent of compound **3** for targeting DDR1/2 kinase. Gratifyingly, the measured IC_{50} values of **30** and **31** for DDR1/2 kinases were significantly lower than IC_{50} values of earlier compounds. For **30**, IC_{50} values of 23 nM and 18 nM were determined for DDR1 and DDR2, respectively. For compound **31**, harboring a methyl-stabilized benzyl linker, potencies were only slightly reduced. However, activity for p38 α kinase remained for both inhibitors, **30** and **31**, with potencies 5-6 times higher for p38 α than for DDR1.

To understand the differences in inhibitor binding in p38 α and DDR1 kinase, a crystal structure in complex with **30** was determined for both targets (Figure 4).

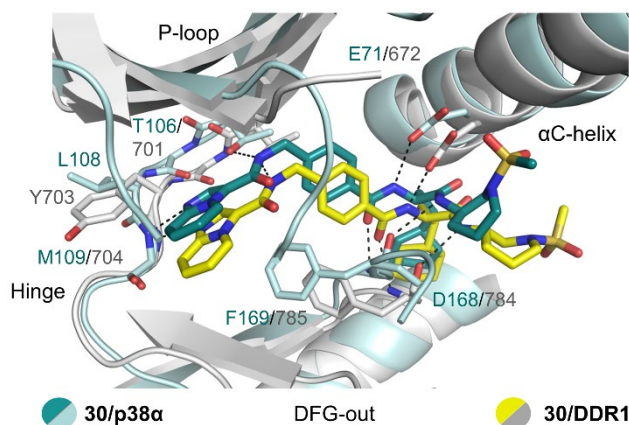


Figure 4. Binding mode of dual DDR/p38 inhibitor 30. Crystal structure of DDR1 kinase in complex with **30** (yellow inhibitor, PDB: 7BCM) showing an extended P-loop. In contrast, in the p38 α kinase complex with **30** (teal, PDB: 7BDO), the P-loop adopts a folded conformation (teal, PDB: 7BDO) where the ligand interacts with the P-loop (light blue). In both cases, the tip of the P-loop was partly disordered, though. Hydrogen bonds are highlighted as black dashed lines; important structural motifs are labeled.

Overall, **30** adopted a similar binding mode in both kinases, targeting an inactive DFG-out state, with the cyclohexyl decoration interacting with the allosteric deep pocket, which is slightly smaller in DDR1 kinase. The sulfonamide moiety pointed toward the solvent. In both structures, a similar hydrogen network was seen with engaging the Glu-Asp salt bridge of the DFG-motif and the conserved glutamate in α C, and an additional hydrogen bond formed with the DFG aspartate and the terminal amide. However, differences were observed in interactions with the hinge region and the P-loop. While in p38 α , Met109 is preceded by a leucine (Leu108), an aromatic tyrosine residue (Tyr703) is found in DDR1 at this position. The side chain of Tyr703 pointed towards the ATP-binding pocket and interacted with the imidazo[1,2-*a*]pyridine hinge-binding decoration. The flat geometry of this hinge binder was probably the main driver for the improved potency of **30** for DDR1/2 kinase. In the DDR1-**13** complex (Figure 2A), an orthogonal orientation of aminopyrazole and its phenyl decoration was found, negatively influencing aromatic interactions with Tyr703. In addition to the potency toward DDR1/2 kinase, **30** also showed potent binding of p38 α / β . The reason for this can also be explained

based on the crystal structure, which showed that **30** traps the P-loop of p38 α in a conformation that forms a lid over the inhibitor binding site, reminiscent of the folded P-loop seen with **13**. However not all residues in the P-loop region were fully resolved in the crystal structure, and π -stacking interaction with Tyr35 and Phe169 from the DFG-motif were not visible in this structure, indicating that the P-loop retained a certain degree of flexibility. As discussed above, **13** showed a very low IC_{50} value of 22.5 nM for p38 α , probably mainly due to favorable interactions with the P-loop, which was fully resolved in the crystal structure (Figure 2A). As the hinge decoration of **30** lacked the phenyl-extended hinge-binding head group, interactions with the P-loop Tyr35 were less pronounced, which could explain the 4.8-fold reduced potency for p38 α .

Selectivity profiling

The most interesting and potent compounds were selected to study their kinome-wide selectivity. Therefore, **28**, **29**, and **30** were each profiled against 468 kinases and clinically relevant kinase mutants in total (Figure 5, Supplement Table S6). All compounds showed very clean selectivity profiles, as expected based on earlier studies on structurally related compounds.

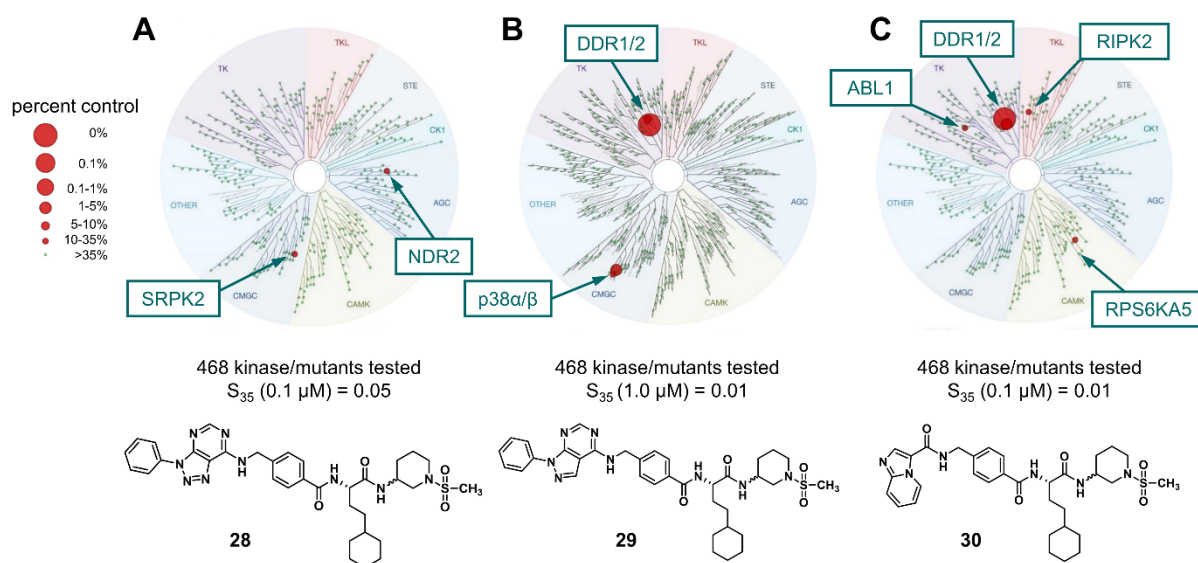


Figure 5. Selectivity profiling against 468 kinases and kinase mutants. A) **28** screened at 0.1 μM ; B) **29** screened at 1.0 μM ; C) **30** screened at 0.1 μM ; selectivity score S_{35} is given for compound comparison; mutants not shown; selectivity screen was performed by Eurofins scanMAX technology.

Compound **29** which contained a bridged pyridazo[3,4-*d*]pyrimidine structure was screened at a concentration of 1 μM (Figure 5B) and a remarkably clean selectivity profile was obtained. From the 468 kinases and mutations screened with **29**, only DDR1/2 and p38 α / β kinases were inhibited by more than 50% (selectivity score of S_{35} (1 μM) = 0.01). To understand the reason for this kinome-wide selectivity, a crystal structure in complex with p38 α was determined (Figure 6).

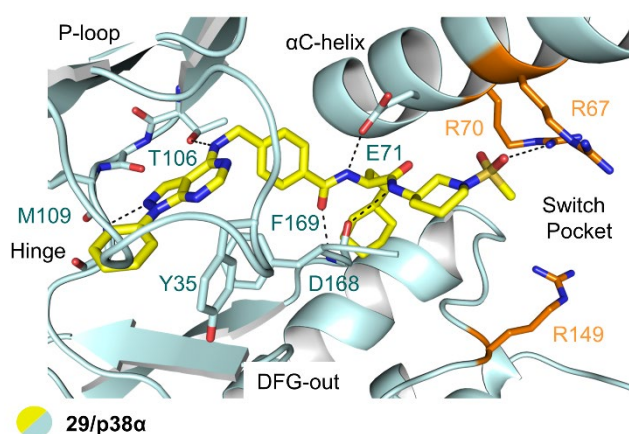


Figure 6. Selectivity by targeting the switch-pocket residues in p38 α . Compound **29** (teal, PDB: 7BDQ) in complex with p38 α MAPK. Important structural elements are highlighted, including the switch-pocket residues Arg70, Arg67 and Arg149 (shown in orange). The structure reveals a folded P-loop conformation stabilized by inhibitor binding. Hydrogen bonds between inhibitor and the kinase are highlighted by black broken lines.

In this crystal structure, **29** bound as expected as a typical type-II inhibitor occupying the DFG-out deep pocket and made contacts with the backbone amide of Met109 in the hinge region via its pyrazole nitrogen atom. Besides this canonical binding mode, **29** engaged the P-loop in a

folded conformation that acted as a lid over the hinge-binding moiety, which improved inhibitor selectivity as seen for other inhibitors crystallized in this study. However, none of those inhibitors matched the excellent kinome-wide selectivity of **29**. The reason for this selectivity might be due to an unexpected hydrogen bond formed between Arg70 from the α C helix and one of the sulfonamide *O*-atoms, which was not seen in the p38 complexes with **13**, **32**, and **30**. Like Arg67 (α C helix) and Arg149 (HRD segment), Arg70 belongs to the so-called switch pocket residues. Targeting those amino acids was previously studied by Deciphera Pharmaceuticals, who developed highly selective p38 α/β inhibitors.²⁶ Since Arg70 is a non-conserved amino acid found exclusively in p38 α/β , the superior kinome-wide selectivity of **29** may be primarily caused by the additional interaction with the basic arginine side chain. However, the binding mode of **29** was unique as it represented the first switch-pocket inhibitor simultaneously making contacts with the hinge region. Another unique feature was that it trapped the P-loop in an unusual distorted conformation.

The most potent compound of our SAR series, **30**, was screened against the kinome at a concentration of 0.1 μ M to obtain insights into its selectivity (Figure 5C). In addition to DDR1/2, which were bound the strongest, three other kinases were detected with residual activity of <35% of the uninhibited control at this concentration: ABL1, RIPK2, and RPS6KA5. The cellular activity of these targets and p38 α/β was studied by NanoBRET and revealed potent inhibitory potencies of **30** on DDR1/2 (IC_{50} = 23/18 nM) and p38 α/β (IC_{50} = 125/196 nM) kinases. A significantly lower cellular activity was found for the additional targets, with IC_{50} values >25 μ M, making **30** a very valuable tool compound (Supplement Figure S1, Table S3, Table S4).

Table 4. Selectivity profiling and target activity of **30**.

Kinome targets	% Activity compared with uninhibited control at 0.1 μ M	NanoBRET IC_{50} [μ M] ^a
DDR2	0	0.018 \pm 0.002
DDR1	0.1	0.023 \pm 0.002
ABL1-nonphosphorylated	14	> 25 μ M
RIPK2	30	> 25 μ M
RPS6KA5(Kin.Dom.2-C-terminal)	35	> 25 μ M
p38-beta	36	0.196 \pm 0.008
p38-alpha	77	0.125 \pm 0.011

^a IC_{50} values \pm SEM were derived from triplicates (n = 3).

Compound **28**, which had no significant inhibitory activity on p38 α and DDR1/2 in the DSF screen, was screened at a concentration of 0.1 μ M (Figure 5A). Interestingly, **28** also showed a very clean selectivity profile in the kinome scan assay. With a cut-off value of >35% activity of the control in the assay, only two kinases, SRPK2 and NDR2, were detected (S_{35} (0.1 μ M) = 0.005). Compared with the potent inhibitor **30**, compound **28** showed a more than 850-fold reduced potency for DDR1/2 kinases (IC_{50} = 21.9/15.5 μ M), a 43/8-fold decreased IC_{50} value for p38 α/β (IC_{50} = 5.4/1.6 μ M), and no additional off-targets. It, therefore, represents a valuable negative control of this compound series for cell-based assays.

In compounds **31** and **33**, a methyl group was introduced in the benzylic position to strengthen the interaction with the hydrophobic pocket behind the gatekeeper (Thr701) and to stabilize the compounds metabolically. This methyl group is part of many previously published DDR1/2 kinase inhibitors, such as DDR-TRK-1, DDR1-IN-1, as well as **3**, and it is believed to be responsible for the off-target inhibition of TRKs.²⁷ Since none of the previously synthesized compounds based on the VPC-00628 scaffold showed any binding of TRKs in Eurofins

scanMAX, it was of interest whether a methyl group at this position in the molecule also leads to the aforementioned interaction. Compound **31** was therefore investigated for its kinome-wide selectivity at a concentration of 0.1 μ M (Supplement Table S6). Interestingly, screening of **31** revealed a clean profile, and high-affinity targets such as DDR1/2, p38 α , and MELK were detected at a cut-off value of >35% activity of the control. The anticipated inhibition of TRKA, TRKB, and TRKC based on the scaffold **31** was, however, not confirmed, and 100% activity of the control was retained in the Eurofins scanMAX kinase assay panel. For compound **33**, which was studied at the same concentration, a similar clean selectivity profile, without inhibition of TRKs, was observed (Supplement Table S6). It can therefore be assumed that the methyl group is not the only reason for the inhibition of TRKs, as discussed by Zhu et al.²⁷, but that this activity is rather dependent on the hinge-binding scaffold of the inhibitor used.

Cytotoxicity, TNF- α release and drug-like properties

We investigated the dose- and time-dependent effects of the compounds **28**, **30**, **38**, and **39** on cell viability in three different cell types, human embryonic kidney cells (HEK293T), osteosarcoma cells (U2OS), and non-transformed human lung fibroblasts (MRC-9) (Figure 7 and Supplemental Figures S2-S4). Collagen-activated DDR1/2 cell signaling is mediated by mitogen-activated protein kinases, such as ERK1/2, JNK, and p38 α / β .²⁸ To exclude p38 off-target cytotoxicity, our previously published p38 α / β selective chemical probe **38** (SR-318) and its control **39** (SR-321) were included in this assay.²⁵ The cells were treated with fluorescent dyes to detect apoptosis (Alexa Fluor 680 conjugate), nuclei/DNA (Hoechst33342), mitochondria (Mitotracker red), and microtubule (BioTracker™ 488 Green Microtubule Cytoskeleton Dye) effects. Fluorescence and cellular shape were measured before compound treatment and 12 h, 24 h, and 48 h after compound exposure, respectively, using the CQ1 high-content confocal microscope (Yokogawa). Staurosporine at a concentration of 10 μ M was used as a reference compound.

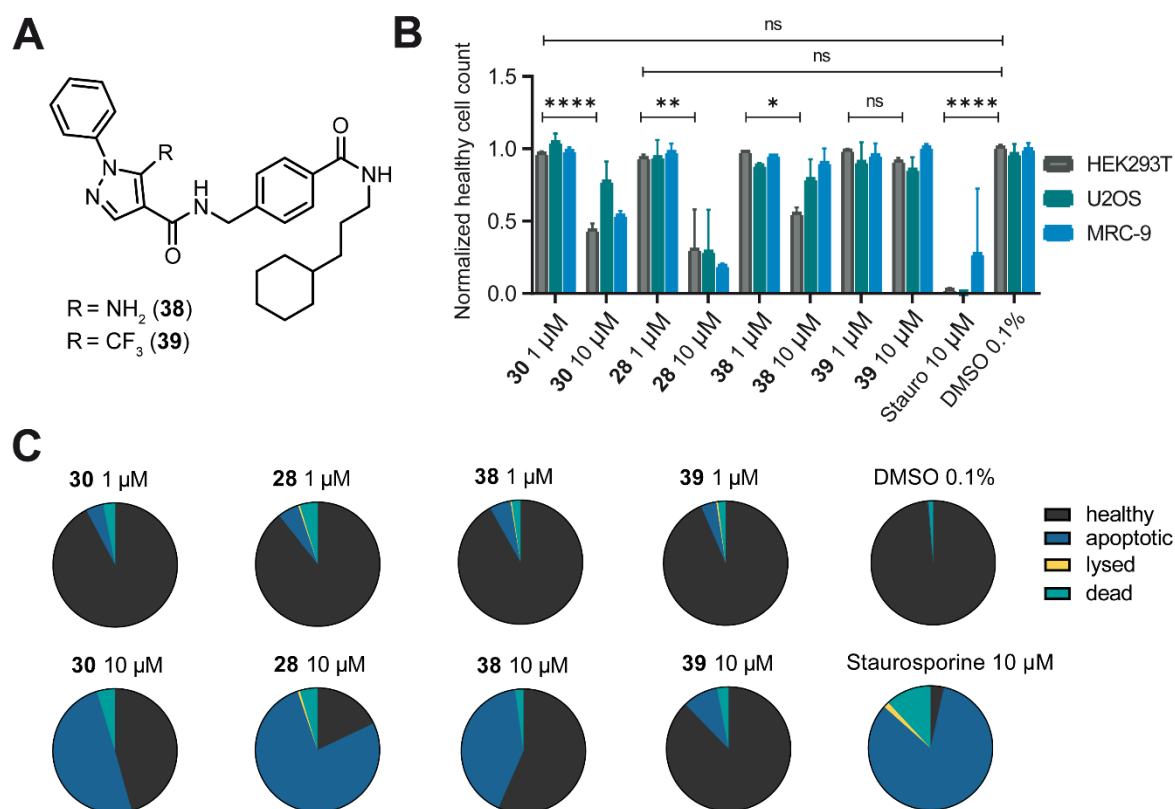


Figure 7. Live cell high-content screen of HEK293T, U2OS and MRC-9 cells. A) Structure of recently published p38 probe **38** (SR-318) and control **39** (SR-321). B) Healthy cell count after 24 h of 1 μM and 10 μM compound exposure (**30**, **28**, **38**, **39**, staurosporine) normalized against healthy cells exposed to DMSO 0.1% in HEK293T, U2OS and MRC-9 cells. Error bars show SEM of three technical duplicates. The significance was calculated using a two-way ANOVA analysis. C) Fraction of healthy, apoptotic, lysed and dead HEK293T cells after 24 h exposure to 1 and 10 μM of compound (**30**, **28**, **38**, **39**, and staurosporine) compared with a 0.1% DMSO control. Additional cytotoxicity data with all three cells lines are shown in Supplemental Figures S2, S3, and S4.

After 24 h, the DDR/p38α/β probe compound, **30**, and the corresponding negative control (**28**) showed no significant cytotoxicity at a compound concentration of 1 μM. At 10 μM, however, there was a pronounced cytotoxic effect and a drastic increase in the percentage of apoptotic cells in all three cell lines for those two inhibitors compared with the DMSO-treated controls (Figure 7C and Supplemental Figure S4). Interestingly, **28** was more toxic than **30** at 10 μM, which was also reflected in a higher proportion of apoptotic cells. For the p38 α/β probe **38**

(SR-318) and its control **39** (SR-321), there was also no notable cytotoxicity detected after 24 h in all three cell lines at an inhibitor concentration of 1 μ M. No major effect on microtubule function was observed after treatment with any of the compounds from the two probe sets, and none of the compounds resulted in increased levels of cell lysis at a concentration of 1 μ M (Supplemental Figures S3 and S4). Thus, the developed probe, **30**, and its corresponding negative control, **28**, represent a versatile toolset to study DDR1/2 function in normal or disease physiology.

In our NanoBRET target engagement studies we showed that **30** also inhibited p38 α/β with a 5-/8-fold lower potency compared with DDR1/2. Recent studies indicated that the collagen-activated DDR receptor may upregulate the expression and release of cytokines in macrophages.²⁹ This process is dependent on NF- κ B signaling and has been suggested to be mediated by the p38 MAPK pathway. To assess the phenotypic effect of our dual DDR/p38 probe, **30**, we measured the TNF- α release in whole blood. Besides **30**, the negative control **28** as well as our recently published p38 selective probe set (**38**, **39**) and the p38 inhibitor SB203580 were studied in this assay. Both p38 inhibitors, **38** and SB203580, potently inhibited the TNF- α release with IC_{50} values of 0.17 μ M and 1.82 μ M, while no inhibition was seen for **30** and the control **39** (Supplemental Figure S5). Based on these results, we concluded that the phenotypic effect of **30** on the p38 α/β MAPK pathway is less pronounced.

We next tested the metabolic stability of compounds **13**, **29**, and **30** using human liver microsomes over a time interval of 240 min (Figure 8). We observed that **29** was metabolized slightly faster than **13** and **30**, and a slightly higher proportion of metabolites was thus detected. After a reaction time of 240 min, only $44.0 \pm 4.0\%$ of the compound remained for **13**, $43.6 \pm 4.5\%$ for **30** and $28.4 \pm 0.8\%$ for **29**. In summary, all derivatives modified for targeting DDR1/2 showed modest metabolic stability.

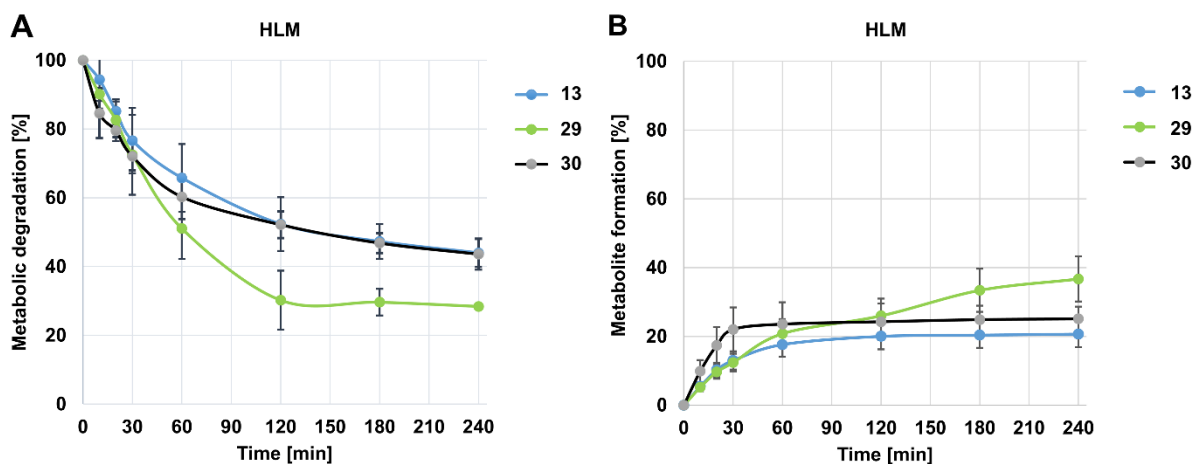


Figure 8. Metabolic stability of compounds 13, 29 and 30 in human liver microsomes (HLM). A) Metabolic degradation over 240 min. B) Metabolite formation over 240 min. Experiments were performed in triplicates. The values represent the mean with standard deviation.

To more comprehensively assess drug-like properties of **30**, ADME properties were predicted using the QikProp software (Schrödinger, 2020, Supplemental Table S9). Overall, **30** fulfilled all criteria limits for drug-like compounds, such as having a good predicted cell permeability in Caco-2 and MDCK cells, which was supported by our nanoBRET assay data. In addition, compound **30** had a good predicted oral absorption of 60% and may therefore show reasonable bioavailability *in vivo*.

CONCLUSION

A comprehensive set of 127 previously published p38 inhibitors was evaluated by DSF against p38 and the main off-targets of VPC-0062825 derived lead compound, **7**, which lead to the identification of suitable chemical starting points for the development of selective DDR1/2 inhibitors. A series of potent DDR1/2 kinase inhibitors were synthesized by targeting the hinge-binding moiety and the back-pocket decorations present in the lead structure **7**. Characterization of these compounds and the determination of crystal structures of selected inhibitor complexes highlighted the importance of the P-loop conformation for potent interaction with p38,

including a rarely seen π -stacking interaction with the inhibitor. Furthermore, we demonstrated the possibility of targeting the non-conserved switch-pocket residue Arg70 in p38 α with a type-II inhibitor to achieve p38 selectivity. Our SAR optimization resulted in a very potent DDR inhibitor, **30** (SR-302), with IC_{50} values of 0.023 and 0.018 μ M for DDR1/2 and more than 5 times lower cellular IC_{50} values for p38 α/β (IC_{50} = 0.125/0.196 μ M). Compound **30** displayed an excellent kinome-wide selectivity, as demonstrated in a screen against 468 kinases and mutants at a concentration of 1 μ M (S-score (35) = 0.01). In addition, we synthesized an appropriate negative control compound, **28** (SR-301), based on the same scaffold, for the use of our compound series in cell-based assays. Taken together, our data suggest that the DDR/p38 probe set is a valuable tool for in-depth mechanistic studies of DDR1/2 signaling under physiological and pathophysiological conditions.

EXPERIMENTAL SECTION

Chemistry. All reagents and water-free solvents were purchased from commercial suppliers and were used, if not otherwise stated, without further purification, or solvents were dried using standard procedures. Column chromatography on silica was performed on silica 60, 0.04-0.63 mm from Machery-Nagel GmbH & Co.KG. Fully characterized compounds were chromatographically homogeneous. Analytical thin-layer chromatography was carried out using aluminum-backed plates coated with Merck TLC Silicagel 60 F254. Plates were visualized under UV light (at λ 254 and/or 360 nm) and/or with ninhydrin solution. ^1H -NMR and ^{13}C -NMR spectra were recorded either on a Bruker Avance 250, 300, 400, 500 or a Bruker DRX 600 using TMS as internal standard. The chemical shifts (δ) are reported in ppm and are calibrated against the residual proton peak of the deuterated solvent. J values were recorded in Hz, and multiplicities were expressed using the usual conventions. Mass spectrometry (ESI) was measured on a VG Plattform II spectrometer from Fisons. High-resolution mass

spectrometry (FTMS +p MALDI-HRMS) was performed using a MALDI LTQ XL Orbitrap spectrometer from Thermo Scientific. Determination of the compound purity by HPLC was carried out on an Agilent 1260 Infinity II device with a 1260 DAD HS detector (G7117C; 254 nm, 280 nm) and a LC/MSD device (G6125B, ESI pos. 100-1000). The compounds were analyzed on a Poroshell 120 EC-C18 (Agilent, 3 x 150 mm, 2.7 μ m) reversed phase column using 0.1% formic acid in water (A) and 0.1% formic acid in acetonitrile (B) as a mobile phase. The following gradient was used: 0 min. 5% B - 2 min. 5% B - 8 min. 98% B (flow rate of 0.5 mL/min.). UV-detection was performed at 254 and 280 nm and all compounds used for further biological characterizations showed > 95% purity, if not otherwise stated. For compound **28**, purity was determined by a HPLC instrument LC-20A Prominence from Shimadzu. Separations were performed on a C18 column (Luna 10 μ C18 (2) 100 Å; 250 x 4.6 mm) from Phenomenex using the following gradient profile: 0 - 2 min 95% B, 2 - 14 min 95% B, 14 - 21 min 10% B, 21 min 95% B. As solvent A) acetonitrile Ultra MS-Grade was used and as solvent B) MS-Grade H₂O with 0.1% formic acid at a flow rate of 1 mL/min. The detection was carried out with an LCMS-2020 mass spectrometric detector from Shimadzu at a wavelength of 254 and 280 nm respectively.

General procedure A for Fmoc-cleavage and the preparation of amines 11a-11g. Amines **11a-11g** used in the amide coupling reaction for general procedure B were freshly prepared directly before coupling to the acid. The corresponding Fmoc protected amine (**10a-10g**, 1.2 eq) was dissolved in DMF (12 mL), and piperidine (20%) was added. The mixture was stirred for 1 h at RT, and CH₂Cl₂ (30 mL) or EtOAc (30 mL) was added. The organic phase was washed 5 times with water (30 mL) and dried over MgSO₄. The solvent was evaporated under reduced pressure, and the crude product (quantitative) was used without further purification.

General procedure B for amide coupling reaction using HATU for the preparation of final compounds 12-15, 20-24, and 30-33. The corresponding carboxylic acid (1 eq) and HATU (1.2 eq) were dissolved in DMF (8 mL) and DIPEA (1.5 eq) was added. The solution was stirred at RT for 1.5 h, and a solution of the corresponding amine (**11a-11g**, 1.2 eq) in DMF (8 mL) with DIPEA (1.5 eq) was added. The mixture was stirred for 20 h at RT. CH₂Cl₂ or EtOAc (50 mL) was added, and the organic phase was washed 4 times with water (50 mL) and dried over MgSO₄. The solvent was evaporated under reduced pressure, and the crude product was purified by column chromatography on silica (eluent: cyclohexane/EtOAc, CH₂Cl₂/MeOH, or EtOAc/MeOH) if not stated otherwise.

(S)-5-Amino-N-(4-((4-cyclohexyl-1-(ethylamino)-1-oxobutan-2-yl)carbamoyl)benzyl)-1-phenyl-1H-pyrazole-4-carboxamide (7), 4-((5-Amino-1-phenyl-1H-pyrazole-4-carboxamido)methyl)benzoic acid (8) and (9H-Fluoren-9-yl)methyl (S)-(4-cyclohexyl-1-(ethylamino)-1-oxobutan-2-yl)carbamate (10a) were prepared as previously published.²⁴

(9H-Fluoren-9-yl)methyl (S)-(4-cyclohexyl-1-oxo-1-(propylamino)butan-2-yl)carbamate (10b)

(S)-2-((((9H-Fluoren-9-yl)methoxy)carbonyl)amino)-4-cyclohexylbutanoic acid (**9**, 400 mg, 0.98 mmol) and HATU (448 mg, 1.18 mmol) were dissolved in DMF (dry, 10 mL) and DIPEA (152 mg, 1.18 mmol) was added. The reaction mixture was stirred for 2 h at RT and propan-1-amine (97 µL, 1.18 mmol) was added. The mixture was stirred for additional 20 h at RT. DCM (50 mL) was added, and the organic phase was washed 5 times with H₂O (20 mL) and dried over MgSO₄. The solvent was evaporated under reduced pressure, and the crude product was purified by column chromatography on silica (cyclohexane/EtOAc 1:1). Compound **10b** was obtained in a yield of 248 mg (0.55 mmol, 56%) as a colorless solid. TLC: R_f = 0.15 (SiO₂, cyclohexane/EtOAc, 1:1). ¹H-NMR (500 MHz, CDCl₃, 300 K): δ = 7.76 (d, ³J = 7.5 Hz, 2H),

7.57 (d, $^3J = 7.5$ Hz, 2H), 7.39 (t, $^3J = 7.4$ Hz, 2H), 7.30 (t, $^3J = 7.4$ Hz, 2H), 6.13 (s, 1H), 5.48 (d, $^3J = 7.9$ Hz, 1H), 4.48–4.28 (m, 2H), 4.20 (t, $^3J = 7.0$ Hz, 1H), 4.12–4.02 (m, 1H), 3.30–3.11 (m, 2H), 1.91–1.76 (m, 1H), 1.73–1.58 (m, 6H), 1.56–1.43 (m, 2H), 1.36–1.06 (m, 6H), 0.94–0.79 (m, 5H) ppm. ^{13}C -NMR (126 MHz, CDCl_3 , 300 K): $\delta = 171.8, 156.3, 143.9, 141.4, 127.9, 127.2, 125.2, 120.1, 67.1, 55.5, 47.2, 41.3, 37.6, 33.4, 33.3, 33.1, 30.4, 26.7, 26.4, 22.9, 11.4$ ppm. MS (ESI pos.): m/z (%) = 897.62 (84) ($[\text{2M}+\text{H}]^+$, calcd. 897.54), 449.24 (92) ($[\text{M}+\text{H}]^+$, calcd. 449.27), 227.18 (100) ($[\text{M-Fmoc}+\text{H}]^+$, calcd. 227.20).

(9H-Fluoren-9-yl)methyl ((S)-4-cyclohexyl-1-(((SR)-1-(cyclopropanecarbonyl)piperidin-3-yl)amino)-1-oxobutan-2-yl)carbamate (10c)

(S)-2-((((9H-Fluoren-9-yl)methoxy)carbonyl)amino)-4-cyclohexylbutanoic acid (**9**, 500 mg, 1.23 mmol) and HATU (560 mg, 1.47 mmol) were dissolved in DMF (dry, 10 mL), and DIPEA (190 mg, 1.47 mmol) was added. The reaction mixture was stirred for 1.5 h at RT, and *rac*-(3-aminopiperidin-1-yl)(cyclopropyl)methanone (**37d**, 248 mg, 1.47 mmol) dissolved in DMF (dry, 5 mL) was added. The mixture was stirred for additional 20 h at RT. EtOAc (100 mL) was added, and the organic phase was washed 4 times with H_2O (50 mL) and dried over MgSO_4 . The solvent was evaporated under reduced pressure, and the crude product was purified using column chromatography on silica (cyclohexane/EtOAc 1:3 \rightarrow 1:9). Compound **10c** was obtained in a yield of 553 mg (0.992 mmol, 81%), as a colorless solid. TLC: $R_f = 0.37$ (SiO_2 , cyclohexane/EtOAc, 1:3). ^1H -NMR (400 MHz, DMSO-d_6 , 300 K): (mixture of diastereomeres) $\delta = 7.96\text{--}7.80$ (m, 3H), 7.77–7.68 (m, 2H), 7.46–7.37 (m, 3H), 7.32 (t, $^3J = 7.4$ Hz, 2H), 4.33–4.13 (m, 3H), 4.09–3.78 (m, 2H), 3.76–3.47 (m, 2H), 3.39–3.05 (m, 2H), 2.00–1.29 (m, 12H), 1.27–1.03 (m, 6H), 0.91–0.77 (m, 2H), 0.76–0.53 (m, 4H) ppm. ^{13}C -NMR (101 MHz, DMSO-d_6 , 300 K): (mixture of diastereomeres) $\delta = 171.0, 170.9, 152.0$ (2x), 143.9, 143.8, 140.7 (2x), 138.6, 127.6, 127.0, 125.3, 120.1 (2x), 65.5, 46.6, 36.8, 33.0, 32.9, 32.7, 32.6, 26.1, 25.8 (2x), 10.4, 6.8 ppm. MS (ESI pos.): m/z (%) = 580.43 (100) ($[\text{M}+\text{Na}]^+$, calcd. 580.32).

(9H-Fluoren-9-yl)methyl ((S)-4-cyclohexyl-1-(((SR)-1-(methylsulfonyl)piperidin-3-yl)amino)-1-oxobutan-2-yl)carbamate (10d)

(S)-2-((((9H-Fluoren-9-yl)methoxy)carbonyl)amino)-4-cyclohexylbutanoic acid (**9**, 500 mg, 1.23 mmol) and HATU (560 mg, 1.47 mmol) were dissolved in DMF (dry, 10 mL) and DIPEA (190 mg, 1.47 mmol) was added. The reaction mixture was stirred for 1.5 h at RT, and *rac*-1-(methylsulfonyl)piperidin-3-amine (**37a**, 262 mg, 1.47 mmol) dissolved in DMF (dry, 5 mL) was added. The mixture was stirred for additional 20 h at RT. H₂O (50 mL) was added, and the resulting precipitate was filtered off, washed with H₂O and dried in a vacuum oven to afford 655 mg (1.15 mmol, 94%) of compound **10d** as a colorless solid. TLC: R_f = 0.44 (SiO₂, cyclohexane/EtOAc, 1:3). ¹H-NMR (500 MHz, DMSO-d₆, 300 K): (mixture of diastereomers) δ = 7.94 (d, ³J = 7.4 Hz, 1H), 7.89 (d, ³J = 7.5 Hz, 2H), 7.76–7.70 (m, 2H), 7.46 (dd, ³J = 8.3, 3.0 Hz, 1H), 7.42 (t, ³J = 7.5 Hz, 2H), 7.32 (td, ³J = 7.5, 3.4 Hz, 2H), 4.31–4.17 (m, 3H), 3.99–3.90 (m, 1H), 3.75–3.67 (m, 1H), 3.51–3.39 (m, 1H), 3.37–3.27 (m, 1H), 2.87–2.82 (m, 3H), 2.81–2.73 (m, 1H), 2.56–2.49 (m, 1H), 1.83–1.69 (m, 2H), 1.68–1.45 (m, 8H), 1.42–1.27 (m, 1H), 1.26–1.05 (m, 6H), 0.90–0.77 (m, 2H) ppm. ¹³C-NMR (126 MHz, DMSO-d₆, 300 K): (mixture of diastereomers) δ = 170.7 (2x), 155.9 (2x), 143.9, 143.8, 140.7 (2x), 127.6, 127.0, 125.4, 120.1, 65.6, 54.8, 54.7, 49.6, 49.4, 46.7, 45.4, 45.1, 45.0, 36.8 (2x), 34.6, 34.2, 33.1, 32.9 (2x), 32.7, 32.6, 29.7, 28.9, 28.6, 26.2, 25.8 (2x), 23.0, 22.9 ppm. MS (ESI pos.): *m/z* (%) = 586.32 (100) ([M+H]⁺, calcd. 586.29), 346.21 (62) ([M-Fmoc+H]⁺, calcd. 346.22).

(9H-Fluoren-9-yl)methyl ((S)-4-cyclohexyl-1-(((SR)-1-(oxetan-3-yl)piperidin-3-yl)amino)-1-oxobutan-2-yl)carbamate (10e)

(S)-2-((((9H-Fluoren-9-yl)methoxy)carbonyl)amino)-4-cyclohexylbutanoic acid (**9**, 463 mg, 1.14 mmol) and HATU (432 mg, 1.36 mmol) were dissolved in DMF (dry, 4 mL) and DIPEA (147 mg, 1.36 mmol) was added. The reaction mixture was stirred for 1.5 h at RT, and *rac*-1-(oxetan-3-yl)piperidin-3-amine (**37e**, 213 mg, 1.36 mmol) dissolved in DMF (dry, 4 mL) was

added. The mixture was stirred for additional 4 h at RT. DCM (50 mL) was added, and the organic phase was washed 4 times with H₂O (50 mL) and dried over MgSO₄. The solvent was evaporated under reduced pressure, and the crude product was purified by column chromatography on silica (cyclohexane/EtOAc 1:1 → 1:20 → EtOAc). Compound **10e** was obtained in a yield of 595 mg (1.09 mmol, 96%), as a colorless solid. TLC: R_f = 0.20 (SiO₂, cyclohexane/EtOAc, 1:20). ¹H-NMR (500 MHz, DMSO-d₆, 300 K): (mixture of diastereomers) δ = 7.89 (d, ³J = 7.6 Hz, 2H), 7.78–7.69 (m, 3H), 7.47–7.38 (m, 3H), 7.31 (t, ³J = 7.4 Hz, 2H), 4.52–4.43 (m, 2H), 4.41–4.31 (m, 2H), 4.30–4.17 (m, 3H), 3.96–3.87 (m, 1H), 3.76–3.66 (m, 1H), 3.40–3.28 (m, 3H), 2.55–2.32 (m, 2H), 1.92–1.39 (m, 11H), 1.31–1.04 (m, 6H), 0.91–0.76 (m, 2H) ppm. ¹³C-NMR (126 MHz, DMSO-d₆, 300 K): (mixture of diastereomers) δ = 171.3, 171.2, 155.9 (2x), 143.9, 143.8, 140.7, 127.6, 127.0, 125.3 (2x), 120.1, 74.6 (3x), 74.5, 65.6 (2x), 58.4 (2x), 54.8, 54.4, 54.3, 49.2, 46.7, 45.1, 38.3, 36.8, 36.7, 33.0, 32.9, 32.7 (2x), 29.7, 29.6, 29.5, 26.2, 25.8, 22.9 ppm. MS (ESI pos.): *m/z* (%) = 546.31 (100) ([M+H]⁺, calcd. 546.34).

(9*H*-Fluoren-9-yl)methyl ((*S*)-4-cyclohexyl-1-(((*S*)-1-(methylsulfonyl)piperidin-3-yl)amino)-1-oxobutan-2-yl)carbamate (10f**)**

The synthesis of (9*H*-fluoren-9-yl)methyl ((*S*)-4-cyclohexyl-1-(((*R*)-1-(methylsulfonyl)piperidin-3-yl)amino)-1-oxobutan-2-yl)carbamate (**10f**) was performed analogously to compound **10d**. (*S*)-1-(Methylsulfonyl)piperidin-3-amine (**37b**, 262 mg, 1.47 mmol) was used as starting material to afford 663 mg (1.17 mmol, 95%) of compound **10f** as a colorless solid. TLC: R_f = 0.76 (SiO₂, EtOAc/MeOH, 9:1). ¹H-NMR (500 MHz, DMSO-d₆, 300 K): δ = 7.91–7.78 (m, 4H), 7.76–7.70 (m, 2H), 7.46–7.59 (m, 1H), 7.41 (td, ³J = 7.4, 1.2 Hz, 2H), 7.34 (td, ³J = 7.4, 1.2 Hz, 2H), 6.66 (d, ³J = 8.5 Hz, 1H), 4.32–4.18 (m, 3H), 3.92–3.84 (m, 1H), 3.78–3.66 (m, 1H), 3.56–3.22 (m, 2H), 2.84 (s, 3H), 2.85–2.74 (m, 1H), 2.67–2.49 (m, 1H), 1.86–1.31 (m, 11H), 1.28–1.04 (m, 6H), 0.90–0.74 (m, 2H) ppm. ¹³C-NMR (126 MHz,

DMSO- d_6 , 300 K): δ = 174.6, 172.1, 156.8 (2x), 143.9, 143.8, 140.7 (2x), 128.9, 127.7, 127.3, 123.9, 121.4, 120.0, 61.8, 54.6, 54.5, 49.5, 49.4, 45.4 (2x), 45.0, 44.6, 37.0, 36.8, 34.3, 34.2, 32.9 (2x), 32.8, 32.7, 32.6, 32.4, 29.8, 28.9, 28.7, 26.2 (2x), 25.7, 22.9, 22.7 ppm. MS (ESI pos.): m/z (%) = 590.34 (100) ($[M+Na]^+$, calcd. 590.27).

(9H-Fluoren-9-yl)methyl ((S)-4-cyclohexyl-1-(((R)-1-(methylsulfonyl)piperidin-3-yl)amino)-1-oxobutan-2-yl)carbamate (10g)

The synthesis of (9H-Fluoren-9-yl)methyl ((S)-4-cyclohexyl-1-(((S)-1-(methylsulfonyl)piperidin-3-yl)amino)-1-oxobutan-2-yl)carbamate (**10g**) was performed analogously to compound **10d**. (R)-1-(Methylsulfonyl)piperidin-3-amine (**37c**, 262 mg, 1.47 mmol) was used as starting material to afford 655 mg (1.15 mmol, 94%) of compound **10g** as a light brownish solid. TLC: R_f = 0.76 (SiO₂, EtOAc/MeOH, 9:1). ¹H-NMR (500 MHz, DMSO- d_6 , 300 K): δ = 7.92–7.73 (m, 4H), 7.46–7.59 (m, 1H, NHCOO), 7.42–7.31 (m, 4H), 6.65 (d, ³J = 8.5 Hz, 1H), 4.33–4.22 (m, 3H), 3.89–3.82 (m, 1H), 3.78–3.66 (m, 1H), 3.53–3.25 (m, 2H), 2.85 (s, 3H), 2.89–2.71 (m, 1H), 2.64–2.47 (m, 1H), 1.82–1.69 (m, 2H), 1.68–1.28 (m, 9H), 1.26–1.02 (m, 6H), 0.90–0.74 (m, 2H) ppm. ¹³C-NMR (126 MHz, DMSO- d_6 , 300 K): δ = 174.6, 172.1, 156.8, 143.9, 140.6 140.4, 128.9, 127.7, 127.3, 123.9, 121.4, 120.0, 61.8, 54.7 (2x), 49.6, 49.5, 45.4, 45.3, 45.1, 44.6, 36.9, 36.8, 34.4, 34.3, 32.9 (2x), 32.8, 32.7 (2x), 32.3, 29.8, 28.9, 28.8, 26.1 (2x), 25.8, 23.0, 22.9 ppm. MS (ESI pos.): m/z (%) = 590.34 (100) ($[M+H]^+$, calcd. 590.27), 346.22 (38) ($[M-Fmoc+H]^+$, calcd. 346.22).

(S)-2-Amino-4-cyclohexyl-N-ethylbutanamide (11a) was prepared as previously published.²⁴

(S)-2-Amino-4-cyclohexyl-N-propylbutanamide (11b)

The synthesis of (S)-2-amino-4-cyclohexyl-N-propylbutanamide (**11b**) was performed according to the general procedure for Fmoc deprotection. The starting material was (9H-fluoren-9-yl)methyl((S)-4-cyclohexyl-1-(((SR)-1-(cyclopropanecarbonyl)piperidin-3-

yl)amino)-1-oxobutan-2-yl)carbamate (**10a**, 405 mg, 0.716 mmol). The amine was freshly prepared prior to the synthesis of **11b**.

(S)-2-Amino-4-cyclohexyl-N-((SR)-1-(cyclopropanecarbonyl)piperidin-3-yl)butanamide (11c)

The synthesis of (S)-2-amino-4-cyclohexyl-N-((SR)-1-(cyclopropanecarbonyl)piperidin-3-yl)butanamide (**11c**) was performed according to the general procedure for Fmoc deprotection. The starting material was (9H-fluoren-9-yl)methyl((S)-4-cyclohexyl-1-(((SR)-1-(cyclopropanecarbonyl)piperidin-3-yl)amino)-1-oxobutan-2-yl)carbamate (**10c**, 405 mg, 0.716 mmol). The amine was freshly prepared prior to the synthesis of **11c**.

(S)-2-Amino-4-cyclohexyl-N-((SR)-1-(methylsulfonyl)piperidin-3-yl)butanamide (11d)

The synthesis of (S)-2-amino-4-cyclohexyl-N-((SR)-1-(methylsulfonyl)piperidin-3-yl)butanamide (**11d**) was performed according to the general procedure for Fmoc deprotection. The starting material was (9H-fluoren-9-yl)methyl ((S)-4-cyclohexyl-1-(((SR)-1-(methylsulfonyl)piperidin-3-yl)amino)-1-oxobutan-2-yl)carbamate (**10d**, 405 mg, 0.714 mmol). The amine was freshly prepared prior to the synthesis of **11d**.

(S)-2-Amino-4-cyclohexyl-N-((RS)-1-(oxetan-3-yl)piperidin-3-yl)butanamide (11e)

The synthesis of (S)-2-Amino-4-cyclohexyl-N-((RS)-1-(oxetan-3-yl)piperidin-3-yl)butanamide (**11e**) was performed according to the general procedure for Fmoc deprotections. The starting material was (9H-fluoren-9-yl)methyl ((S)-4-cyclohexyl-1-(((S)-1-(methylsulfonyl)piperidin-3-yl)amino)-1-oxobutan-2-yl)carbamate (**10e**, 453 mg, 0.830 mmol). The amine was freshly prepared prior to the synthesis of **11e**.

(S)-2-Amino-4-cyclohexyl-N-((S)-1-(methylsulfonyl)piperidin-3-yl)butanamide (11f)

The synthesis of (*S*)-2-amino-4-cyclohexyl-*N*-((*S*)-1-(methylsulfonyl)piperidin-3-yl) (**11f**) was performed according to the general procedure for Fmoc deprotection. The starting material was (9*H*-fluoren-9-yl)methyl((*S*)-4-cyclohexyl-1-(((*S*)-1-(methylsulfonyl)piperidin-3-yl)amino)-1-oxobutan-2-yl)carbamate (**10f**, 406 mg, 0.716 mmol). The amine was freshly prepared prior to the synthesis of **11f**.

(*S*)-2-Amino-4-cyclohexyl-*N*-((*R*)-1-(methylsulfonyl)piperidin-3-yl)butanamide (11g**)**

The synthesis of (*S*)-2-amino-4-cyclohexyl-*N*-((*R*)-1-(methylsulfonyl)piperidin-3-yl) (**11g**) was performed according to the general procedure for Fmoc deprotection. The starting material was (9*H*-fluoren-9-yl)methyl ((*S*)-4-cyclohexyl-1-(((*R*)-1-(methylsulfonyl)piperidin-3-yl)amino)-1-oxobutan-2-yl)carbamate (**10g**, 835 mg, 1.47 mmol). The amine was freshly prepared prior to the synthesis of **11g**.

(*S*)-5-Amino-*N*-(4-((4-cyclohexyl-1-oxo-1-(propylamino)butan-2-yl)carbamoyl)benzyl)-1-phenyl-1*H*-pyrazole-4-carboxamide (12**)**

4-((5-Amino-1-phenyl-1*H*-pyrazole-4-carboxamido)methyl)benzoic acid (**12**, 100 mg, 0.30 mmol) and HATU (152 mg, 0.40 mmol) were dissolved in DMF (5 mL), and DIPEA (58 mg, 0.45 mmol) was added. The solution was stirred for 1.5 h at RT and (*S*)-2-amino-4-cyclohexyl-*N*-propylbutanamide (**11b**, 81 mg, 0.36 mmol), diluted in DMF (5 mL) and DIPEA (58 mg, 0.45 mmol), was added. The mixture was stirred for 20 h at RT. DCM (100 mL) was added, and the organic phase was washed 5 times with H₂O (20 mL) and dried over MgSO₄. The solvent was evaporated under reduced pressure, and the crude product was purified using column chromatography on silica (DCM/MeOH 20:1). Compound **12** was obtained in a yield of 121 mg (0.22 mmol, 75%), as a yellowish solid. TLC: *R*_f = 0.17 (SiO₂, DCM/MeOH 20:1). HPLC: *t*_R = 9.31 min, purity: >95%. ¹H-NMR (500 MHz, DMSO-*d*₆, 300 K): δ = 8.55–8.47 (m, 1H), 8.28 (d, ³*J* = 8.1 Hz, 1H), 7.98 (s, 1H), 7.92 (t, ³*J* = 5.7 Hz, 1H), 7.85 (d, ³*J* = 8.3 Hz, 2H),

7.59–7.49 (m, 4H), 7.41–7.31 (m, 3H), 6.38 (br s, 2H), 4.49–4.43 (m, 2H), 4.39–4.32 (m, 1H), 3.10–2.93 (m, 2H), 1.81–1.71 (m, 1H), 1.70–1.55 (m, 6H), 1.40 (sext, $^3J = 7.3$ Hz, 2H), 1.28–1.04 (m, 6H), 0.90–0.77 (m, 5H) ppm. ^{13}C -NMR (126 MHz, DMSO- d_6 , 300 K): $\delta = 171.7$, 166.0, 164.2, 149.2, 143.6, 141.4, 138.4, 138.2, 132.7, 129.4, 127.6, 127.1, 127.0, 126.8 (2x), 123.1, 97.4, 53.6, 41.3, 36.8, 33.3, 32.9, 32.7, 29.4, 26.2, 25.8 (2x), 22.3, 11.4 ppm. MS (ESI pos.): m/z (%) = 545.32 (100) ($[\text{M}+\text{H}]^+$, calcd. 545.33), 486.27 (30) ($[\text{M}_{\text{H}}]^+$, calcd. 486.25). HRMS (FTMS + p MALDI): $m/z = 545.3222$ $[\text{M}+\text{H}]^+$, calcd. for $[\text{C}_{31}\text{H}_{41}\text{N}_6\text{O}_3]^+ = 545.3240$.

5-Amino-*N*-(4-(((*S*)-4-cyclohexyl-1-(((*SR*)-1-(methylsulfonyl)piperidin-3-yl)amino)-1-oxobutan-2-yl)carbamoyl)benzyl)-1-phenyl-1*H*-pyrazole-4-carboxamide (13)

4-((5-Amino-1-phenyl-1*H*-pyrazole-4-carboxamido)methyl)benzoic acid (**8**, 200 mg, 0.59 mmol) and HATU (280 mg, 0.74 mmol) were dissolved in DMF (5 mL), and DIPEA (115 mg, 0.89 mmol) was added. The solution was stirred for 1.5 h at RT and (*S*)-2-amino-4-cyclohexyl-*N*-((*SR*)-1-(methylsulfonyl)piperidin-3-yl)butanamide (**11d**, 247 mg, 0.71 mmol), diluted in DMF (5 mL) and DIPEA (115 mg, 0.89 mmol), was added. The mixture was stirred for 20 h at RT. DCM (50 mL) was added, and the organic phase was washed 5 times with H₂O (20 mL) and dried over MgSO₄. The solvent was evaporated under reduced pressure, and the crude product was triturated with cyclohexane/EtOAc (1:1) to afford 78 mg (0.11 mmol, 19%) of compound **13** as a colorless solid. TLC: $R_f = 0.14$ (SiO₂, cyclohexane/EtOAc 1:3). HPLC: (mixture of diastereomeres) $t_{R,1} = 8.90$, $t_{R,2} = 9.08$ min, purity: >95%. ^1H -NMR (500 MHz, DMSO- d_6 , 300 K): (mixture of diastereomeres) $\delta = 8.52$ (t, $^3J = 6.0$ Hz, 1H), 8.32 (d, $^3J = 8.1$ Hz, 1H), 8.03 (d, $^3J = 7.5$ Hz, 1H), 7.99 (s, 1H), 7.85 (d, $^3J = 8.4$ Hz, 2H), 7.60–7.49 (m, 4H), 7.42–7.34 (m, 3H), 6.38 (br s, 2H), 4.47 (d, $^3J = 6.0$ Hz, 2H), 4.44–4.35 (m, 1H), 3.78–3.67 (m, 1H), 3.53–3.40 (m, 1H), 3.37–3.28 (m, 1H), 2.87–2.82 (m, 3H), 2.81–2.71 (m, 1H), 2.58–2.51 (m, 1H), 1.85–1.46 (m, 10H), 1.45–1.30 (m, 1H), 1.29–1.04 (m, 6H), 0.90–0.77 (m, 2H) ppm. ^{13}C -NMR (126 MHz, DMSO- d_6 , 300 K): (mixture of diastereomeres) $\delta = 171.7$, 166.1

(2x), 164.1, 149.2, 143.6, 138.4, 138.2, 132.7, 129.4, 127.6, 127.1, 126.8, 123.1, 97.4, 53.6, 53.5, 49.6, 49.4, 45.4, 45.2, 45.1, 41.3, 36.8 (2x), 34.3 (2x), 33.3, 32.9 (2x), 32.7 (2x), 29.5, 29.0, 28.7, 26.2, 25.8 (2x), 23.0 (2x) ppm. MS (ESI neg.): m/z (%) = 662.27 (100) ($[M-H]^-$, calcd. 662.31), 698.30 (50) ($[M+Cl]^-$, calcd. 698.77). HRMS (FTMS + p MALDI): m/z = 702.2830 $[M+K]^+$, calcd. for $[C_{34}H_{45}KN_7O_5S]^+ = 702.2840$.

5-Amino-*N*-(4-(((*S*)-4-cyclohexyl-1-(((*SR*)-1-(cyclopropanecarbonyl)piperidin-3-yl)amino)-1-oxobutan-2-yl)carbamoyl)benzyl)-1-phenyl-1*H*-pyrazole-4-carboxamide (14)

4-((5-Amino-1-phenyl-1*H*-pyrazole-4-carboxamido)methyl)benzoic acid (**8**, 200 mg, 0.59 mmol) and HATU (280 mg, 0.74 mmol) were dissolved in DMF (5 mL) and DIPEA (115 mg, 0.89 mmol) was added. The solution was stirred for 1.5 h at RT, and (*S*)-2-amino-4-cyclohexyl-*N*-(((*SR*)-1-(cyclopropanecarbonyl)piperidin-3-yl)butanamide (**11c**, 240 mg, 0.71 mmol), diluted in DMF (5 mL) and DIPEA (115 mg, 0.89 mmol) was added. The mixture was stirred for 20 h at RT. DCM (50 mL) was added, and the organic phase was washed 5 times with H₂O (20 mL) and dried over MgSO₄. The solvent was evaporated under reduced pressure, and the crude product was triturated with cyclohexane/EtOAc (1:1) to afford 120 mg (0.18 mmol, 31%) of compound **14** as a colorless solid. TLC: R_f = 0.21 (SiO₂, EtOAc/MeOH 10:1). HPLC: (mixture of diastereomers) $t_{R,1}$ = 8.96, $t_{R,2}$ = 9.08 min, purity: 91%. ¹H-NMR (500 MHz, DMSO-*d*₆, 300 K): (mixture of diastereomers) δ = 8.52 (t, ³*J* = 6.1 Hz, 1H), 8.30 (d, ³*J* = 8.1 Hz, 1H), 8.07–7.88 (m, 2H), 7.85 (d, ³*J* = 8.3 Hz, 2H), 7.60–7.49 (m, 4H), 7.43–7.34 (m, 3H), 6.38 (br s, 2H), 4.53–4.31 (m, 3H), 4.20–3.46 (m, 3H), 3.27–3.01 (m, 1H), 2.76–2.56 (m, 1H), 2.54–2.45 (m, 1H), 2.02–1.31 (m, 12H), 1.30–1.02 (m, 6H), 0.92–0.77 (m, 2H), 0.92–0.77 (m, 4H) ppm. ¹³C-NMR (126 MHz, DMSO-*d*₆, 300 K): (mixture of diastereomers) δ = 172.0, 171.4, 171.0, 170.9, 166.1, 164.1, 149.2, 143.6, 138.4, 138.2, 132.7, 132.6, 129.4, 127.6, 127.1, 126.8, 123.1, 97.4, 53.4, 49.0, 46.1, 45.9, 45.1, 41.8, 41.3, 36.9, 33.5, 33.3, 33.0, 32.7, 29.9, 29.7, 29.4, 29.3, 26.2, 25.8 (2x), 24.1, 22.5, 10.4, 10.3, 7.0, 6.8 ppm. MS (ESI neg.): m/z (%) =

652.31 (100) ($[M-H]^-$, calcd. 652.36). HRMS (FTMS + p MALDI): $m/z = 692.3311 [M+K]^+$, calcd. for $[C_{37}H_{47}KN_7O_4]^+ = 692.3321$.

5-Amino-*N*-(4-(((*S*)-4-cyclohexyl-1-(((*SR*)-1-(oxetan-3-yl)piperidin-3-yl)amino)-1-oxobutan-2-yl)carbamoyl)benzyl)-1-phenyl-1*H*-pyrazole-4-carboxamide (15)

4-((5-Amino-1-phenyl-1*H*-pyrazole-4-carboxamido)methyl)benzoic acid (**8**, 233 mg, 0.69 mmol) and HATU (316 mg, 0.83 mmol) were dissolved in DMF (5 mL), and DIPEA (134 mg, 1.038 mmol) was added. The solution was stirred for 1 h at RT and (*S*)-2-amino-4-cyclohexyl-*N*-(((*SR*)-1-(oxetan-3-yl)piperidin-3-yl)butanamide (**11e**, 268 mg, 0.83 mmol), diluted in DMF (5 mL), was added. The mixture was stirred for 20 h at RT. DCM (50 mL) was added, and the organic phase was washed 5 times with H₂O (20 mL) and dried over MgSO₄. The solvent was evaporated under reduced pressure, and the crude product was purified using column chromatography on silica (cyclohexane/EtOAc 1:20 → EtOAc → EtOH) to afford 175 mg (0.273 mmol, 39%) of compound **15** as a colorless solid. TLC: $R_f = 0.16$ (SiO₂, EtOAc/MeOH 10:1). HPLC: (mixture of diastereomers) $t_{R,1} = 7.57$, $t_{R,2} = 7.61$ min, purity: >95%. ¹H-NMR (500 MHz, DMSO-*d*₆, 300 K): (mixture of diastereomers) $\delta = 8.60$ (t, $^3J = 5.9$ Hz, 1H), 8.40 (d, $^3J = 8.2$ Hz, 1H), 8.02 (s, 1H), 7.91 (d, $^3J = 7.9$ Hz, 1H), 7.85 (dd, $^3J = 8.5$, 1.9 Hz, 2H), 7.59–7.49 (m, 4H), 7.41–7.35 (m, 3H), 6.38 (br s, 2H), 4.53–4.44 (m, 4H), 4.43–4.31 (m, 3H), 3.76–3.67 (m, 1H), 3.48–3.26 (m, 3H), 2.55–2.46 (m, 1H), 2.45–2.35 (m, 1H), 1.89–1.54 (m, 10H), 1.51–1.38 (m, 1H), 1.31–1.04 (m, 6H), 0.89–0.77 (m, 2H) ppm. ¹³C-NMR (126 MHz, DMSO-*d*₆, 300 K): (mixture of diastereomers) $\delta = 171.3$ (2x), 166.1 (2x), 164.2, 149.2, 143.7, 143.6, 138.5, 138.3, 132.7 (2x), 129.4, 127.6, 127.1, 126.8, 123.1, 97.5, 74.7, 74.6, 58.4, 54.4 (2x), 53.7, 53.6, 49.2, 45.2 (2x), 41.3, 36.8 (2x), 33.3, 33.0, 32.7, 29.7, 29.5, 29.4, 26.2, 25.8 (2x), 23.0, 29.9 ppm. MS (ESI pos.): m/z (%) = 642.51 (100) ($[M-H]^+$, calcd. 642.38). HRMS (FTMS + p MALDI): $m/z = 642.3760 [M+H]^+$, calcd. for $[C_{36}H_{48}N_7O_4]^+ = 642.3762$.

Methyl 4-((3-phenyl-1*H*-pyrazole-5-carboxamido)methyl)benzoate (18a)

3-Phenyl-1*H*-pyrazole-5-carboxylic acid (**16**, 500 mg, 2.66 mmol), HOBt (431 mg, 3.19 mmol) and EDC-HCl (611 mg, 3.19 mmol) were dissolved in DMF (dry, 10 mL) and DIPEA (512 mg, 3.99 mmol) was added. The mixture was stirred for 1 h at RT and a solution of methyl 4-(aminomethyl)benzoate hydrochloride (**17a**, 688 mg, 3.19 mmol) dissolved in DMF (dry, 15 mL), and DIPEA (512 mg, 3.99 mmol) was added. The reaction mixture was stirred for additional 20 h at RT. DCM (150 mL) was added, and the organic phase was washed 4 times with H₂O (150 mL). The organic phase was separated, dried over MgSO₄ and the solvent was removed under reduced pressure. The crude product was dissolved in DCM and precipitated with cyclohexane to afford 711 mg (2.12 mmol, 80%) of compound **18a**, as a colorless solid. TLC: R_f = 0.70 (SiO₂, cyclohexane/EtOAc 1:3). ¹H-NMR (600 MHz, DMSO-d₆, 300 K): δ = 13.70 (s, 1H), 9.22–8.73 (s, 1H), 7.93 (d, ³J = 8.1 Hz, 2H), 7.80 (d, ³J = 7.3 Hz, 2H), 7.51–7.42 (m, 4H), 7.39–7.32 (m, 1H), 4.60–4.48 (m, 2H), 3.84 (s, 3H) ppm. ¹³C-NMR (150 MHz, DMSO-d₆, 300 K): δ = 166.1, 161.8, 147.7, 145.4, 140.8, 129.2 (2x), 128.9, 128.1, 127.3, 125.2, 102.5, 52.0, 41.8 ppm. MS (ESI neg.): *m/z* (%) = 334.07 (100) ([M-H]⁻, calcd. 334.12).

Methyl 4-(1-(3-phenyl-1*H*-pyrazole-5-carboxamido)ethyl)benzoate (18b**)**

3-Phenyl-1*H*-pyrazole-5-carboxylic acid (**16**, 1.00 g, 5.314 mmol), HOBt (862 mg, 6.38 mmol) and EDC-HCl (1.22 g, 6.38 mmol) were dissolved in DMF (dry, 10 mL) and DIPEA (1.03 g, 7.97 mmol) was added. The mixture was stirred for 1.5 h at RT, and a solution of methyl 4-(1-aminoethyl)benzoate hydrochloride (**17b**, 1.38 g, 6.38 mmol) dissolved in DMF (dry, 10 mL) and DIPEA (1.03 g, 7.97 mmol) was added. The reaction mixture was stirred for additional 20 h at RT. DCM (100 mL) and H₂O (200 mL) were added, and the aqueous phase was extracted 2 times with DCM (50 mL). The organic phase was separated, dried over MgSO₄, and the solvent was removed under reduced pressure. The crude product was purified using column chromatography on silica (cyclohexane/EtOAc 1:1 → 1:3). Compound **18b** was obtained in a yield of 1.606 g (4.80 mmol, 90%), as a colorless solid. TLC: R_f = 0.29 (SiO₂,

cyclohexane/EtOAc 1:1). ¹H-NMR (500 MHz, DMSO-d₆, 300 K): δ = 7.94 (d, ³J = 8.5 Hz, 2H), 7.58 (d, ³J = 6.9 Hz, 2H), 7.41 (d, ³J = 8.3 Hz, 2H), 7.38–7.30 (m, 4H), 7.06 (s, 1H), 5.35 (p, ³J = 7.4 Hz, 1H), 3.88 (s, 3H), 1.56 (d, ³J = 7.0 Hz, 3H) ppm. ¹³C-NMR (126 MHz, DMSO-d₆, 300 K): δ = 167.1, 161.4, 148.6, 146.2, 130.1, 129.2 (2x), 128.9, 126.3, 126.2, 125.7, 103.4, 52.3, 48.7, 22.1 ppm. MS (ESI neg.): *m/z* (%) = 348.11 (100) ([M-H]⁻, calcd. 348.13), 697.20 (24) ([2M-H]⁻, calcd. 697.27).

4-((3-Phenyl-1*H*-pyrazole-5-carboxamido)methyl)benzoic acid (**19a**)

Methyl 4-((3-phenyl-1*H*-pyrazole-5-carboxamido)methyl)benzoate (**18a**, 600 mg, 1.79 mmol) was dissolved in a mixture of THF/H₂O (10 mL, 1:1) and LiOH·H₂O (214 mg, 8.95 mmol) was added. The suspension was stirred for 24 h at RT and then acidified with HCl (aq., 10 mL, 1 M). The precipitate was filtered, washed with H₂O and dried under reduced pressure in a vacuum oven to afford 544 mg (1.69 mmol, 95%) of compound **19a** as a colorless solid. TLC: R_f = 0.30 (SiO₂, cyclohexane/EtOAc 1:3). ¹H-NMR (600 MHz, DMSO-d₆, 300 K): δ = 13.70–12.68 (m, 2H), 8.95 (s, 1H), 7.91 (d, ³J = 8.0 Hz, 2H), 7.80 (d, ³J = 7.6 Hz, 2H), 7.50–7.41 (m, 4H), 7.36 (t, ³J = 7.6 Hz, 1H), 7.17 (s, 1H), 4.54 (d, ³J = 6.2 Hz, 2H) ppm. ¹³C-NMR (150 MHz, DMSO-d₆, 300 K): δ = 167.2, 157.0, 147.7, 144.8, 140.8, 129.4, 129.3, 129.0, 128.2, 127.2 (2x), 125.2, 102.5, 41.8 ppm. MS (ESI neg.): *m/z* (%) = 320.10 (100) ([M-H]⁻, calcd. 320.10), 356.08 (56) ([M+Cl]⁻, calcd. 356.56).

4-(1-(3-Phenyl-1*H*-pyrazole-5-carboxamido)ethyl)benzoic acid (**19b**)

Methyl 4-(1-(3-phenyl-1*H*-pyrazole-5-carboxamido)ethyl)benzoate (**18b**, 200 mg, 0.57 mmol) was dissolved in a mixture of THF/H₂O (10 mL, 1:1), and LiOH·H₂O (69 mg, 2.86 mmol) was added. The suspension was stirred for 24 h at RT and then acidified with HCl (aq., 10 mL, 1 M). The precipitate was filtered, washed with H₂O and dried under reduced pressure in a vacuum oven to yield 178 mg (0.531 mmol, 93%) of compound **19b** as a colorless solid. TLC: R_f = 0.33 (SiO₂, cyclohexane/EtOAc 1:3). ¹H-NMR (600 MHz, DMSO-d₆, 300 K): δ = 13.95–12.45 (m,

2H), 8.72 (s, 1H), 7.91 (d, $^3J = 8.2$ Hz, 2H), 7.80 (d, $^3J = 7.6$ Hz, 2H), 7.52 (d, $^3J = 8.2$ Hz, 2H), 7.46 (t, $^3J = 7.6$ Hz, 2H), 7.35 (t, $^3J = 7.5$ Hz, 1H), 7.19 (s, 1H), 5.21 (p, $^3J = 7.1$ Hz, 1H), 1.56 (d, $^3J = 7.1$ Hz, 3H) ppm. ^{13}C -NMR (150 MHz, DMSO- d_6 , 300 K): $\delta = 168.1, 150.7, 148.6, 146.2, 130.4, 103.2, 129.9, 129.1, 127.3, 126.2, 125.2, 103.6, 47.8, 21.8$ ppm. MS (ESI neg.): m/z (%) = 334.10 (100) ($[\text{M-H}]^-$, calcd. 334.12), 370.05 (22) ($[\text{M+Cl}]^-$, calcd. 370.58).

***N*-(4-(((*S*)-4-Cyclohexyl-1-(((*SR*)-1-(methylsulfonyl)piperidin-3-yl)amino)-1-oxobutan-2-yl)carbamoyl)benzyl)-3-phenyl-1*H*-pyrazole-5-carboxamide (**20**)**

4-(((3-Phenyl-1*H*-pyrazole-5-carboxamido)methyl)benzoic acid (**19a**, 200 mg, 0.62 mmol) and HATU (284 mg, 0.75 mmol) were dissolved in DMF (5 mL), and DIPEA (96 mg, 0.75 mmol) was added. The solution was stirred for 1.5 h at RT and (*S*)-2-amino-4-cyclohexyl-*N*-(((*SR*)-1-(methylsulfonyl)piperidin-3-yl)butanamide (**11d**, 258 mg, 0.75 mmol), diluted in DMF (5 mL), was added. The mixture was stirred for 20 h at RT. DCM (100 mL) was added, and the organic phase was washed 4 times with H₂O (100 mL) and dried over MgSO₄. The solvent was evaporated under reduced pressure, and the crude product was purified using flashcolumn chromatography on silica (cyclohexane/EtOAc 1:1 \rightarrow 1:3 \rightarrow 1:20 \rightarrow EtOAc) to afford 113 mg (0.17 mmol, 28%) of compound **20** as a colorless solid. TLC: $R_f = 0.44$ (SiO₂, cyclohexane/EtOAc 1:10). HPLC: (mixture of diastereomers) $t_{R,1} = 9.03$ min; $t_{R,2} = 9.20$ min, purity: >95%. ^1H -NMR (600 MHz, DMSO- d_6 , 300 K): (mixture of diastereomers) $\delta = 13.68$ (br s, 1H), 8.86 (br s, 1H), 8.32 (d, $^3J = 8.0$ Hz, 1H), 8.01 (d, $^3J = 7.6$ Hz, 1H), 7.91–7.71 (m, 4H), 7.54–7.29 (m, 5H), 7.12 (br s, 1H), 4.60–4.32 (m, 3H), 3.82–3.64 (m, 1H), 3.55–3.41 (m, 1H), 3.37–3.24 (m, 1H), 2.85 (s, 3H), 2.82–2.70 (m, 1H), 2.60–2.53 (m, 1H), 1.85–1.46 (m, 10H), 1.44–1.31 (m, 1H), 1.26–1.02 (m, 6H), 0.90–0.76 (m, 2H) ppm. ^{13}C -NMR (150 MHz, DMSO- d_6 , 300 K): (mixture of diastereomers) $\delta = 171.6, 166.0, 162.1, 149.5, 143.9, 132.7, 128.9, 127.5, 126.9, 125.2, 102.9, 53.6, 53.4, 49.5, 49.4, 45.3, 45.3, 45.2, 45.1, 41.8, 36.8, 34.4, 34.3, 33.2, 32.9, 32.6, 29.4, 28.9, 28.6, 26.1, 25.7, 22.9$ ppm. MS (ESI neg.): m/z (%) = 647.22 (100) ($[\text{M-H}]^-$,

calcd. 647.30). HRMS (FTMS + p MALDI): m/z = 671.2980 $[M+Na]^+$, calcd. for $[C_{34}H_{44}N_6NaO_5S]^+ = 671.2992$.

***N*-((*SR*)-1-(4-(((*S*)-4-Cyclohexyl-1-(((*SR*)-1-(methylsulfonyl)piperidin-3-yl)amino)-1-oxobutan-2-yl)carbamoyl)phenyl)ethyl)-3-phenyl-1*H*-pyrazole-5-carboxamide carboxamide (**21**)**

4-(1-(3-Phenyl-1*H*-pyrazole-5-carboxamido)ethyl)benzoic acid (**19b**, 200 mg, 0.60 mmol) and HATU (309 mg, 0.72 mmol) were dissolved in DMF (5 mL) and DIPEA (105 mg, 0.72 mmol) was added. The solution was stirred for 1.5 h at RT and (*S*)-2-amino-4-cyclohexyl-*N*-((*SR*)-1-(methylsulfonyl)piperidin-3-yl)butanamide (**11d**, 281 mg, 0.72 mmol), diluted in DMF (5 mL), was added. The mixture was stirred for 20 h at RT. DCM (100 mL) was added, and the organic phase was washed 4 times with H₂O (100 mL) and dried over MgSO₄. The solvent was evaporated under reduced pressure, and the crude product was purified using flash column chromatography on silica (cyclohexane/EtOAc 1:3 → EtOAc) to afford 89 mg (0.13 mmol, 30%) of compound **21** as a colorless solid. TLC: R_f = 0.70 (SiO₂, EtOAc/MeOH 1:10). HPLC: (mixture of diastereomers) $t_{R,1}$ = 9.21 min; $t_{R,2}$ = 9.34 min, purity: >95%. ¹H-NMR (400 MHz, DMSO-*d*₆, 300 K): (mixture of diastereomers) δ = 13.64 (br s, 1H), 8.97–8.76 (m, 0.4H), 8.66–8.45 (m, 0.6H), 8.30 (d, ³*J* = 7.6 Hz, 1H), 8.04–7.93 (m, 1H), 7.89–7.82 (m, 2H), 7.80 (d, ³*J* = 7.2 Hz, 2H), 7.54–7.29 (m, 5.4H), 7.06 (s, 0.6H), 5.20 (p, ³*J* = 7.6 Hz, 1H), 4.45–4.33 (m, 1H), 3.81–3.66 (m, 1H), 3.54–3.40 (m, 1H), 3.39–3.27 (m, 1H), 2.85 (s, 3H), 2.81–2.70 (m, 1H), 2.59–2.51 (m, 1H), 1.85–1.46 (m, 13H), 1.44–1.31 (m, 1H), 1.29–1.05 (m, 6H), 0.92–0.72 (m, 2H) ppm. ¹³C-NMR (101 MHz, DMSO-*d*₆, 300 K): (mixture of diastereomers) δ = 171.6, 166.2, 161.9, 147.7, 144.9, 132.7, 129.1, 128.8, 127.9, 127.7, 127.6, 126.0, 125.4, 102.8, 53.5, 53.4, 49.6, 49.4, 45.4, 45.2, 45.1, 36.8, 34.4, 33.3 (2x), 32.9 (2x), 32.7, 29.4, 28.9, 28.7, 26.1, 25.8 (2x), 23.0 (2x), 22.0 (2x) ppm. MS (ESI neg.): m/z (%) = 707.29 (93) ($[M+EtOH-H]^-$, calcd. 707.36), 661.29 (100) ($[M-H]^-$, calcd. 661.32), 418.17 (30) ($[M_{fr.}+EtOH-H]^-$, calcd. 418.23),

372.19 (42) ($[M_{fr}]^-$, calcd. 372.20). HRMS (FTMS + p MALDI): $m/z = 685.3138 [M+Na]^+$, calcd. for $[C_{35}H_{46}N_6NaO_5S]^+ = 685.3148$.

***N*-((*SR*)-1-(4-(((*S*)-4-Cyclohexyl-1-(((*S*)-1-(methylsulfonyl)piperidin-3-yl)amino)-1-oxobutan-2-yl)carbamoyl)phenyl)ethyl)-3-phenyl-1*H*-pyrazole-5-carboxamide (**22**)**

4-(1-(3-Phenyl-1*H*-pyrazole-5-carboxamido)ethyl)benzoic acid (**19b**, 200 mg, 0.60 mmol) and HATU (272 mg, 0.72 mmol) were dissolved in DMF (5 mL) and DIPEA (93 mg, 0.72 mmol) was added. The solution was stirred for 1.5 h at RT and (*S*)-2-amino-4-cyclohexyl-*N*-((*S*)-1-(methylsulfonyl)piperidin-3-yl)butanamide (**11f**, 248 mg, 0.72 mmol), diluted in DMF (5 mL), was added. The mixture was stirred for 20 h at RT. DCM (100 mL) was added and the organic phase was washed 4 times with H₂O (100 mL) and dried over MgSO₄. The solvent was evaporated under reduced pressure, and the crude product was purified using flashcolumn chromatography on silica (cyclohexane/EtOAc 1:1 → 1:3 → 1:20) to afford 121 mg (0.18 mmol, 41%) of compound **22** as a colorless solid. TLC: $R_f = 0.07$ (SiO₂, cyclohexane/EtOAc 1:3). HPLC: (mixture of diastereomers) $t_R = 9.21$ min, purity: >95%. ¹H-NMR (600 MHz, DMSO-d₆, 300 K): (mixture of diastereomers) $\delta = 13.66$ – 13.57 (m, 1H), 8.88 (d, $^3J = 8.0$ Hz, 0.4H), 8.56 (d, $^3J = 8.4$ Hz, 0.6H), 8.34–8.27 (m, 1H), 8.03–7.96 (m, 1H), 7.89–7.82 (m, 2H), 7.80 (d, $^3J = 7.6$ Hz, 2H), 7.52–7.42 (m, 4H), 7.40–7.30 (m, 1.4H), 7.06 (s, 0.6H), 5.20 (p, $^3J = 7.3$ Hz, 1H), 4.39 (q, $^3J = 8.0$ Hz, 1H), 3.77–3.67 (m, 1H), 3.52–3.46 (m, 1H), 3.37–3.31 (m, 1H), 2.85 (s, 3H), 2.78–2.71 (m, 1H), 2.56–2.49 (m, 1H), 1.81–1.46 (m, 13H), 1.39–1.30 (m, 1H), 1.28–1.04 (m, 6H), 0.89–0.79 (m, 2H) ppm. ¹³C-NMR (150 MHz, DMSO-d₆, 300 K): (mixture of diastereomers) $\delta = 171.6, 166.1, 161.0, 148.2, 147.8, 143.5, 132.6, 129.1, 128.8, 128.4, 127.5, 125.9, 125.8, 125.4, 125.0, 102.8, 102.2, 53.5, 49.5, 47.7, 45.3, 45.2, 36.8, 34.4, 33.2, 32.9, 32.7, 29.4, 28.9, 26.1, 25.8, 25.7, 23.0, 21.9$ ppm. MS (ESI neg.): m/z (%) = 707.35 (71) ($[M+EtOH-H]^-$, calcd. 707.36), 661.26 (100) ($[M-H]^-$, calcd. 661.31), 372.24 (65) ($[M_{fr}]^-$, calcd.

372.20). HRMS (FTMS + p MALDI): $m/z = 685.3140$ $[M+Na]^+$, calcd. for $[C_{35}H_{46}N_6NaO_5S]^+$ = 685.3148.

***N*-((*SR*)-1-(4-(((*S*)-4-Cyclohexyl-1-(((*R*)-1-(methylsulfonyl)piperidin-3-yl)amino)-1-oxobutan-2-yl)carbamoyl)phenyl)ethyl)-3-phenyl-1*H*-pyrazole-5-carboxamide (**23**)**

4-(1-(3-Phenyl-1*H*-pyrazole-5-carboxamido)ethyl)benzoic acid (**19b**, 200 mg, 0.60 mmol) and HATU (309 mg, 0.72 mmol) were dissolved in DMF (5 mL) and DIPEA (105 mg, 0.72 mmol) was added. The solution was stirred for 1.5 h at RT, and (*S*)-2-amino-4-cyclohexyl-*N*-((*R*)-1-(methylsulfonyl)piperidin-3-yl)butanamide (**11g**, 281 mg, 0.72 mmol), diluted in DMF (5 mL), was added. The mixture was stirred for 20 h at RT. DCM (100 mL) was added, and the organic phase was washed 4 times with H₂O (100 mL) and dried over MgSO₄. The solvent was evaporated under reduced pressure, and the crude product was purified using flash column chromatography on silica (cyclohexane/EtOAc 1:1 → 1:3 → 1:20) to afford 102 mg (0.15 mmol, 34%) of compound **23** as a colorless solid. TLC: $R_f = 0.63$ (SiO₂, EtOAc/MeOH 1:10). HPLC: (mixture of diastereomers) $t_R = 9.31$ min, purity: >95%. ¹H-NMR (600 MHz, DMSO-*d*₆, 300 K): (mixture of diastereomers) $\delta = 13.68$ –13.56 (m, 1H), 8.94–8.82 (m, 0.4H), 8.63–8.51 (m, 0.6H), 8.35–8.26 (m, 1H), 7.99 (d, $^3J = 7.9$ Hz, 1H), 7.88–7.81 (m, 2H), 7.79 (d, $^3J = 7.7$ Hz, 2H), 7.51–7.29 (m, 5.4H), 7.06 (s, 0.6H), 5.20 (p, $^3J = 7.4$ Hz, 1H), 4.44–4.36 (m, 1H), 3.76–3.67 (m, 1H), 3.46–3.41 (m, 1H), 3.34–3.27 (m, 1H), 2.84 (s, 3H), 2.80–2.77 (m, 1H), 2.58–2.51 (m, 1H), 1.84–1.33 (m, 14H), 1.30–1.05 (m, 6H), 0.90–0.77 (m, 2H) ppm. ¹³C-NMR (150 MHz, DMSO-*d*₆, 300 K): (mixture of diastereomers) $\delta = 171.6, 166.1, 160.7, 148.2, 147.8, 143.4, 132.6, 129.0$ (2x), 127.5, 125.9, 125.3 (2x), 125.0, 102.1, 53.4, 49.4, 45.3, 45.1, 45.0, 36.8, 34.3, 33.2, 32.9, 32.6, 29.4, 28.6, 26.1, 25.8, 23.0, 21.9 (2x) ppm. MS (ESI neg.): m/z (%) = 707.32 (48) ($[M+EtOH-H]^-$, calcd. 707.36), 661.31 (41) ($[M-H]^-$, calcd. 661.32), 418.19 (57) ($[M_{fr}+EtOH-H]^-$, calcd. 418.23), 372.19 (100) ($[M_{fr}]^-$, calcd. 372.20). HRMS (FTMS + p MALDI): $m/z = 685.3144$ $[M+Na]^+$, calcd. for $[C_{35}H_{46}N_6NaO_5S]^+ = 685.3148$.

(S)-N-(4-((4-Cyclohexyl-1-oxo-1-(propylamino)butan-2-yl)carbamoyl)benzyl)-3-phenyl-1H-pyrazole-5-carboxamide (24)

4-((3-Phenyl-1H-pyrazole-5-carboxamido)methyl)benzoic acid (**19a**, 200 mg, 0.62 mmol) and HATU (284 mg, 0.75 mmol) were dissolved in DMF (5 mL), and DIPEA (96 mg, 0.75 mmol) was added. The solution was stirred for 1.5 h at RT. (S)-2-amino-4-cyclohexyl-N-propylbutanamide (**11b**, 169 mg, 0.75 mmol), diluted in DMF (5 mL), was added. The mixture was stirred for 20 h at RT. DCM (100 mL) was added, and the organic phase was washed 4 times with H₂O (150 mL), once with a NaCl solution (sat., 50 mL) and dried over MgSO₄. The solvent was evaporated under reduced pressure, and the crude product was precipitated from EtOAc to afford 197 mg (0.37 mmol, 60%) of compound **24** as a colorless solid. TLC: R_f = 0.34 (SiO₂, cyclohexane/ EtOAc 1:3). HPLC: t_R = 9.44 min, purity: >95%. ¹H-NMR (250 MHz, DMSO-d₆, 300 K): (mixture of rotamers) δ = 13.67 (s, 1H), 9.18–9.02 (m, 0.4H), 8.89–8.73 (m, 0.6H), 8.26 (d, ³J = 7.9 Hz, 1H), 7.98–7.71 (m, 5H), 7.55–7.25 (m, 5.4H), 7.09 (s, 0.6H), 4.60–4.42 (m, 2H), 4.41–4.28 (m, 1H), 3.15–2.90 (m, 2H), 1.80–1.51 (m, 7H), 1.40 (sext., ³J = 7.3 Hz, 2H), 1.28–1.04 (m, 6H), 0.92–0.72 (m, 5H) ppm. ¹³C-NMR (126 MHz, DMSO-d₆, 300 K): (mixture of rotamers) δ = 171.7, 166.0, 161.8, 147.7, 143.5, 143.3, 132.7, 129.1, 128.8, 128.5, 127.6, 126.9, 125.3, 125.1, 102.8, 53.7, 41.8, 36.8, 33.3, 32.9, 32.7, 29.4, 26.2, 25.8 (2x), 22.3, 11.4 ppm. MS (ESI neg.): m/z (%) = 528.14 (100) ([M-H]⁻, calcd. 528.30). HRMS (FTMS + p MALDI): m/z 552.2922 [M+Na]⁺, calcd. for [C₃₁H₃₉N₅NaO₃]⁺ = 552.2945.

Methyl 4-(((3-phenyl-3H-[1,2,3]triazolo[4,5-d]pyrimidin-7-yl)amino)methyl)benzoate (26a)

7-Chloro-3-phenyl-3H-[1,2,3]triazolo[4,5-d]pyrimidine (**25a**, 250 mg, 1.08 mmol) was diluted in THF (dry, 10 mL) and DIPEA (140 mg, 1.08 mmol) was added. In a separate flask methyl 4-(aminomethyl)benzoate hydrochloride (**17a**, 218 mg, 1.08 mmol) and DIPEA (140 mg, 1.08 mmol) were dissolved in THF (dry, 10 mL) and stirred at RT for 5 min. This suspension

was then added to the first solution, and the mixture was heated to 60 °C for 20 h. EtOAc (150 mL) was added, and the organic phase was washed 3 times with H₂O (50 mL). The organic phase was separated, dried over MgSO₄, and the solvent was removed under reduced pressure. The crude product was precipitated from cyclohexane to afford 324 mg (0.899 mmol, 83%) of compound **26a** as a colorless solid. TLC: R_f = 0.72 (SiO₂, cyclohexane/EtOAc 1:1). ¹H-NMR (600 MHz, DMSO-d₆, 300 K): (mixture of rotamers): δ = 9.73 (t, ³J = 6.1 Hz, 0.8H), 9.35 (t, ³J = 7.0 Hz, 0.2H), 8.47 (s, 0.8H), 8.43 (s, 0.2H), 8.15 (d, ³J = 7.9 Hz, 1.6H), 8.15 (d, ³J = 7.9 Hz, 0.4H), 7.92 (d, ³J = 7.9 Hz, 2H), 7.66 (t, ³J = 7.9 Hz, 2H), 7.58–7.49 (m, 3H), 5.32 (d, ³J = 7.0 Hz, 0.4H), 4.88 (d, ³J = 6.1 Hz, 1.6H), 3.83 (s, 3H) ppm. ¹³C-NMR (150 MHz, DMSO-d₆, 300 K): (mixture of rotamers) δ = 166.0, 157.4, 157.0, 154.5, 148.1, 144.5, 135.7, 129.6, 129.4, 129.3, 128.5, 128.3, 127.4, 124.8, 121.5, 121.4, 52.0, 43.0 ppm. MS (ESI neg.): m/z (%) = 359.05 (100) ([M-H]⁻, calcd. 359.12).

Methyl 4-(((1-phenyl-1*H*-pyrazolo[3,4-*d*]pyrimidin-4-yl)amino)methyl)benzoate (26b)

4-Chloro-1-phenyl-1*H*-pyrazolo[3,4-*d*]pyrimidine (**25b**, 250 mg, 1.08 mmol) was diluted in THF (dry, 10 mL), and DIPEA (140 mg, 1.08 mmol) was added. In a separate flask methyl 4-(aminomethyl)benzoate hydrochloride (**17a**, 219 mg, 1.08 mmol) and DIPEA (140 mg, 1.08 mmol) were dissolved in THF (dry, 10 mL) and stirred at RT for 5 min. The latter suspension was added to the first solution, and the mixture was heated to 60 °C for 20 h. EtOAc (150 mL) was added, and the organic phase was washed 3 times with H₂O (50 mL). The organic phase was separated, dried over MgSO₄, and the solvent was removed under reduced pressure. The crude product was purified using column chromatography on silica (cyclohexane/EtOAc 10:1) to afford 358 mg (0.996 mmol, 92%) of compound **26b** as a colorless solid. TLC: R_f = 0.59 (SiO₂, cyclohexane/EtOAc 1:1). ¹H-NMR (400 MHz, DMSO-d₆, 300 K): δ = 9.07 (t, ³J = 5.6 Hz, 1H), 8.45 (s, 1H), 8.38 (s, 1H), 8.20 (d, ³J = 8.1 Hz, 2H), 7.95 (d, ³J = 8.1 Hz, 2H), 7.59–7.49 (m, 4H), 7.35 (t, ³J = 7.3 Hz, 1H), 4.88 (d, ³J = 5.8 Hz, 2H) 3.84 (s, 3H) ppm. ¹³C-NMR

(150 MHz, DMSO- d_6 , 300 K): δ = 166.0, 156.4 (2x), 152.8, 144.8, 138.9, 133.7, 129.3 (2x), 129.1, 127.5, 126.1, 120.6, 101.8, 52.2, 42.9 ppm. MS (ESI pos.): m/z (%) = 359.89 (100) ($[M-H]^+$, calcd. 360.15).

Methyl 4-((imidazo[1,2-*a*]pyridine-3-carboxamido)methyl)benzoate (26c)

Imidazo[1,2-*a*]pyridine-3-carboxylic acid (**25c**, 500 mg, 3.08 mmol), HOBt (500 mg, 3.70 mmol) and EDC-HCl (709 mg, 3.70 mmol) were dissolved in DMF (dry, 8 mL), and DIPEA (598 mg, 4.63 mmol) was added. The mixture was stirred for 1 h at RT, and a solution of methyl 4-(aminomethyl)benzoate hydrochloride (**17a**, 789 mg, 3.91 mmol) dissolved in DMF (dry, 7 mL), DMSO (dry, 3 mL) and DIPEA (598 mg, 4.63 mmol) was added. The reaction mixture was stirred for additional 20 h at RT. DCM (200 mL) was added, and the organic phase was washed 4 times with H₂O (150 mL). The organic phase was separated, dried over MgSO₄, and the solvent was removed under reduced pressure. The crude product was dissolved in DCM and precipitated with cyclohexane to afford 837 mg (2.71 mmol, 88%) of compound **26c** as a colorless solid. TLC: R_f = 0.26 (SiO₂, cyclohexane/EtOAc 1:3). ¹H-NMR (600 MHz, DMSO- d_6 , 300 K): δ = 9.47 (d, ³*J* = 7.0 Hz, 1H), 9.13 (t, ³*J* = 5.8 Hz, 1H), 8.42 (s, 1H), 7.93 (d, ³*J* = 8.2 Hz, 2H), 7.72 (d, ³*J* = 9.2 Hz, 1H), 7.49 (d, ³*J* = 8.0 Hz, 2H), 7.46 (t, ³*J* = 7.7 Hz, 1H), 7.11 (t, ³*J* = 6.9 Hz, 1H), 4.60 (d, ³*J* = 5.8 Hz, 2H), 3.83 (s, 3H) ppm. ¹³C-NMR (150 MHz, DMSO- d_6 , 300 K): δ = 166.1, 160.2, 146.9, 145.3, 136.9, 129.3, 128.2, 127.5, 127.4, 126.9, 117.9, 117.2, 113.8, 52.0, 41.6 ppm. MS (ESI neg.): m/z (%) = 308.09 (100) ($[M-H]^-$, calcd. 308.10).

Methyl 4-((5-amino-1-methyl-1*H*-pyrazole-4-carboxamido)methyl)benzoate (26d)

5-Amino-1-methyl-1*H*-pyrazole-4-carboxylic acid (**25d**, 500 mg, 3.54 mmol), HOBt (574 mg, 4.25 mmol) and EDC-HCl (815 mg, 4.25 mmol) were dissolved in DMF (dry, 10 mL), and DIPEA (687 mg, 5.31 mmol) was added. The mixture was stirred for 1 h at RT, and a solution of methyl 4-(aminomethyl)benzoate hydrochloride (**17a**, 857 mg, 4.25 mmol) dissolved in

DMF (dry, 10 mL) and DIPEA (687 mg, 5.31 mmol) was added. The reaction mixture was stirred for additional 20 h at RT. DCM (100 mL) was added, the organic phase was washed 4 times with H₂O (100 mL) and once with brine (100 mL). The organic phase was separated, dried over MgSO₄, and the solvent was removed under reduced pressure. The crude product was precipitated from cyclohexane to afford 722 mg (2.50 mmol, 71%) of compound **26d** as a colorless solid. TLC: R_f = 0.25 (SiO₂, cyclohexane/EtOAc 1:3). ¹H-NMR (600 MHz, DMSO-d₆, 300 K): δ = 8.32 (t, ³J = 5.9 Hz, 1H), 7.92 (d, ³J = 8.1 Hz, 2H), 7.68 (s, 1H), 7.41 (d, ³J = 8.1 Hz, 2H), 6.16 (s, 2H), 4.45 (d, ³J = 6.1 Hz, 2H), 3.84 (s, 3H), 3.51 (s, 3H) ppm. ¹³C-NMR (150 MHz, DMSO-d₆, 300 K): δ = 166.1, 164.1, 149.4, 146.1, 136.1, 129.2, 128.0, 127.2, 96.7, 52.0, 41.3, 33.9 ppm. MS (ESI pos.): *m/z* (%) = 289.03 (100) ([M+H]⁺, calcd. 289.13).

Methyl 4-(1-(5-amino-1-methyl-1*H*-pyrazole-4-carboxamido)ethyl)benzoate (26e)

5-Amino-1-methyl-1*H*-pyrazole-4-carboxylic acid (**25d**, 436 mg, 3.09 mmol), HOBt (501 mg, 3.71 mmol) and EDC-HCl (711 mg, 3.71 mmol) were dissolved in DMF (dry, 8 mL), and DIPEA (600 mg, 4.64 mmol) was added. The mixture was stirred for 1 h at RT, and a solution of methyl 4-(1-aminoethyl)benzoate hydrochloride (**17b**, 800 mg, 3.71 mmol) dissolved in DMF (dry, 7 mL), and DIPEA (600 mg, 4.64 mmol) was added. The reaction mixture was stirred for additional 20 h at RT. Then DCM (100 mL) was added, and the organic phase was washed 4 times with H₂O (50 mL) and once with a NaCl solution (sat., 50 mL). The organic phase was separated, dried over MgSO₄, and the solvent was removed under reduced pressure. The crude product was precipitated from cyclohexane to afford 632 mg (2.09 mmol, 68%) of compound **26e** as a colorless solid. TLC: R_f = 0.20 (SiO₂, cyclohexane/EtOAc 1:3). ¹H-NMR (600 MHz, DMSO-d₆, 300 K): δ = 8.25–7.68 (m, 4H), 7.65–7.28 (m, 2H), 6.11 (s, 2H), 5.30–4.95 (m, 1H), 3.83 (s, 3H), 3.50 (s, 3H), 1.43 (s, 3H) ppm. ¹³C-NMR (150 MHz, DMSO-d₆, 300 K): δ = 166.1, 163.4, 151.2, 149.4, 136.3, 129.2, 127.8, 126.2, 96.7, 52.0, 47.2, 33.8, 22.1 ppm.

MS (ESI neg.): m/z (%) = 301.14 (100) ($[M-H]^-$, calcd. 301.13), 347.06 (35) ($[M-H+EtOH]^-$, calcd. 347.17).

Methyl 4-(1-(imidazo[1,2-*a*]pyridine-3-carboxamido)ethyl)benzoate (26f)

Imidazo[1,2-*a*]pyridine-3-carboxylic acid (**25c**, 251 mg, 1.55 mmol), HOBt (209 mg, 1.85 mmol) and EDC-HCl (296 mg, 1.85 mmol) were dissolved in DMF (dry, 8 mL), and DIPEA (300 mg, 2.32 mmol) was added. The mixture was stirred for 1 h at RT, and a solution of methyl 4-(1-aminoethyl)benzoate hydrochloride (**17b**, 400 mg, 3.71 mmol) dissolved in DMF (dry, 7 mL), DMSO (dry, 5 mL) and DIPEA (300 mg, 2.32 mmol) was added. The reaction mixture was stirred for additional 20 h at RT, then DCM (150 mL) was added, and the organic phase was washed 4 times with H₂O (100 mL). The organic phase was separated, dried over MgSO₄, and the solvent was removed under reduced pressure. The crude product was purified using column chromatography on silica (cyclohexane/EtOAc 1:10) to afford 365 mg (1.13 mmol, 73%) of compound **26f** as a yellowish solid. TLC: R_f = 0.31 (SiO₂, cyclohexane/EtOAc 1:3). ¹H-NMR (600 MHz, DMSO-*d*₆, 300 K): δ = 9.40 (d, ³*J* = 7.2 Hz, 1H), 8.88 (d, ³*J* = 7.6 Hz, 1H), 8.51 (s, 1H), 7.93 (d, ³*J* = 8.3 Hz, 2H), 7.70 (d, ³*J* = 8.9 Hz, 1H), 7.55 (d, ³*J* = 8.1 Hz, 2H), 7.44 (t, ³*J* = 7.6 Hz, 1H), 7.08 (t, ³*J* = 6.9 Hz, 1H), 5.27 (p, ³*J* = 7.2 Hz, 1H), 3.83 (s, 3H), 1.52 (d, ³*J* = 7.1 Hz, 3H) ppm. ¹³C-NMR (150 MHz, DMSO-*d*₆, 300 K): δ = 166.1, 159.5, 150.4, 146.9, 137.1, 129.3, 128.1, 127.5, 126.9, 126.3, 117.9, 117.2, 113.8, 52.0, 47.7, 21.9 ppm. MS (ESI neg.): m/z (%) = 322.08 (100) ($[M-H]^-$, calcd. 322.12).

4-(((3-Phenyl-3*H*-[1,2,3]triazolo[4,5-*d*]pyrimidin-7-yl)amino)methyl)benzoic acid (27a)

Methyl 4-(((3-phenyl-3*H*-[1,2,3]triazolo[4,5-*d*]pyrimidin-7-yl)amino)methyl)benzoate (**26a**, 290 mg, 0.81 mmol) was dissolved in a mixture of THF/H₂O (20 mL, 1:1) and LiOH·H₂O (96 mg, 4.03 mmol) was added. The suspension was stirred for 4 d at RT and then acidified with HCl (aq., 10 mL, 1 M). The precipitate was filtered, washed with H₂O and dried under reduced pressure in a vacuum oven to afford 231 mg (0.67 mmol, 83%) of compound **27a** as a colorless

solid. TLC: R_f = 0.60 (SiO₂, cyclohexane /EtOAc 1:10). ¹H-NMR (300 MHz, DMSO-d₆, 300 K): (mixture of rotamers) δ = 12.86 (s, 1H), 9.81–9.60 (m, 0.8H), 9.42–9.26 (m, 0.2H), 8.56–8.37 (m, 1H), 8.15 (d, ³ J = 8.1 Hz, 2H), 7.91 (d, ³ J = 7.8 Hz, 2H), 7.73–7.37 (m, 5H), 5.39–5.25 (m, 0.4H), 4.97–4.77 (m, 1.6H) ppm. ¹³C-NMR (75 MHz, DMSO-d₆, 300 K): (mixture of rotamers) δ = 167.1, 157.5, 154.5, 148.1, 144.0, 135.8, 129.6, 129.4, 128.5, 127.3, 127.2, 124.9, 121.4, 43.1 ppm. MS (ESI neg.): m/z (%) = 345.07 (100) ([M-H]⁻, calcd. 345.11).

4-(((1-Phenyl-1*H*-pyrazolo[3,4-*d*]pyrimidin-4-yl)amino)methyl)benzoic acid (**27b**)

Methyl 4-(((1-phenyl-1*H*-pyrazolo[3,4-*d*]pyrimidin-4-yl)amino)methyl)benzoate (**26b**, 500 mg, 1.39 mmol) was dissolved in a mixture of THF/H₂O (20 mL, 1:1) and LiOH·H₂O (166 mg, 6.96 mmol) was added. The suspension was stirred for 4 d at RT and then acidified with HCl (aq., 10 mL, 1 M). The precipitate was filtered, washed with H₂O and dried under reduced pressure in a vacuum oven to afford 455 mg (1.32 mmol, 95%) of compound **27b** as a colorless solid. TLC: R_f = 0.02 (SiO₂, cyclohexane/EtOAc 1:10). ¹H-NMR (300 MHz, DMSO-d₆, 300 K): δ = 13.41–12.35 (br s, 1H), 9.16 (t, ³ J = 6.1 Hz, 1H), 8.48 (s, 1H), 8.38 (s, 1H), 8.19 (d, ³ J = 7.8 Hz, 2H), 7.92 (d, ³ J = 8.3 Hz, 2H), 7.60–7.45 (m, 4H), 7.34 (tt, ³ J = 7.4, 1.1 Hz, 1H), 4.86 (d, ³ J = 5.9 Hz, 2H) ppm. ¹³C-NMR (75 MHz, DMSO-d₆, 300 K): δ = 167.1, 156.4 (2x), 152.8, 144.3, 138.9, 133.8, 129.5, 129.1 (2x), 127.4, 126.2, 120.7, 101.9, 43.1 ppm. MS (ESI neg.): m/z (%) = 344.04 (100) ([M-H]⁻, calcd. 344.10).

4-((Imidazo[1,2-*a*]pyridine-3-carboxamido)methyl)benzoic acid (**27c**)

Methyl 4-((imidazo[1,2-*a*]pyridine-3-carboxamido)methyl)benzoate (**26c**, 600 mg, 1.94 mmol) was dissolved in a mixture of THF/H₂O (20 mL, 1:1) and LiOH·H₂O (232 mg, 9.70 mmol) was added. The suspension was stirred for 3 d at RT and then acidified with HCl (aq., 10 mL, 1 M). The precipitate was filtered, washed with H₂O and dried under reduced pressure in a vacuum oven to afford 367 mg (1.24 mmol, 64%) of compound **27c** as a yellowish solid. TLC: R_f = 0.02 (SiO₂, cyclohexane/EtOAc 1:10). ¹H-NMR (300 MHz, DMSO-d₆, 300 K): δ = 9.89 (t, ³ J = 5.9

Hz, 1H), 9.69 (d, $^3J = 7.0$ Hz, 1H), 9.03 (s, 1H), 8.08–7.67 (m, 4H), 7.58–7.45 (m, 3H), 4.59 (d, $^3J = 5.8$ Hz, 2H) ppm. ^{13}C -NMR (75 MHz, DMSO- d_6 , 300 K): $\delta = 167.1, 158.7, 144.1, 141.5, 133.3, 129.5, 129.4, 129.2, 127.7, 127.4, 118.8, 117.4, 113.5, 41.8$ ppm. MS (ESI neg.): m/z (%) = 294.10 (100) ($[\text{M}-\text{H}]^-$, calcd. 294.09).

4-((5-Amino-1-methyl-1*H*-pyrazole-4-carboxamido)methyl)benzoic acid (27d)

Methyl 4-((5-amino-1-methyl-1*H*-pyrazole-4-carboxamido)methyl)benzoate (**26d**, 600 mg, 2.08 mmol) was dissolved in a mixture of THF/ H_2O (10 mL, 1:1), and $\text{LiOH}\cdot\text{H}_2\text{O}$ (249 mg, 10.4 mmol) was added. The suspension was stirred for 24 h at RT and then acidified with HCl (aq., 10 mL, 1 M). The precipitate was filtered, washed with H_2O and dried under reduced pressure in a vacuum oven to afford 504 mg (1.84 mmol, 88%) of compound **27d** as a colorless solid. TLC: $R_f = 0.08$ (SiO_2 , cyclohexane/EtOAc 1:3). ^1H -NMR (600 MHz, DMSO- d_6 , 300 K): $\delta = 8.50\text{--}8.44$ (m, 1H), 7.90 (d, $^3J = 8.2$ Hz, 2H), 7.84 (s, 1H), 7.39 (d, $^3J = 8.2$ Hz, 2H), 6.34–4.64 (m, 3H), 4.47–4.42 (m, 2H), 3.55 (s, 3H) ppm. ^{13}C -NMR (150 MHz, DMSO- d_6 , 300 K): $\delta = 167.2, 163.8, 149.6, 145.5, 135.7, 129.4, 129.2, 127.1, 97.0, 41.4, 33.8$ ppm. MS (ESI neg.): m/z (%) = 273.08 (100) ($[\text{M}-\text{H}]^-$, calcd. 273.10), 309.07 (47) ($[\text{M}+\text{Cl}]^-$, calcd. 308.53), 229.11 (28) ($[\text{M}-\text{COOH}]^-$, calcd. 229.11).

4-(1-(5-Amino-1-methyl-1*H*-pyrazole-4-carboxamido)ethyl)benzoic acid (27e)

Methyl 4-(1-(5-amino-1-methyl-1*H*-pyrazole-4-carboxamido)ethyl)benzoate (**26e**, 500 mg, 1.65 mmol) was dissolved in a mixture of THF/ H_2O (10 mL, 1:1) and $\text{LiOH}\cdot\text{H}_2\text{O}$ (198 mg, 8.27 mmol) was added. The solvent was removed under reduced pressure. The crude product was triturated with DCM/ H_2O (1:1), filtered, washed with H_2O and dried under reduced pressure in a vacuum oven to afford 368 mg (1.28 mmol, 77%) of compound **27e** as a colorless solid. TLC: $R_f = 0.13$ (SiO_2 , DCM/MeOH 10:1). ^1H -NMR (600 MHz, DMSO- d_6 , 300 K): $\delta = 12.83$ (br s, 1H), 8.06 (d, $^3J = 7.9$ Hz, 1H), 7.89 (d, $^3J = 7.9$ Hz, 2H), 7.78 (s, 1H), 7.44 (d, $^3J = 8.0$ Hz, 2H), 6.11 (br s, 2H), 5.13 (p, $^3J = 7.3$ Hz, 1H), 3.50 (s, 3H), 1.43 (d, $^3J = 7.2$ Hz, 3H)

ppm. ^{13}C -NMR (150 MHz, DMSO- d_6 , 300 K): δ = 167.2, 163.4, 150.7, 149.5, 136.3, 129.3, 129.0, 126.1, 96.7, 47.2, 33.9, 22.1 ppm. MS (ESI neg.): m/z (%) = 287.10 (100) ($[\text{M-H}]^-$, calcd. 287.29), 243.12 (20) ($[\text{M-COOH}]^-$, calcd. 243.12).

4-(1-(Imidazo[1,2-*a*]pyridine-3-carboxamido)ethyl)benzoic acid (27f)

Methyl 4-(1-(imidazo[1,2-*a*]pyridine-3-carboxamido)ethyl)benzoate (**26f**, 337 mg, 1.04 mmol) was dissolved in a mixture of THF/ H_2O (20 mL, 1:1) and $\text{LiOH}\cdot\text{H}_2\text{O}$ (125 mg, 5.21 mmol) was added. The suspension was stirred for 4 d at RT and then acidified with HCl (aq., 10 mL, 1 M). The precipitate was filtered, washed with H_2O and dried under reduced pressure in a vacuum oven to afford 308 mg (1.00 mmol, 96%) of compound **27f** as a yellowish solid. TLC: R_f = 0.07 (SiO_2 , cyclohexane/EtOAc 1:3). ^1H -NMR (300 MHz, DMSO- d_6 , 300 K): δ = 12.85 (s, 1H), 9.41 (d, 3J = 7.1 Hz, 1H), 8.93 (d, 3J = 7.7 Hz, 1H), 8.55 (s, 1H), 7.91 (d, 3J = 8.3 Hz, 2H), 7.71 (d, 3J = 9.0 Hz, 1H), 7.53 (d, 3J = 8.3 Hz, 2H), 7.45 (t, 3J = 7.7 Hz, 1H), 7.09 (t, 3J = 7.0 Hz, 1H), 5.26 (p, 3J = 7.3 Hz, 1H), 1.52 (d, 3J = 7.1 Hz, 3H) ppm. ^{13}C -NMR (75 MHz, DMSO- d_6 , 300 K): δ = 167.2, 159.5, 150.4, 146.8, 137.0, 129.5, 129.3, 127.6, 127.1, 126.2, 118.0, 117.2, 113.9, 47.8, 22.0 ppm. MS (ESI neg.): m/z (%) = 308.12 (100) ($[\text{M-H}]^-$, calcd. 308.10).

***N*-((*S*)-4-Cyclohexyl-1-(((*SR*)-1-(methylsulfonyl)piperidin-3-yl)amino)-1-oxobutan-2-yl)-4-(((3-phenyl-3*H*-[1,2,3]triazolo[4,5-*d*]pyrimidin-7-yl)amino)methyl)benzamide (28)**

4-(((3-Phenyl-3*H*-[1,2,3]triazolo[4,5-*d*]pyrimidin-7-yl)amino)methyl)benzoic acid (**27a**, 200 mg, 0.58 mmol) and HATU (263 mg, 0.69 mmol) were dissolved in DMF (5 mL) and DIPEA (90 mg, 0.693 mmol) was added. The solution was stirred for 1.5 h at RT and (*S*)-2-amino-4-cyclohexyl-*N*-((*SR*)-1-(methylsulfonyl)piperidin-3-yl)butanamide (**11d**, 239 mg, 0.70 mmol), diluted in DMF (5 mL), was added. The mixture was stirred for 20 h at RT. DCM (150 mL) was added, and the organic phase was washed 5 times with H_2O (150 mL) and dried over MgSO_4 . The solvent was evaporated under reduced pressure, and the crude product was triturated with EtOAc/cyclohexane (1:1) and recrystallized from DCM to afford 51 mg

(0.075 mmol, 13%) of compound **28** as a colorless solid. TLC: R_f = 0.20 (SiO₂, cyclohexane/EtOAc 1:10). HPLC: (mixture of diastereomers) $t_{R,1}$ = 15.97 min; $t_{R,2}$ = 16.27 min, purity: >95%. ¹H-NMR (400 MHz, DMSO-*d*₆, 300 K): (mixture of diastereomers/ rotamers) δ = 9.77–9.63 (m, 1H) 8.56–8.39 (m, 2H), 8.22–8.09 (m, 3H), 7.72–7.60 (m, 2H), 7.58–7.39 (m, 3H), 7.32 (d, ³*J* = 7.5 Hz, 2H), 4.84 (d, ³*J* = 5.6 Hz, 2H), 3.89–3.10 (m, 4H), 2.95–2.79 (m, 5H), 1.87–1.38 (m, 12H), 1.30–1.03 (m, 5H), 0.94–0.76 (m, 2H). MS (ESI pos.): *m/z* (%) = 696.30 (100) ([*M*+Na]⁺, calcd. 696.31). HRMS (FTMS + *p* MALDI): *m/z* 696.3054 [*M*+Na]⁺, calcd. for [C₃₄H₄₃N₉NaO₄S]⁺ = 696.3056.

***N*-((*S*)-4-Cyclohexyl-1-(((*SR*)-1-(methylsulfonyl)piperidin-3-yl)amino)-1-oxobutan-2-yl)-4-(((1-phenyl-1*H*-pyrazolo[3,4-*d*]pyrimidin-4-yl)amino)methyl)benzamide (**29**)**

4-(((1-Phenyl-1*H*-pyrazolo[3,4-*d*]pyrimidin-4-yl)amino)methyl)benzoic acid (**27b**, 200 mg, 0.58 mmol) and HATU (264 mg, 0.70 mmol) were dissolved in DMF (5 mL), and DIPEA (90 mg, 0.70 mmol) was added. The solution was stirred for 1.5 h at RT, and (*S*)-2-amino-4-cyclohexyl-*N*-((*SR*)-1-(methylsulfonyl)piperidin-3-yl)butanamide (**11d**, 240 mg, 0.70 mmol), diluted in DMF (5 mL), was added. The mixture was stirred for 20 h at RT. DCM (150 mL) was added, and the organic phase was washed 5 times with H₂O (100 mL) and dried over MgSO₄. The solvent was evaporated under reduced pressure, and the crude product was triturated with EtOAc/cyclohexane (1:1) and recrystallized from DCM to afford 125 mg (0.19 mmol, 32%) of compound **29** as a colorless solid. TLC: R_f = 0.21 (SiO₂, cyclohexane/EtOAc 1:10). HPLC: (mixture of diastereomers) $t_{R,1}$ = 9.76 min; $t_{R,2}$ = 9.92 min, purity: >95%. ¹H-NMR (300 MHz, DMSO-*d*₆, 300 K): (mixture of diastereomers) δ = 9.03 (t, ³*J* = 5.8 Hz, 1H), 8.45 (s, 1H), 8.38 (s, 1H), 8.31 (d, ³*J* = 8.0 Hz, 1H), 8.19 (d, ³*J* = 8.0 Hz, 2H), 8.00 (d, ³*J* = 7.6 Hz, 1H), 7.86 (d, ³*J* = 7.8 Hz, 2H), 7.55 (t, ³*J* = 7.8 Hz, 2H), 7.45 (d, ³*J* = 8.0 Hz, 2H), 7.34 (t, ³*J* = 7.6 Hz, 1H), 4.84 (d, ³*J* = 5.8 Hz, 2H), 4.46–4.34 (m, 1H), 3.79–3.64 (m, 1H), 3.53–3.40 (m, 1H), 3.37–3.23 (m, 1H), 2.84 (s, 3H), 2.83–2.69 (m, 1H), 2.59–2.41 (m, 1H), 1.86–1.32 (m, 11H),

1.30–1.01 (m, 6H), 0.95–0.72 (m, 2H) ppm. ^{13}C -NMR (150 MHz, DMSO- d_6 , 300 K): (mixture of diastereomers) δ = 171.6, 166.1, 156.4, 152.9, 142.4, 138.9, 133.7, 132.9, 129.1, 127.7, 127.0, 126.1, 120.7, 101.8, 53.4, 49.5, 49.4, 45.3, 45.2, 45.1, 43.0, 36.8, 34.4, 34.3, 33.2, 32.9, 32.6, 29.4, 28.6, 26.1, 25.7, 22.9 ppm. MS (ESI pos.): m/z (%) = 673.25 (100) ($[\text{M}+\text{H}]^+$, calcd. 673.33), 494.98 (26) ($[\text{M}_{\text{fr}}]^+$, calcd. 495.28). HRMS (FTMS + p MALDI): m/z = 695.3099 ($[\text{M}+\text{Na}]^+$, calcd. for $[\text{C}_{35}\text{H}_{44}\text{N}_8\text{NaO}_4\text{S}]^+$ = 695.3104).

***N*-(4-(((*S*)-4-Cyclohexyl-1-(((*SR*)-1-(methylsulfonyl)piperidin-3-yl)amino)-1-oxobutan-2-yl)carbamoyl)benzyl)imidazo[1,2-*a*]pyridine-3-carboxamide (30)**

4-((Imidazo[1,2-*a*]pyridine-3-carboxamido)methyl)benzoic acid (**27c**, 200 mg, 0.677 mmol) and HATU (309 mg, 0.813 mmol) were dissolved in DMF (5 mL), and DIPEA (105 mg, 0.813 mmol) was added. The solution was stirred for 1.5 h at RT, and (*S*)-2-amino-4-cyclohexyl-*N*-((*SR*)-1-(methylsulfonyl)piperidin-3-yl)butanamide (**11d**, 281 mg, 0.813 mmol), diluted in DMF (5 mL), was added. The mixture was stirred for 20 h at RT. DCM (150 mL) was added, and the organic phase was washed 5 times with H₂O (150 mL) and dried over MgSO₄. The solvent was evaporated under reduced pressure, and the crude product was purified using column chromatography on silica (EtOAc/MeOH 10:1) to afford 48 mg (0.077 mmol, 11%) of compound **30** as a colorless solid. TLC: R_f = 0.19 (SiO₂, EtOAc/MeOH 10:1). HPLC: (mixture of diastereomers) $t_{R,1}$ = 7.88 min; $t_{R,2}$ = 8.04 min, purity: 93%. ^1H -NMR (300 MHz, DMSO- d_6 , 300 K): (mixture of diastereomers) δ = 9.47 (d, 3J = 7.0 Hz, 1H), 9.09 (t, 3J = 6.1 Hz, 1H), 8.40 (s, 1H), 8.31 (d, 3J = 8.0 Hz, 1H), 8.00 (d, 3J = 7.5 Hz, 1H), 7.85 (d, 3J = 8.3 Hz, 2H), 7.72 (d, 3J = 9.0 Hz, 1H), 7.51–7.31 (m, 3H), 7.12 (td, 3J = 6.9, 1.3 Hz, 1H), 4.57 (d, 3J = 6.1 Hz, 2H), 4.45–4.33 (m, 1H), 3.79–3.65 (m, 1H), 3.53–3.37 (m, 1H), 3.36–3.25 (m, 1H), 2.85 (s, 3H), 2.83–2.70 (m, 1H), 2.59–2.41 (m, 1H), 1.88–1.31 (m, 11H), 1.29–1.00 (m, 6H), 0.93–0.71 (m, 2H) ppm. ^{13}C -NMR (75 MHz, DMSO- d_6 , 300 K): (mixture of diastereomers) δ = 171.7, 166.1, 160.2, 146.9, 143.0, 136.9, 132.8, 127.6 (2x), 127.0, 126.9, 118.0, 117.3, 113.9,

107.0, 53.6, 53.4, 49.4, 45.4, 45.2, 45.1, 41.6, 36.8, 34.4, 34.3, 33.3, 32.9, 32.7, 29.4, 28.6, 26.1 (2x), 25.8, 23.0 ppm. MS (ESI neg.): m/z (%) = 667.29 (100) ($[M+EtOH-H]^-$, calcd. 667.32), 621.30 (94) ($[M-H]^-$, calcd. 621.28), 361.24 (48) ($[M_{fr}+EtOH+H]^-$, calcd. 361.24). HRMS (FTMS + p MALDI): m/z 645.2801 $[M+Na]^+$, calcd. for $[C_{32}H_{42}N_7NaO_5S]^+ = 645.2835$.

***N*-(((*SR*)-1-(4-(((*S*)-4-Cyclohexyl-1-(((*SR*)-1-(methylsulfonyl)piperidin-3-yl)amino)-1-oxobutan-2-yl)carbamoyl)phenyl)ethyl)imidazo[1,2-*a*]pyridine-3-carboxamide (**31**)**

4-(1-(imidazo[1,2-*a*]pyridine-3-carboxamido)ethyl)benzoic acid (**27f**, 200 mg, 0.65 mmol) and HATU (295 mg, 0.78 mmol) were dissolved in DMF (6 mL), and DIPEA (100 mg, 0.78 mmol) was added. The solution was stirred for 1.5 h at RT and (*S*)-2-amino-4-cyclohexyl-*N*-(((*SR*)-1-(methylsulfonyl)piperidin-3-yl)butanamide (**11d**, 268 mg, 0.78 mmol), diluted in DMF (6 mL), was added. The mixture was stirred for 20 h at RT. DCM (100 mL) was added, and the organic phase was washed 4 times with H₂O (100 mL) and dried over MgSO₄. The solvent was evaporated under reduced pressure, and the crude product was purified using column chromatography on silica (hexane/EtOAc 1:1 → EtOAc → EtOAc/MeOH 10:1) to afford 209 mg (0.33 mmol, 51%) of compound **31** as a colorless solid. TLC: R_f = 0.20 (SiO₂, EtOAc/MeOH 10:1). HPLC: (mixture of diastereomers) $t_{R,1}$ = 7.96 min; $t_{R,2}$ = 8.12 min, purity: >95%. ¹H-NMR (600 MHz, DMSO-*d*₆, 300 K): (mixture of diastereomers) δ = 9.41 (d, ³*J* = 6.9 Hz, 1H), 8.84 (d, ³*J* = 7.9 Hz, 1H), 8.49 (d, ⁴*J* = 1.5 Hz, 1H), 8.30 (d, ³*J* = 8.1 Hz, 1H), 7.99 (d, ³*J* = 7.5 Hz, 1H), 7.85 (dt, ³*J* = 8.3, 3.0 Hz, 2H), 7.70 (dt, ³*J* = 9.0, 1.1 Hz, 1H), 7.49 (d, ³*J* = 8.3 Hz, 2H), 7.44 (ddd, ³*J* = 9.0, 6.8, 1.3 Hz, 1H), 7.08 (td, ³*J* = 6.9, 1.1 Hz, 1H), 5.25 (p, ³*J* = 7.2 Hz, 1H), 4.43–4.36 (m, 1H), 3.76–3.69 (m, 1H), 3.51–3.41 (m, 1H), 3.36–3.29 (m, 1H), 2.84 (s, 3H), 2.79–2.71 (m, 1H), 2.57–2.52 (m, 1H), 1.84–1.55 (m, 10H), 1.52 (d, ³*J* = 7.1 Hz, 3H), 1.44–1.31 (m, 1H), 1.28–1.06 (m, 6H), 0.89–0.77 (m, 2H) ppm. ¹³C-NMR (150 MHz, DMSO-*d*₆, 300 K): (mixture of diastereomers) δ = 171.6, 166.1, 159.4, 148.2, 146.9, 137.0, 132.7, 127.6, 127.5, 126.9, 125.8, 118.0, 117.2, 113.8, 53.5, 53.4, 49.6, 49.4, 47.7, 45.4, 45.2, 45.1, 36.8 (2x), 34.4,

34.3, 33.2, 32.9, 32.6, 29.4, 28.9, 28.6, 26.1, 25.8, 25.7, 23.0 (2x), 22.2, 22.1 ppm. MS (ESI pos.): m/z (%) = 637.50 (100) ($[M+H]^+$, calcd. 637.32), 459.31 (60) ($[M_{fr.}]^+$, calcd. 459.24). HRMS (FTMS + p MALDI): m/z 637.3173 $[M+H]^+$, calcd. for $[C_{33}H_{45}N_6O_5S]^+ = 637.3172$.

5-Amino-*N*-(4-(((*S*)-4-cyclohexyl-1-(((*SR*)-1-(methylsulfonyl)piperidin-3-yl)amino)-1-oxobutan-2-yl)carbamoyl)benzyl)-1-methyl-1*H*-pyrazole-4-carboxamide (32)

4-((5-Amino-1-methyl-1*H*-pyrazole-4-carboxamido)methyl)benzoic acid (**27d**, 200 mg, 0.73 mmol) and HATU (333 mg, 0.88 mmol) were dissolved in DMF (5 mL), and DIPEA (113 mg, 0.88 mmol) was added. The solution was stirred for 1.5 h at RT (*S*)-2-amino-4-cyclohexyl-*N*-(((*SR*)-1-(methylsulfonyl)piperidin-3-yl)butanamide (**11d**, 302 mg, 0.875 mmol), diluted in DMF (5 mL), was added. The mixture was stirred for 20 h at RT. DCM (100 mL) was added, and the organic phase was washed 4 times with H₂O (100 mL) and dried over MgSO₄. The solvent was evaporated under reduced pressure, the crude product was triturated with EtOAc/cyclohexane (1:1) and recrystallized from DCM to afford 281 mg (0.47 mmol, 64%) of compound **32** as a colorless solid. TLC: R_f = 0.37 (SiO₂, DCM/MeOH 10:1). HPLC: (mixture of diastereomers) $t_{R,1}$ = 8.17 min; $t_{R,2}$ = 8.34 min, purity: 94%. ¹H-NMR (300 MHz, DMSO-*d*₆, 300 K): (mixture of diastereomers) δ = 8.35–8.24 (m, 2H), 8.01 (d, ³*J* = 7.6 Hz, 1H), 7.83 (d, ³*J* = 7.2 Hz, 2H), 7.68 (s, 1H), 7.36–7.28 (m, 2H), 6.15 (s, 2H), 4.46–4.35 (m, 3H), 3.77–3.67 (m, 1H), 3.51 (s, 3H), 3.50–3.40 (m, 1H), 3.36–3.28 (m, 1H), 2.90–2.71 (m, 4H), 2.58–2.47 (m), 1.82–1.48 (m, 10H), 1.45–1.31 (m, 1H), 1.28–1.03 (m, 6H), 0.90–0.79 (m, 2H) ppm. ¹³C-NMR (75 MHz, DMSO-*d*₆, 300 K): (mixture of diastereomers) δ = 171.6 (2x), 166.1 (2x), 164.1, 149.4, 143.8, 136.1, 132.6, 132.5, 127.5, 127.0, 126.7, 126.6, 96.7, 53.5, 53.4, 49.6, 49.4, 45.4, 45.2, 45.1, 41.2, 36.8, 34.4, 34.3, 33.9, 33.2, 32.9, 32.8, 32.7, 32.6, 29.4, 28.9, 28.6, 26.1, 25.8 (2x), 23.0, 22.9 ppm. MS (ESI neg.): m/z (%) = 646.16 (39) ($[M+EtOH-H]^-$, calcd. 646.33), 600.19 (100) ($[M-H]^-$, calcd. 600-29). HRMS (FTMS + p MALDI): m/z = 624.2950 $[M+Na]^+$, calcd. for $[C_{29}H_{43}N_7NaO_5S]^+ = 624.2944$.

5-Amino-*N*-((*SR*)-1-(4-(((*S*)-4-cyclohexyl-1-(((*SR*)-1-(methylsulfonyl)piperidin-3-yl)amino)-1-oxobutan-2-yl)carbamoyl)phenyl)ethyl)-1-methyl-1*H*-pyrazole-4-carboxamide (33**)**

4-(1-(5-Amino-1-methyl-1*H*-pyrazole-4-carboxamido)ethyl)benzoic acid (**27e**, 125 mg, 0.40 mmol) and HATU (184 mg, 0.49 mmol) were dissolved in DMF (5 mL) and DIPEA (63 mg, 0.40 mmol) was added. The solution was stirred for 1.5 h at RT (*S*)-2-amino-4-cyclohexyl-*N*-((*SR*)-1-(methylsulfonyl)piperidin-3-yl)butanamide (**11d**, 168 mg, 0.49 mmol), diluted in DMF (5 mL) was added. The mixture was stirred for 20 h at RT. DCM (100 mL) was added, and the organic phase was washed 3 times with H₂O (100 mL), once with a NaCl solution (sat., 50 mL) and dried over MgSO₄. The solvent was evaporated under reduced pressure, and the crude product was purified using flashcolumn chromatography on silica (cyclohexane/EtOAc 1:1 → EtOAc → EtOAc/MeOH 10:1) to afford 162 mg (0.26 mmol, 65%) of compound **33** as a colorless solid. TLC: R_f = 0.24 (SiO₂, EtOAc/MeOH 10:1). HPLC: (mixture of diastereomers) $t_{R,1}$ = 8.34 min; $t_{R,2}$ = 8.51 min, purity: >95%. ¹H-NMR (600 MHz, DMSO-*d*₆, 300 K): (mixture of diastereomers) δ = 8.28 (d, ³*J* = 8.1 Hz, 1H), 8.02 (d, ³*J* = 7.8 Hz, 1H), 7.99 (d, ³*J* = 8.0 Hz, 1H), 7.82 (dt, ³*J* = 8.4, 2.6 Hz, 2H), 7.77 (s, 1H), 7.40 (d, ³*J* = 8.4 Hz, 2H), 6.10 (s, 2H), 5.11 (p, ³*J* = 7.3 Hz, 1H), 4.43–4.35 (m, 1H), 3.80–3.68 (m, 1H), 3.52–3.47 (m, 1H), 3.49 (s, 3H), 3.46–3.42 (m, 1H), 2.86–2.68 (m, 4H), 2.57–2.48 (m, 1H), 1.84–1.48 (m, 10H), 1.42 (d, ³*J* = 7.1 Hz, 3H), 1.45–1.30 (m, 1H), 1.28–1.05 (m, 6H), 0.92–0.78 (m, 2H) ppm. ¹³C-NMR (150 MHz, DMSO-*d*₆, 300 K): (mixture of diastereomers) δ = 171.6 (2x), 166.2, 166.1, 163.4, 149.4, 148.9, 136.2, 132.4, 127.4, 125.7, 113.7, 96.7, 53.5, 53.4, 49.5, 49.4, 49.2, 47.1, 45.4 (2x), 45.2, 45.1, 36.9, 36.8, 34.4, 34.3, 33.8, 33.2, 32.9, 32.6, 29.4, 28.9, 28.6, 26.1 (2x), 26.1 (2x), 25.8 (2x), 25.7, 23.0 (2x), 22.3, 22.2 ppm. MS (ESI pos.): m/z (%) = 616.22 (100) ([*M*+*H*]⁺, calcd. 616.33), 438.14 (37) ([*M*_{fr.}]⁺, calcd. 438.25). HRMS (FTMS + p MALDI): m/z 638.3092 [*M*+*Na*]⁺, calcd. for [C₃₀H₄₅N₇NaO₅S]⁺ = 638.3101.

rac-tert-Butyl (1-(methanesulfonyl)piperidin-3-yl)carbamate (36a)

rac-tert-Butyl piperidin-3-ylcarbamate (34a, 801 mg, 4.00 mmol) was dissolved in DCM (dry, 20 mL), and triethylamine (405 mg, 4.00 mmol) was added. The solution was cooled to -15 °C, and methanesulfonyl chloride (**35a**, 687 mg, 6.00 mmol) was added dropwise. The mixture was stirred for 6 h at RT. The reaction mixture was acidified with NH₄Cl (sat., 3 mL) and extracted 3 times with DCM. The separated organic phase was washed 3 times with H₂O (20 mL) and dried over MgSO₄. The solvent was evaporated under reduced pressure to afford 1.08 mg (3.88 mmol, 97%) of **36a** as a colorless solid. TLC: R_f = 0.63 (SiO₂, cyclohexane/EtOAc, 1:20, ninhydrin). ¹H-NMR (500 MHz, CDCl₃, 300 K): δ = 4.95–4.78 (m, 1H), 3.89–3.74 (m, 1H), 3.72–2.95 (m, 4H), 2.77 (s, 3H), 1.88–1.57 (m, 4H), 1.43 (s, 9H) ppm. ¹³C-NMR (126 MHz, CDCl₃, 300 K): δ = 155.0, 79.8, 50.8, 46.3, 45.6, 35.2, 29.2, 28.5, 22.1 ppm. MS (ESI neg.): *m/z* (%) = 323.08 (84) ([M+EtOH-H]⁻, calcd. 323.16), 313.06 (100) ([M+Cl]⁻, calcd. 313.58), 162.95 (67) ([M_{fr.}]⁻, calcd. 162.95), 160.92 (60) ([M_{fr.}-H]⁻, calcd. 160.94).

tert-Butyl (S)-(1-(methanesulfonyl)piperidin-3-yl)carbamate (36b)

The synthesis of *tert-butyl (S)-(1-(methanesulfonyl)piperidin-3-yl)carbamate (36b)* was performed in analogy to compound **36a**. *tert-Butyl (S)-piperidin-3-ylcarbamate (34b*, 801 mg, 4.00 mmol) was used as starting material to afford 1.03 g (3.71 mmol, 93%) of compound **36b** as a colorless solid. TLC: R_f = 0.63 (SiO₂, cyclohexane/EtOAc, 1:20, ninhydrin). ¹H-NMR (250 MHz, CDCl₃, 300 K): δ = 6.95 (d, ³*J* = 7.5 Hz, 1H), 3.58–3.46 (m, 1H) 3.40–3.01 (m, 2H), 2.85 (s, 3H), 2.71–2.57 (m, 1H), 2.47–2.35 (m, 1H), 1.84–1.67 (m, 2H), (s, 9H), 1.59–1.11 (m, 2H) ppm. ¹³C-NMR (126 MHz, CDCl₃, 300 K): δ = 155.0, 79.8, 50.8, 46.3, 45.6, 35.2, 29.2, 28.5, 22.1 ppm. MS (ESI neg.): *m/z* (%) = 323.15 (100) ([M+EtOH-H]⁻, calcd. 323.16), 313.13 (39) ([M+Cl]⁻, calcd. 313.58).

tert-Butyl (R)-(1-(methanesulfonyl)piperidin-3-yl)carbamate (36c)

The synthesis of *tert*-butyl (*R*)-(1-(methylsulfonyl)piperidin-3-yl)carbamate (**36c**) was performed analogously to compound **36b**. *tert*-Butyl (*R*)-piperidin-3-ylcarbamate (**34c**, 801 mg, 4.00 mmol), was used as starting material to afford 915 mg (3.29 mmol, 97%) of compound **36c** as a light brownish solid. The analytical data are in accordance with compound **36b**.

***rac-tert*-Butyl (1-(cyclopropanecarbonyl)piperidin-3-yl)carbamate (36d)**

Cyclopropanecarboxylic acid (**35b**, 215 mg, 2.50 mmol) and HATU (1.14 g, 3.00 mmol) were dissolved in DMF (dry, 7 mL) and DIPEA (387 mg, 3.00 mmol) was added. The reaction mixture was stirred for 1.5 h at RT, and *rac-tert*-butyl piperidin-3-ylcarbamate (**34a**, 600 mg, 3.00 mmol) dissolved in DMF (dry, 5 mL) was added. The mixture was stirred for additional 20 h at RT. DCM (100 mL) was added, and the organic phase was washed 4 times with H₂O (100 mL), once with NH₄Cl (sat. 100 mL) and dried over MgSO₄. The solvent was evaporated under reduced pressure, and the crude product was purified using column chromatography on silica (cyclohexane/EtOAc 1:9). Compound **36d** was obtained in a yield of 636 mg (2.37 mmol, 95%) as a colorless solid. TLC: *R*_f = 0.56 (SiO₂, cyclohexane/EtOAc, 1:9, ninhydrin). ¹H-NMR (500 MHz, CDCl₃, 300 K): δ = 4.73–4.54 (m, 1H), 4.05–2.84 (m, 5H), 1.97–1.86 (m, 1H), 1.81–1.49 (m, 4H), 1.42 (s, 9H), 1.01–0.89 (m, 2H), 0.80–0.66 (m, 2H) ppm. ¹³C-NMR (126 MHz, CDCl₃, 300 K): δ = 172.7, 155.3, 79.7, 50.4, 46.9, 42.7, 30.3, 28.8, 22.5, 11.0, 7.7 ppm. MS (ESI pos.): *m/z* (%) = 307.17 (23) ([M+K]⁺, calcd. 307.27), 291.20 (100) ([M+Na]⁺, calcd. 291.17), 269.21 (5) ([M+H]⁺, calcd. 269.19), 169.12 (32) ([M-Boc+H]⁺, calcd. 169.14).

***rac-tert*-Butyl (1-(oxetan-3-yl)piperidin-3-yl)carbamate (36e)**

rac-tert-Butyl piperidin-3-ylcarbamate (**34a**, 400 mg, 2.00 mmol) was dissolved in THF (dry, 10 mL), and oxetan-3-one (**35c**, 107 μL, 1.66 mmol) was added at 0 °C. The mixture was stirred for 1.5 h and allowed to warm to RT. Sodium triacetoxyborohydride (708 mg, 3.33 mmol) was

added, and the suspension was stirred for additional 20 h at RT. The reaction was quenched with NaHCO₃ (sat., 30 mL), and the solvent was evaporated under reduced pressure. The residue was dissolved in EtOAc (30 mL), H₂O (30 mL) was added and extracted 4 times with EtOAc (30 mL). The organic phase was dried over MgSO₄. The solvent was evaporated under reduced pressure, and the crude product was purified using column chromatography on silica (cyclohexane/EtOAc 1:20 + 1% TEA). Compound **36e** was obtained in a yield of 240 mg (0.937 mmol, 47%) as a colorless solid. TLC: R_f = 0.20 (SiO₂, cyclohexane/EtOAc + 1% TEA, 1:20, ninhydrin). ¹H-NMR (500 MHz, CDCl₃, 300 K): δ = 5.16–4.92 (m, 1H, NH), 4.66–4.50 (m, 4H), 3.82–3.69 (m, 1H), 3.41 (p, ³J = 6.4 Hz, 1H), 2.47–1.83 (m, 4H), 1.81–1.33 (m, 4H), 1.43 (s, 9H) ppm. ¹³C-NMR (126 MHz, CDCl₃, 300 K): δ = 155.2, 79.3, 75.9, 59.1, 55.2, 50.2, 45.8, 29.6, 28.6, 21.9 ppm. MS (ESI neg.): m/z (%) = 255.20 (100) ([M-H]⁻, calcd. 255.17).

***rac*-1-(Methylsulfonyl)piperidin-3-amine (37a)**

rac-*tert*-Butyl (1-(methylsulfonyl)piperidin-3-yl)carbamate (**36a**, 450 mg, 1.62 mmol) was dissolved in DCM (10 mL), cooled to 0 °C, and TFA (2 mL) was added dropwise. The mixture was stirred for 1 h allowing to warm up to RT. The solvent was removed under reduced pressure, and the residue was dissolved in MeOH. The mixture was cooled to 5 °C, K₂CO₃ (3.6 g, 26.0 mmol) was added and stirred for 10 min. The solid was filtered off, and the solvent was removed under reduced pressure. The quantitatively obtained crude product was used without further purification in the next step.

(*S*)-1-(Methylsulfonyl)piperidin-3-amine (37b)

The synthesis of (*S*)-1-(methylsulfonyl)piperidin-3-amine (**37b**) was performed analogously to compound **37a**. *tert*-Butyl (*S*)-(1-(methylsulfonyl)piperidin-3-yl)carbamate (**36b**, 420 mg, 1.51 mmol) was used as starting material to afford compound **37b** in quantitative yield. The product was used without further purification in the next step.

(R)-1-(Methylsulfonyl)piperidin-3-amine (37c)

The synthesis of (R)-1-(methylsulfonyl)piperidin-3-amine (**37c**) was performed analogously to compound **37b**. The starting material was *tert*-butyl (R)-(1-(methylsulfonyl)piperidin-3-yl)carbamate (**36c**, 420 mg, 1.51 mmol). The crude product was obtained in quantitative yield and used without further purification in the next step.

***rac*-(3-Aminopiperidin-1-yl) (cyclopropyl)methanone (37d)**

The synthesis of *rac*-(3-aminopiperidin-1-yl) (cyclopropyl)methanone (**37d**) was performed analogously to compound **37a**. *rac-tert*-Butyl (1-(cyclopropanecarbonyl)piperidin-3-yl)carbamate (**36d**, 430 mg, 1.60 mmol) was used as starting material to afford compound **37d** in quantitative yield. The crude product was used without further purification in the next step.

***rac*-1-(Oxetan-3-yl)piperidin-3-amine (37e)**

The synthesis of *rac*-1-(oxetan-3-yl)piperidin-3-amine (**37e**) was performed analogously to compound **37d**. *rac-tert*-Butyl (1-(oxetan-3-yl)piperidin-3-yl)carbamate (**36e**, 350 mg, 1.37 mmol) was used as starting material to afford compound **37e** in quantitative yield. The crude product was used without further purification in the next step.

Biological and Biochemical Methods.

1. Differential scanning fluorimetry (DSF) assay. Differences in the melting temperature (ΔT_m) data were measured as described in Fedorov et al.³⁰

2. NanoBRET assay. The assay was performed as described previously.^{31, 32} In brief, full-length kinase ORF (Promega) cloned in frame with a NanoLuc-vector (as indicated in Table S7) was transfected into HEK293T cells using FuGENE HD (Promega, E2312), and proteins were allowed to express for 20 h. Serially diluted inhibitor and NanoBRETTM kinase tracer at the respective previously determined tracer $K_{d, app}$ (as indicated in Table S7) were pipetted into white 384-well plates (Greiner 781 207) using an ECHO 550 acoustic dispenser (Labcyte). The

corresponding transfected cells were added and reseeded at a density of 2×10^5 cells/mL after trypsinization and resuspension in Opti-MEM without phenol red (Life Technologies). The system was allowed to equilibrate for 2 hours at 37 °C and 5% CO₂ prior to BRET measurements. To measure BRET, NanoBRET™ NanoGlo Substrate + Extracellular NanoLuc Inhibitor (Promega, N2160) were added as per the manufacturer's protocol, and filtered luminescence was measured on a PHERAstar plate reader (BMG Labtech) equipped with a luminescence filter pair (450 nm BP filter (donor) and 610 nm LP filter (acceptor)). Competitive displacement data were then plotted using GraphPad Prism 8 software using a 4-parameter curve fit with the following equation: $Y = \text{Bottom} + (\text{Top} - \text{Bottom}) / (1 + 10^{((\text{Log}IC_{50} - X) * \text{HillSlope}))}$

3. Protein purification and crystallography.

Murine MAP kinase p38α was expressed in *E. coli* and purified as previously described.³³ The kinase domain of human DDR1 (residues 601-913) was expressed in baculovirus and purified following the published procedure.⁹ Crystals of p38α and DDR1 inhibitor complexes were grown in 3-well crystallization plates (SwisSCI) using the sitting-drop vapor diffusion method. Recombinant p38α (10-13 mg/ml) was incubated with 1 mM of the corresponding inhibitor, and the complexes were crystallized at 4 °C using PEG smears-based conditions containing either 17.0-22.5% medium-molecular-weight PEG smears and 0.1 M MES pH 6.0-6.5, or 14% high-molecular-weight PEG smears and 0.1 M MES, pH 6.0. For the DDR1-**13** complex, the protein (10 mg/mL DDR1 in 50 mM HEPES, pH 7.5, 300 mM NaCl, and 1 mM TCEP) was mixed with **13** at a final inhibitor concentration of 1 mM. Crystals were then grown at 20 °C with a reservoir solution consisting of 20% PEG 3350, 10% ethylene glycol, 0.1 M Bis-tris propane, pH 6.5, and 0.2 M sodium sulfate (50 nL protein and 100 nL reservoir). Crystals of the DDR1-**30** complex, were grown at 4 °C by mixing the protein solution (100 nL, 16 mg/mL DDR1, 1 mM **30**) with 100 nL precipitant solution consisting of 20% PEG 10000 and 0.1 M HEPES, pH 7.5). Crystals of the inhibitor complexes were cryoprotected with mother liquor

complemented with 20-25% ethylene glycol and flash frozen in liquid nitrogen. X-ray diffraction data were collected at 100K at Diamond beamlines i04 and i04-1, BESSY beamline 14.1 and Swiss Light Source (SLS) beamline X06SA. The data were processed with either Xia2³⁴ or XDS³⁵ and Aimless.³⁶ The structures were then solved by molecular replacement using Phaser³⁷ and published p38 α (PDB ID: 5LAR) or DDR1 (PDB IDs: 4BKJ and 5FDX) coordinates as a search model. The structural models were then manually rebuilt in COOT³⁸ and refined using either REFMAC³⁹ or PHENIX.⁴⁰ The data collection and refinement statistics are summarized in Table S8. Structure figures were generated using PyMOL (<https://pymol.org/2/>).

4. Live cell high-content screen. To assess the influence of the compounds on cell viability and the potential effect on microtubules, a live cell high-content screen was performed, using a confocal microscope (CQ1, Yokogawa). HEK293T (ATCC® CRL-1573™) and U2OS (ATCC® HTB-96™) were cultured in DMEM plus L-glutamine (High glucose) supplemented with 10% FBS (Gibco) and penicillin/streptomycin (Gibco). MRC-9 fibroblasts (ATCC® CCL-2™) were cultured in EMEM plus L-glutamine supplemented with 10% FBS (Gibco) and penicillin/streptomycin (Gibco). For every cell line, 2000 cells per well were seeded in 384-well plates in culture medium (cell culture microplate, PS, f-bottom, μ Clear®, 781091, Greiner). Cells were stained with 75 nM Hoechst33342 (Thermo Scientific), 75 nM Mitotracker red (Invitrogen), 0.3 μ l/well Annexin V Alexa Fluor 680 conjugate (Invitrogen) and 25 nL /well BioTracker™ 488 Green Microtubule Cytoskeleton Dye (EMD Millipore). Each compound (**28**, **30**, **38**, **39**) was tested at two different concentrations (1 μ M and 10 μ M) in triplicates. Staurosporine 10 μ M was used as a positive control. Cellular shape and fluorescence were measured before compound treatment and 12 h, 24 h, and 48 h after compound exposure, respectively, using the CQ1 high-content confocal microscope (Yokogawa). The following setup parameters were used for image acquisition: Ex 405 nm/Em 447/60 nm, 500 ms, 50%;

Ex 561 nm/Em 617/73 nm, 100 ms, 40%; Ex 488/Em 525/50 nm, 50 ms, 40%; bright field, 300 ms, 100% transmission, one centered field per well, 7 z stacks per well with 55 μ m spacing. Images were analyzed using the CellPathfinder software (Yokogawa). Cells were detected as described previously,⁴¹ gated using a machine learning algorithm and divided into the categories healthy, apoptotic, lysed, and dead cells. The program was trained using a training set of five compounds with known effects (staurosporine, paclitaxel, digitonin, milciclib, daunorubicin). Data were normalized against the average of DMSO (0.1%) treated cells. Significance was shown using a two-way ANOVA analysis. Two biological duplicates were performed.

5. TNF- α release assay in human whole blood. The assay was performed as published by Bauer et al.⁴² The assay principle is summarized here in brief: The tested compounds were preincubated in human whole blood from two different donors for 15 min before TNF- α release was stimulated by addition of LPS. After stimulation, the samples were incubated at 37 °C and 6% CO₂ for 2.5 hours followed by centrifugation to separate cells and plasma. The supernatant was separated, and the TNF- α levels were determined using a sandwich ELISA.

6. *In vitro* metabolism studies. Pooled male human liver microsomes (HLM) were purchased from Xenotech. These microsomes were characterized in protein and cytochrome P-450 content. All incubations were made in the presence of an NADPH-regenerating system, consisting of 5 mM glucose-6-phosphate, 5 U/mL glucose-6-phosphate dehydrogenase, and 1 mM NADP⁺. The substrate (100 μ M), the NADPH regenerating system, and 3.8 mM MgCl₂ x 6 H₂O in 0.1 M Tris buffer (pH 7.4 at 37 °C) were pre-incubated for 5 min in a shaking heating block at 37 °C and 650 rpm. The incubation mix was split into 50 μ L aliquots, and the reaction was started by addition of the HLM. The microsomal protein content was standardized to 1 mg/mL. To follow the course of metabolism, the reaction tubes were quenched at selected time

points (0, 10, 20, 30, 60, 120, 180, and 240 min) by adding 100 μ L ice-cold internal standard at a concentration of 20 μ M in acetonitrile (ACN). The samples were vortexed for 30 s and centrifuged (19800 relative centrifugal force/4 $^{\circ}$ C/20 min). The supernatant was used directly for LC-MS analysis. All incubations were conducted in triplicate, and incubations with heat-inactivated HLM were used to show that analyte reduction results from metabolic degradation only. In all incubations, a limit of 1% organic solvent was not exceeded.

6.1. LC-MS analysis. Chromatographic separation was performed on an Alliance 2695 Separations Module (Waters GmbH, Eschborn) using a Dr. Maisch Nucleosil 100 C18, 5 μ , 53 x 4.6 mm column with water (A) and acetonitrile (B) with 0.1% (v/v) formic acid as mobile phase. The following gradient was applied: 20% B from 0–0.2 min, 20–80% B from 0.2–5.5 min, 20% B from 5.6–14 min at a flow rate of 400 μ L/min. Samples were maintained at 4 $^{\circ}$ C, the column temperature was set to 40 $^{\circ}$ C, and the injection volume was 10 μ L. The detection was performed on a Waters Quattro Micro API mass spectrometer (Waters GmbH, Eschborn) operated in electrospray-ionization (+) mode. The spray voltage was set to 4 kV. The heated capillary operated at 270 $^{\circ}$ C, and the desolvation gas flow was set to 650 L/h.

ASSOCIATED CONTENT

Supporting Information. The following supplemental data are available: Supplement information 1: Biochemical assay and selectivity data, as well as X-ray data collection and refinement statistics. Supplement information 2: NMR and HRMS spectra. Molecular formula strings (CSV).

Accession Codes. Coordinates and structure factors of the p38 α and DDR1 inhibitor complexes were deposited in the Protein Data Bank (PDB). Accession codes: 7BE4 (p38 α -13), 7BE5 (p38 α -32), 7BDQ (p38 α -29), 7BDO (p38 α -30), 7BE6 (DDR1-13), and 7BCM (DDR1-30). Authors will release the atomic coordinates upon article publication.

AUTHOR INFORMATION

Corresponding Author

*E-Mail: knapp@pharmchem.uni-frankfurt.de

Author Contributions

S.R. wrote manuscript, did synthesis and contributed to experimental data; Structural studies were performed by M.S., A.C.J., D.M.P., S.M., D.M.P., J.C.B.; NanoBRET was performed by B.-T.B. and further cellular assays by A.T., M.K., and L.K.; C.P., A.N.B., S.M., S.L., and S.K. supervised research. All authors edited and approved the manuscript.

ACKNOWLEDGMENT

S.R., A.C.J, B-T.B, S.M. and S.K. are grateful for support by the SGC, a registered charity (no: 1097737) that receives funds from; AbbVie, Bayer AG, Boehringer Ingelheim, Canada Foundation for Innovation, Eshelman Institute for Innovation, Genentech, Genome Canada through Ontario Genomics Institute [OGI-196], EU/EFPIA/OICR/McGill/KTH/Diamond, Innovative Medicines Initiative 2 Joint Undertaking [EUbOPEN grant 875510], Janssen, Merck KGaA (aka EMD in Canada and US), Merck & Co (aka MSD outside Canada and US), Pfizer, São Paulo Research Foundation-FAPESP, Takeda and Wellcome [106169/ZZ14/Z]. We thank the staff at BESSY, Diamond and SLS for assistance during data collection. Data collection at SLS was supported by funding from the European Union's Horizon 2020 research and innovation program under grant agreement number 730872, project CALIPSOplus. We thank Thales Kronenberger from the University Hospital of Tübingen for predicting the pharmacokinetic properties of our probe compound.

ABBREVIATIONS

Abl1, abelson tyrosine-protein kinase 1; CSF1R, macrophage colony-stimulating factor 1 receptor; DDR, discoidin domain receptor; DIPEA, *N,N*-diisopropylethylamine; DSF, differential scanning fluorimetry; ΔT_m , Differences in the melting temperature; EDC-HCl, 1-ethyl-3-(3-dimethylaminopropyl)carbodiimid-hydrochlorid; EGFR, epidermal growth factor receptor; HATU, *N*-[(dimethylamino)-1*H*-1,2,3-triazolo-[4,5-*b*]pyridin-1-ylmethylene]-*N*-methylmethanaminium hexafluorophosphate *N*-oxide; HLM, human liver microsomes; HOBt, hydroxybenzotriazole; IRK, insulin receptor kinase; KIT, mast/stem cell growth factor receptor Kit; MAPK, mitogene activated protein kinase; MEK5, dual specificity mitogen-activated protein kinase kinase 5; PDGFR, platelet-derived growth factor receptor; Pyk2, Protein-tyrosine kinase 2-beta; RTK, receptor tyrosine kinase; TEA, triethylamine; Tie, tyrosine-protein kinase receptor Tie; TRK, tropomyosin receptor kinase; YSK4, Mitogen-activated protein kinase kinase kinase 19; ZAK, mitogen-activated protein kinase kinase kinase 20.

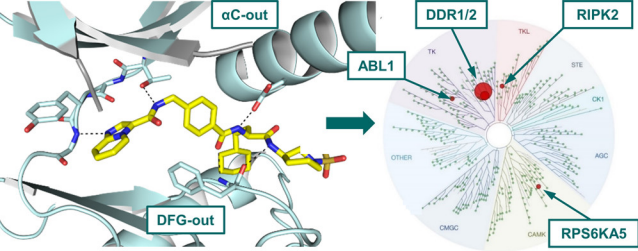
REFERENCES

- (1) Shrivastava, A.; Radziejewski, C.; Campbell, E.; Kovac, L.; McGlynn, M.; Ryan, T. E.; Davis, S.; Goldfarb, M. P.; Glass, D. J.; Lemke, G.; Yancopoulos, G. D. An orphan receptor tyrosine kinase family whose members serve as nonintegrin collagen receptors. *Molecular Cell* **1997**, 1, 25-34.
- (2) Vogel, W.; Gish, G. D.; Alves, F.; Pawson, T. The discoidin domain receptor tyrosine kinases are activated by collagen. *Molecular Cell* **1997**, 1, 13-23.
- (3) Li, Y.; Lu, X.; Ren, X.; Ding, K. Small molecule discoidin domain receptor kinase inhibitors and potential medical applications. *Journal of Medicinal Chemistry* **2015**, 58, 3287-3301.
- (4) Leitinger, B. Molecular analysis of collagen binding by the human discoidin domain receptors, ddr1 and ddr2: Identification of collagen binding sites in ddr2. *Journal of Biological Chemistry* **2003**, 278, 16761-16769.
- (5) Agarwal, G.; Smith, A. W.; Jones, B. Discoidin domain receptors: Micro insights into macro assemblies. *Biochimica et Biophysica Acta (BBA) - Molecular Cell Research* **2019**, 1866, 118496.
- (6) Leitinger, B. Chapter two - discoidin domain receptor functions in physiological and pathological conditions. In *International review of cell and molecular biology*, Jeon, K. W., Ed. Academic Press: 2014; Vol. 310, pp 39-87.
- (7) Yeung, D. A.; Shanker, N.; Sohail, A.; Weiss, B. A.; Wang, C.; Wellmerling, J.; Das, S.; Ganju, R. K.; Miller, J. L. C.; Herr, A. B.; Fridman, R.; Agarwal, G. Clustering, spatial distribution, and phosphorylation of discoidin domain receptors 1 and 2 in response to soluble collagen i. *Journal of Molecular Biology* **2019**, 431, 368-390.

- (8) Artim, S. C.; Mendrola, J. M.; Lemmon, M. A. Assessing the range of kinase autoinhibition mechanisms in the insulin receptor family. *The Biochemical journal* **2012**, 448, 213-220.
- (9) Canning, P.; Tan, L.; Chu, K.; Lee, S. W.; Gray, N. S.; Bullock, A. N. Structural mechanisms determining inhibition of the collagen receptor ddr1 by selective and multi-targeted type ii kinase inhibitors. *Journal of molecular biology* **2014**, 426, 2457-2470.
- (10) Hanson, S. M.; Georghiou, G.; Thakur, M. K.; Miller, W. T.; Rest, J. S.; Chodera, J. D.; Seeliger, M. A. What makes a kinase promiscuous for inhibitors? *Cell Chemical Biology* **2019**, 26, 390-399.e5.
- (11) Richters, A.; Nguyen, H. D.; Phan, T.; Simard, J. R.; Grütter, C.; Engel, J.; Rauh, D. Identification of type ii and iii ddr2 inhibitors. *Journal of Medicinal Chemistry* **2014**, 57, 4252-4262.
- (12) Murray, C. W.; Berdini, V.; Buck, I. M.; Carr, M. E.; Cleasby, A.; Coyle, J. E.; Curry, J. E.; Day, J. E. H.; Day, P. J.; Hearn, K.; Iqbal, A.; Lee, L. Y. W.; Martins, V.; Mortenson, P. N.; Munck, J. M.; Page, L. W.; Patel, S.; Roomans, S.; Smith, K.; Tamanini, E.; Saxty, G. Fragment-based discovery of potent and selective ddr1/2 inhibitors. *ACS medicinal chemistry letters* **2015**, 6, 798-803.
- (13) Liu, L.; Hussain, M.; Luo, J.; Duan, A.; Chen, C.; Tu, Z.; Zhang, J. Synthesis and biological evaluation of novel dasatinib analogues as potent ddr1 and ddr2 kinase inhibitors. *Chemical Biology & Drug Design* **2017**, 89, 420-427.
- (14) Gao, M.; Duan, L.; Luo, J.; Zhang, L.; Lu, X.; Zhang, Y.; Zhang, Z.; Tu, Z.; Xu, Y.; Ren, X.; Ding, K. Discovery and optimization of 3-(2-(pyrazolo[1,5-a]pyrimidin-6-yl)ethynyl)benzamides as novel selective and orally bioavailable discoidin domain receptor 1 (ddr1) inhibitors. *Journal of Medicinal Chemistry* **2013**, 56, 3281-3295.
- (15) Wang, Z.; Zhang, Y.; Pinkas, D. M.; Fox, A. E.; Luo, J.; Huang, H.; Cui, S.; Xiang, Q.; Xu, T.; Xun, Q.; Zhu, D.; Tu, Z.; Ren, X.; Brekken, R. A.; Bullock, A. N.; Liang, G.; Ding, K.; Lu, X. Design, synthesis, and biological evaluation of 3-(imidazo[1,2-a]pyrazin-3-ylethynyl)-4-isopropyl- n-(3-((4-methylpiperazin-1-yl)methyl)-5-(trifluoromethyl)phenyl)benzamide as a dual inhibitor of discoidin domain receptors 1 and 2. *Journal of medicinal chemistry* **2018**, 61, 7977-7990.
- (16) Wang, Z.; Bian, H.; Bartual, S. G.; Du, W.; Luo, J.; Zhao, H.; Zhang, S.; Mo, C.; Zhou, Y.; Xu, Y.; Tu, Z.; Ren, X.; Lu, X.; Brekken, R. A.; Yao, L.; Bullock, A. N.; Su, J.; Ding, K. Structure-based design of tetrahydroisoquinoline-7-carboxamides as selective discoidin domain receptor 1 (ddr1) inhibitors. *Journal of medicinal chemistry* **2016**, 59, 5911-5916.
- (17) Wang, Z.; Zhang, Y.; Bartual, S. G.; Luo, J.; Xu, T.; Du, W.; Xun, Q.; Tu, Z.; Brekken, R. A.; Ren, X.; Bullock, A. N.; Liang, G.; Lu, X.; Ding, K. Tetrahydroisoquinoline-7-carboxamide derivatives as new selective discoidin domain receptor 1 (ddr1) inhibitors. *ACS medicinal chemistry letters* **2017**, 8, 327-332.
- (18) Müller, S.; Ackloo, S.; Arrowsmith, C. H.; Bauser, M.; Baryza, J. L.; Blagg, J.; Böttcher, J.; Bountra, C.; Brown, P. J.; Bunnage, M. E.; Carter, A. J.; Damerell, D.; Dötsch, V.; Drewry, D. H.; Edwards, A. M.; Edwards, J.; Elkins, J. M.; Fischer, C.; Frye, S. V.; Gollner, A.; Grimshaw, C. E.; Ijzerman, A.; Hanke, T.; Hartung, I. V.; Hitchcock, S.; Howe, T.; Hughes, T. V.; Laufer, S.; Li, V. M. J.; Liras, S.; Marsden, B. D.; Matsui, H.; Mathias, J.; O'Hagan, R. C.; Owen, D. R.; Pande, V.; Rauh, D.; Rosenberg, S. H.; Roth, B. L.; Schneider, N. S.; Scholten, C.; Singh Saikatendu, K.; Simeonov, A.; Takizawa, M.; Tse, C.; Thompson, P. R.; Treiber, D. K.; Viana, A. Y. I.; Wells, C. I.; Willson, T. M.; Zuercher, W. J.; Knapp, S.; Mueller-Fahrnow, A. Donated chemical probes for open science. *eLife* **2018**, 7, e34311.
- (19) Klein, R.; Silos-Santiago, I.; Smeyne, R. J.; Lira, S. A.; Brambilla, R.; Bryant, S.; Zhang, L.; Snider, W. D.; Barbacid, M. Disruption of the neurotrophin-3 receptor gene trkc eliminates la muscle afferents and results in abnormal movements. *Nature* **1994**, 368, 249-251.

- (20) Smeyne, R. J.; Klein, R.; Schnapp, A.; Long, L. K.; Bryant, S.; Lewin, A.; Lira, S. A.; Barbacid, M. Severe sensory and sympathetic neuropathies in mice carrying a disrupted *trk/ngf* receptor gene. *Nature* **1994**, 368, 246-249.
- (21) Schneider, H.; Szabo, E.; Machado, R. A. C.; Broggini-Tenzer, A.; Walter, A.; Lobell, M.; Heldmann, D.; Süßmeier, F.; Grünwald, S.; Weller, M. Novel tie-2 inhibitor bay-826 displays in vivo efficacy in experimental syngeneic murine glioma models. *Journal of Neurochemistry* **2017**, 140, 170-182.
- (22) Richter, H.; Satz, A. L.; Bedoucha, M.; Buettelmann, B.; Petersen, A. C.; Harmeier, A.; Hermosilla, R.; Hochstrasser, R.; Burger, D.; Gsell, B.; Gasser, R.; Huber, S.; Hug, M. N.; Kocer, B.; Kuhn, B.; Ritter, M.; Rudolph, M. G.; Weibel, F.; Molina-David, J.; Kim, J.-J.; Santos, J. V.; Stihle, M.; Georges, G. J.; Bonfil, R. D.; Fridman, R.; Uhles, S.; Moll, S.; Faul, C.; Fornoni, A.; Prunotto, M. DNA-encoded library-derived *ddr1* inhibitor prevents fibrosis and renal function loss in a genetic mouse model of alport syndrome. *ACS chemical biology* **2019**, 14, 37-49.
- (23) Petersen, L. K.; Blaskjær, P.; Chaikuad, A.; Christensen, A. B.; Dietvorst, J.; Holmkvist, J.; Knapp, S.; Kořínek, M.; Larsen, L. K.; Pedersen, A. E.; Röhm, S.; Sløk, F. A.; Hansen, N. J. V. Novel p38 α map kinase inhibitors identified from yocto reactor dna-encoded small molecule library. *MedChemComm* **2016**, 7, 1332.
- (24) Röhm, S.; Schröder, M.; Dwyer, J. E.; Widdowson, C. S.; Chaikuad, A.; Berger, B.-T.; Joerger, A. C.; Krämer, A.; Harbig, J.; Dauch, D.; Kudolo, M.; Laufer, S.; Bagley, M. C.; Knapp, S. Selective targeting of the α - and dfg-out pocket in p38 mapk. *European Journal of Medicinal Chemistry* **2020**, 112721.
- (25) Röhm, S.; Berger, B.-T.; Schröder, M.; Chaikuad, A.; Winkel, R.; Hekking, K. F. W.; Benningshof, J. J. C.; Müller, G.; Tesch, R.; Kudolo, M.; Forster, M.; Laufer, S.; Knapp, S. Fast iterative synthetic approach toward identification of novel highly selective p38 map kinase inhibitors. *Journal of Medicinal Chemistry* **2019**, 62, 10757-10782.
- (26) Ahn, Y. M.; Clare, M.; Ensinger, C. L.; Hood, M. M.; Lord, J. W.; Lu, W. P.; Miller, D. F.; Patt, W. C.; Smith, B. D.; Vogeti, L.; Kaufman, M. D.; Petillo, P. A.; Wise, S. C.; Abendroth, J.; Chun, L.; Clark, R.; Feese, M.; Kim, H.; Stewart, L.; Flynn, D. L. Switch control pocket inhibitors of p38-map kinase. Durable type ii inhibitors that do not require binding into the canonical atp hinge region. *Bioorg. Med. Chem. Lett.* **2010**, 20, 5793.
- (27) Zhu, D.; Huang, H.; Pinkas, D. M.; Luo, J.; Ganguly, D.; Fox, A. E.; Arner, E.; Xiang, Q.; Tu, Z.-C.; Bullock, A. N.; Brekken, R. A.; Ding, K.; Lu, X. 2-amino-2,3-dihydro-1h-indene-5-carboxamide-based discoidin domain receptor 1 (*ddr1*) inhibitors: Design, synthesis, and in vivo antipancreatic cancer efficacy. *Journal of medicinal chemistry* **2019**, 62, 7431-7444.
- (28) Ruiz-Castro, P. A.; Shaw, D.; Jarai, G. Discoidin domain receptor signaling and pharmacological inhibitors. In *Discoidin domain receptors in health and disease*, Fridman, R.; Huang, P. H., Eds. Springer New York: New York, NY, 2016; pp 217-238.
- (29) Matsuyama, W.; Wang, L.; Farrar, W. L.; Faure, M.; Yoshimura, T. Activation of discoidin domain receptor 1 isoform b with collagen up-regulates chemokine production in human macrophages: Role of p38 mitogen-activated protein kinase and nf- κ b. *The Journal of Immunology* **2004**, 172, 2332-2340.
- (30) Fedorov, O.; Niesen, F. H.; Knapp, S. Kinase inhibitor selectivity profiling using differential scanning fluorimetry. In *Kinase inhibitors: Methods and protocols*, Kuster, B., Ed. Humana Press: Totowa, NJ, 2012; pp 109-118.
- (31) Vasta, J. D.; Corona, C. R.; Wilkinson, J.; Zimprich, C. A.; Hartnett, J. R.; Ingold, M. R.; Zimmerman, K.; Machleidt, T.; Kirkland, T. A.; Huwiler, K. G.; Ohana, R. F.; Slater, M.; Otto, P.; Cong, M.; Wells, C. I.; Berger, B. T.; Hanke, T.; Glas, C.; Ding, K.; Drewry, D. H.; Huber, K. V. M.; Willson, T. M.; Knapp, S.; Müller, S.; Meisenheimer, P. L.; Fan, F.; Wood, K. V.; Robers, M. B. Quantitative, wide-spectrum kinase profiling in live cells for assessing the effect of cellular atp on target engagement. *Cell Chem. Biol.* **2018**, 25, 206.

- (32) Machleidt, T.; Woodroffe, C. C.; Schwinn, M. K.; Méndez, J.; Robers, M. B.; Zimmerman, K.; Otto, P.; Daniels, D. L.; Kirkland, T. A.; Wood, K. V. Nanobret—a novel bret platform for the analysis of protein–protein interactions. *ACS Chem. Biol.* **2015**, 10, 1797.
- (33) De Nicola, G. F.; Martin, E. D.; Chaikuad, A.; Bassi, R.; Clark, J.; Martino, L.; Verma, S.; Sicard, P.; Tata, R.; Atkinson, R. A.; Knapp, S.; Conte, M. R.; Marber, M. S. Mechanism and consequence of the autoactivation of p38 α mitogen-activated protein kinase promoted by tab1. *Nature Structural & Molecular Biology* **2013**, 20, 1182-1190.
- (34) Winter, G.; Lobley, C. M. C.; Prince, S. M. Decision making in xia2. *Acta crystallographica. Section D, Biological crystallography* **2013**, 69, 1260-1273.
- (35) Kabsch, W. Xds. *Acta Crystallogr., Sect. D: Biol. Crystallogr.* **2010**, 66, 125.
- (36) Evans, P. R.; Murshudov, G. N. How good are my data and what is the resolution? *Acta Crystallogr., Sect. D: Biol. Crystallogr.* **2013**, 69, 1204.
- (37) McCoy, A. J.; Grosse-Kunstleve, R. W.; Adams, P. D.; Winn, M. D.; Storoni, L. C.; Read, R. J. Phaser crystallographic software. *J. Appl. Crystallogr.* **2007**, 40, 658.
- (38) Emsley, P.; Lohkamp, B.; Scott, W. G.; Cowtan, K. D. Features and development of coot. *Acta Crystallogr., Sect. D: Biol. Crystallogr.* **2010**, 66, 486.
- (39) Kovalevskiy, O.; Nicholls, R. A.; Long, F.; Carlon, A.; Murshudov, G. N. Overview of refinement procedures within refmac5: Utilizing data from different sources. *Acta Crystallogr., Sect. D: Biol. Crystallogr.* **2018**, 74, 215-227.
- (40) Adams, P. D.; Afonine, P. V.; Bunkóczi, G.; Chen, V. B.; Davis, I. W.; Echols, N.; Headd, J. J.; Hung, L.-W.; Kapral, G. J.; Grosse-Kunstleve, R. W.; McCoy, A. J.; Moriarty, N. W.; Oeffner, R.; Read, R. J.; Richardson, D. C.; Richardson, J. S.; Terwilliger, T. C.; Zwart, P. H. Phenix: A comprehensive python-based system for macromolecular structure solution. *Acta crystallographica. Section D, Biological crystallography* **2010**, 66, 213-221.
- (41) Howarth, A.; Schröder, M.; Montenegro, R. C.; Drewry, D. H.; Sailem, H.; Millar, V.; Müller, S.; Ebner, D. V. Highvia-a flexible live-cell high-content screening pipeline to assess cellular toxicity. *SLAS discovery : advancing life sciences R & D* **2020**, 25, 801-811.
- (42) Bauer, S.; M Kubiak, J.; Rothbauer, U.; Laufer, S. *From enzyme to whole blood: Sequential screening procedure for identification and evaluation of p38 mapk inhibitors*. 2015; Vol. 1360, p 123-148.



Dual DDR/p38 inhibitor probe SR-302:
DDR1/2: $IC_{50} = 23/ 18$ nM, p38 α/β : $IC_{50} = 125/ 196$ nM